Seismic Fragility Analysis of Highway Bridges

Sponsored by

Mid-America Earthquake Center

Technical Report

MAEC RR-4 Project

Prepared by

Howard Hwang, Jing Bo Liu, and Yi-Huei Chiu

Center for Earthquake Research and Information

The University of Memphis

July 2001

ABSTRACT

Past earthquakes, such as the 1971 San Fernando earthquake, the 1994 Northridge earthquake, the 1995 Great Hanshin earthquake in Japan, and the 1999 Chi-Chi earthquake in Taiwan, have demonstrated that bridges are vulnerable to earthquakes. The seismic vulnerability of highway bridges is usually expressed in the form of fragility curves, which display the conditional probability that the structural demand (structural response) caused by various levels of ground shaking exceeds the structural capacity defined by a damage state. Fragility curves of structures can be generated empirically and analytically. Empirical fragility curves are usually developed based on the damage reports from past earthquakes, while analytical fragility curves are developed from seismic response analysis of structures and the resulting fragility curves are verified with actual earthquake data, if available. Since earthquake damage data are very scarce in the central and eastern United States, the analytical method is the only feasible approach to develop fragility curves for structures in this region.

This report presents an analytical method for the development of fragility curves of highway bridges. In this method, uncertainties in the parameters used in modeling ground motion, site conditions, and bridges are identified and quantified to establish a set of earthquake-site-bridge samples. A nonlinear time history response analysis is performed for each earthquake-site-bridge sample to establish the probabilistic characteristics of structural demand as a function of a ground shaking parameter, for example, spectral acceleration or peak ground acceleration. Furthermore, bridge damage states are defined and the probabilistic characteristics of structural capacity corresponding to each damage state are established. Then, the conditional probabilities that structural demand exceeds structural capacity are computed and the results are displayed as fragility curves. The advantage of this approach is that the assessment of uncertainties in the modeling parameters can be easily verified and refined. To illustrate the proposed method, the method is applied to a continuous concrete bridge commonly found in the highway systems affected by the New Madrid seismic zone.

ACKNOWLEDGMENTS

The work described in this report was conducted as part of the Mid-America Earthquake (MAE) Center RR-4 Project. This work was supported primarily by the Earthquake Engineering Research Centers Program of the National Science Foundation under Award Number EEC-9701785. Any opinions, findings, and conclusions expressed in the report are those of the writers and do not necessarily reflect the views of the MAE Center, or the NSF of the United States.

TABLE OF CONTENTS

LIST OF TABLES

LIST OF ILLUSTRATIONS

SECTION 1
INTRODUCTION

Past earthquakes, such as the 1971 San Fernando earthquake, the 1994 Northridge earthquake, the 1995 Great Hanshin earthquake in Japan, and the 1999 Chi-Chi earthquake in Taiwan, have demonstrated that bridges are vulnerable to earthquakes. Since bridges are one of the most critical components of highway systems, it is necessary to evaluate the seismic vulnerability of highway bridges in order to assess economic losses caused by damage to highway systems in the event of an earthquake. The seismic vulnerability of highway bridges is usually expressed in the form of fragility curves, which display the conditional probability that the structural demand (structural response) caused by various levels of ground shaking exceeds the structural capacity defined by a damage state.

Fragility curves of bridges can be developed empirically and analytically. Empirical fragility curves are usually developed based on the damage reports from past earthquakes (Basoz and Kiremidjian, 1998; Shinozuka, 2000). On the other hand, analytical fragility curves are developed from seismic response analysis of bridges, and the resulting curves are verified with actual earthquake data, if available (Hwang and Huo; 1998; Mander and Basoz, 1999). Since earthquake damage data are very scarce in the central and eastern United States (CEUS), the analytical method is the only feasible approach to develop fragility curves for bridges in this region. This report presents an analytical method for the development of fragility curves of highway bridges.

The procedure for the seismic fragility analysis of highway bridges is briefly described as follows:

1. Establish an appropriate model of the bridge of interest in the study.
2. Generate a set of earthquake acceleration time histories, which cover various levels of ground shaking intensity.
3. Quantify uncertainties in the modeling seismic source, path attenuation, local site condition, and bridge to establish a set of earthquake-site-bridge samples.

4. Perform a nonlinear time history response analysis for each earthquake-site-bridge sample to simulate a set of bridge response data.
5. Perform a regression analysis of simulated response data to establish the probabilistic characteristics of structural demand as a function of a ground shaking parameter, for example, spectral acceleration or peak ground acceleration.
6. Define bridge damage states and establish the probabilistic characteristics of structural capacity corresponding to each damage state.
7. Compute the conditional probabilities that structural demand exceeds structural capacity for various levels of ground shaking.
8. Plot the fragility curves as a function of the selected ground shaking parameter.

The highway bridges affected by the New Madrid seismic zone have been collected by the Mid-America Earthquake Center (French and Bachman, 1999). To illustrate the proposed method, the method is applied to a continuous concrete bridge commonly found in the highway systems affected by the New Madrid seismic zone.

SECTION 2
DESCRIPTION AND MODELING OF BRIDGE

2.1 Description of Bridge

The bridge selected for this study is a bridge with a continuous concrete deck supported by concrete column bents, denoted as a 602-11 bridge according to the bridge classification system established by Hwang et al. (1999). As shown in Figure 2-1, the bridge is a four span structure with two 42.5 ft end spans and two 75 ft interior spans, and thus, the total length of the bridge is 235 ft. The superstructure of the bridge consists of a 58-ft wide, 7-in. thick, continuous cast-in-place concrete deck supported on 11 AASHTO Type III girders spaced at 5.25 ft (Figure 2-2). The girders are supported on reinforced concrete four-column bents. The bearing between the girder and the cap beam of concrete column bent consists of a 1-in. Neoprene pad and two 1-in. diameter A307 Swedge dowel bars projecting 9 in. into the cap beam and 6 in. up into the bottom of the girder (Figure 2-3). At the ends of the bridge, the girders are supported on the abutments (Figure 2-4). As shown in Figures 2-1 and 2-4, the abutment is an integral, open end, spill through abutment with U-shaped wing walls. The back wall is 6 ft 10 in. in height and 58 ft in width. The wing wall is 6 ft 10 in. in height and 9 ft 6 in. in width. The abutment is supported on ten 14 ft × 14 ft concrete piles.

The concrete column bent consists of a 3.25 ft by 4.0 ft cap beam and four 15 ft high, 3 ft diameter columns. The cross sections of the column and the cap beam are shown in Figure 2-5. The vertical reinforcing bars of the column consists of 17-#7, grade 40 vertical bars extending approximately 36 in. straight into the cap beam (Figure 2-6). The vertical bars are spliced at the top of the footing with 17-#7 dowel bars projecting 28 in. into the column (Figure 2-7). The dowels have 90-degree turned out from the column centerlines. The column bents are supported on pile footings. The pile cap is 9 ft × 9 ft × 3.5 ft. The pile cap has a bottom mat of reinforcement consisting of 19-#6 each way located 12 in. up from the bottom of the pile cap. The pile cap has no shear reinforcement. As shown in Figure 2-8, the pile cap is supported on eight 14 in. × 14 in. precast concrete piles. The piles spaced at 2.75 ft are reinforced with 4-#7

vertical bars and #2 square spirals. It is noted that the piles are embedded 12 in. into the bottom of the pile cap and are not tied to the pile caps with reinforcing bars.

2.2 Finite Element Model of Bridge

The bridge is modeled with finite elements as described in the computer program SAP2000 (1996). A three dimensional view of the model is shown in Figure 2-9, and a transverse view of the model is shown in Figure 2-10. The bridge deck is modeled with 4-node plane shell elements. The girders and cap beams are modeled with beam elements. The bearings between girders and cap beams are modeled using Nllink elements. As shown in Figure 2-10, the corresponding nodes between deck and girder, girder and bearing, bearing and cap beam, and cap beam and top of the column are all connected with rigid elements.

The bridge bent consists of four columns. Each column is modeled with four beam elements and two Nllink elements placed at the top and the bottom of the column. The Nllink element is used to simulate the nonlinear behavior of the column. The pile foundation is modeled as springs. The abutment is modeled using beam elements supported on springs. In the following sections, the modeling of bearings, nonlinear column elements, pile foundations, and abutments are described in detail.

2.3 Modeling of Bearings

The bearings between girders and cap beams are modeled using Nllink elements. A Nllink element has six independent nonlinear springs, one for each of six deformational degrees of freedom (SAP2000, 1996). In this study, a bearing is idealized as a shear element. That is, the stiffness of the axial spring is taken as infinite; the stiffness of torsional spring and bending spring is taken as zero, and the stiffness of two horizontal springs is determined below.

The shear force-displacement relationship for two horizontal springs is taken as bilinear (Figure 2-11). The elastic shear stiffness provided by two 1-in. diameter A307 Swedge bolts is determined as follows:

$$K_{bh} = GA / h \tag{2-1}$$

where G is the shear modulus of a Swedge bolt, A is the gross area of two bolts, and h is the thickness of the Neoprene pad. Substituting G, A and h into Equation (2-1), the shear stiffness of the bearing is determined as $K_{bh} = 17511$ kips/in $= 210132$ kips/ft. The post-yield shear stiffness ratio is the ratio of the post-yield shear stiffness to the elastic shear stiffness. Mander et al. (1996) carried out an experiment to determine the characteristics of the 1-in. diameter Swedge bolt. From their experimental results, the post yield stiffness ratio is taken as 0.3. Also from the test results by Mander et al. (1996), the tensile yield stress of the Swedge bolt is taken as f_y = 380 Mpa = 55 ksi, and the ultimate tensile stress is f_{su} = 545 Mpa = 79 ksi. Thus, the shear yield stress of the Swedge bolt is $f_{ys} = f_y / \sqrt{3} = 55 / \sqrt{3} = 32$ ksi, and the shear yield strength of a bearing (two Swedge bolts) is $V_{by} = f_{ys} A = 32 \times 1.57 = 50$ kips. Similarly, the ultimate shear stress of the Swedge bolt is $f_{sy} = f_{su} / \sqrt{3} = 79 / \sqrt{3} = 46$ ksi, and the ultimate shear strength of one bearing is $V_{bu} = f_{sv} A = 46 \times 1.57 = 72$ kips.

2.4 Modeling of Nonlinear Column Elements

2.4.1 Effect of Lap Splices on Column Flexural Strength

As shown in Figure 2-7, the longitudinal reinforcing bars are spliced at the bottom of the columns. The maximum tensile force T_b that can be developed in a single reinforcing bar at the splice is (Priestley et al., 1996)

$$T_b = f_t p l_s \tag{2-2}$$

Where l_s is the lap length, f_t is the tension strength of the concrete, p is the perimeter of the crack surface around a bar. For a circular column, p is determined as follows:

$$p = \min\left\{\frac{\pi D'}{2n} + 2(d_b + c),\ 2\sqrt{2}(d_b + c)\right\} \tag{2-3}$$

where n is the number of longitudinal bars. Given $d_b = 7/8$ in, $D' = 32$ in, $c = 2$ in, and $n = 17$, p is determined as

$$p = \min\left\{\frac{\pi D'}{2n} + 2(d_b + c),\ 2\sqrt{2}(d_b + c)\right\} = \min\{\ 8.71,\ 8.13\ \} = 8.13\ in$$

In this study, f_t is taken as the direct tension strength of concrete and is determined as $f_t = 4\sqrt{f_c'}$. Given $f_c' = 4500$ psi, f_t is equal to 0.268 ksi.

Substituting p = 8.13 in, f_t = 0.268 ksi, and $l_s = 28$ in into Equation (2-2), the maximum tensile force T_b is determined as

$$T_b = 0.268 \times 8.13 \times 28 = 61\ kips$$

Given $A_b = 0.6$ in^2 and $f_y = 48.8$ ksi, the yield strength of a reinforcing bar is

$$A_b f_y = 0.6 \times 48.8 = 29\ kips$$

Since T_b is larger than $A_b f_y$, the yield strength of a reinforcing bar can be developed. As a result, the ideal flexural strength of a column section with lap splices can be developed.

2.4.2 Moment-Curvature Relationship for a Column Section

The nonlinear characteristics of a column section are affected by the axial force acting on the column. In this study, the axial force from dead load is used. Given the geometry of a column section and reinforcement, the moment-curvature interaction diagram of a column section is determined using the program BIAX (Wallace, 1992). Figure 2-12 shows the moment-curvature interaction diagram for a column section with the concrete compression strain of the outer concrete fiber ε_c equal to 0.004. Figures 2-13 and 2-14 show the moment-curvature relationship for column sections with the axial force P = 249 kips and 338 kips, which correspond to the case of the axial force being minimum and maximum. As shown in these figures, the moment-curvature relation of a column section is idealized as elastoplastic. The idealized yield moment M_y is taken as M_4, which is the ultimate capacity of a column section with ε_c equal to 0.004. The corresponding yield curvature ϕ_y is computed as

$$\phi_y = \frac{M_y}{M_1}\phi_1 \tag{2-4}$$

where M_1 and ϕ_1 are the moment and curvature at the first yielding, that is, the vertical reinforcing bars reach the steel yield strength at the first time.

2.4.3 Properties of Nonlinear Column Elements

The nonlinear behavior of a column is modeled using an Nllink element. The force-deformation relations for axial deformation, shear deformation, and rotations are assumed to be linear. The bending moment-deformation relationship is considered as bilinear as shown in Figure 2-15. In this figure, *K* is the elastic spring constant, *YIELD* is the yield moment, and *RATIO* is the ratio of post-yield stiffness to elastic stiffness. *EXP* is an exponent greater than or equal to unity, and a larger value of *EXP* increases the sharpness of the curve at the yield point as shown in Figure 2-15. The value of *YIELD* is equal to the yield flexural strength of a column section as described in Section 2.4.2. The values of *RATIO* and *EXP* are taken as 0 and 10, respectively, in this study.

It is noted that the bilinear model is selected because of the limitation of the SAP2000 program. In the future, other hysteretic models will be explored.

2.5 Modeling of Pile Footings

The soils surrounding the piles are taken as loose granular soils. According to ATC-32 (1996), the lateral stiffness k_p of one concrete pile in loose granular soils is $k_p = 20$ kips/in and the ultimate capacity f_p of one pile is $f_p = 40$ kips.

The pile foundation is modeled as springs as shown in Figure 2-16. The stiffness of springs in the vertical direction and two rotational directions are taken as infinite. The contribution of pile cap to the stiffness of the spring is not included, and following the suggestions by Priestly et al. (1996), the group effect of pile foundation is also not included.

The horizontal stiffness and the ultimate capacity of the spring are derived from concrete piles as follows:

$$K = n_p \times k_p \tag{2-5}$$

$$F = n_p \times f_p \tag{2-6}$$

where n_p is the number of piles in a pile footing. As shown in Figure 2-16, the pile footing has 8 piles, and the horizontal stiffness of the pile footing is

$$K = 8 \times 20 = 160 \ kips/in = 1920 \ kips/ft$$

and the ultimate capacity of the pile footing is

$$F = 8 \times 40 = 320 \ kips$$

The torsional stiffness K_t and torsional capacity T of the pile footing can be obtained by using following equation:

$$K_t = \sum_{i=1}^{n} r_i k_p \tag{2-7}$$

$$T = \sum_{i=1}^{n} r_i f_p \tag{2-8}$$

Where r_i is the distance from the column axis to the pile axe. For the pile footing shown in Figure 2-16,

$$K_t = \sum_{i=1}^{8} r_i \times 20 = (4 \times 33 + 4 \times 33\sqrt{2}) \times 20 = 6374 \; kips/rad$$

and

$$T = \sum_{i=1}^{8} r_i f_p = 12747 \; kips\text{-}in = 1062 \; kips\text{-}ft.$$

2.6 Modeling of Abutments

The abutment is modeled using beam elements supported on 11 sub-springs. The beam elements are used to model the back wall and wing walls of the abutment. The springs are used to model the effect of passive soil pressure on the walls and piles. The stiffness of vertical springs is taken as infinite, and the stiffness of horizontal springs is determined below.

The stiffness and ultimate capacity of the spring are determined according to ATC-32 (1996). For loose granular soils, the ultimate passive soil pressure on the back wall F_b is

$$F_b = 7.7 \times \left(\frac{H}{8(ft)} \right) A \tag{2-9}$$

where H is the wall height and A is the projected wall area in the loading direction. The ultimate passive pressure on the wing wall F_w is taken as 8/9 of that determined from Equation (2-9) in order to account for the differences in participation of two wing walls (Priestley et al., 1996).

The ultimate passive pressure on the back wall is

$$F_b = 7.7 \times \frac{6.833}{8} \times 58 \times 6.833 = 2607 \ kips$$

The ultimate passive pressure on the wing wall is

$$F_w = \left(7.7 \times \frac{6.833}{8} \times 9.5 \times 6.833 \right) \times \frac{8}{9} = 380 \ kips$$

The lateral ultimate capacity of piles is

$$F_p = 40 \times n_p \tag{2-10}$$

where n_p is the number of piles in an abutment. There are 10 piles in an abutment, and the ultimate shear force of these piles is $F_p = 40 \times 10 = 400$ kips.

The equivalent stiffness of the abutment in the longitudinal direction is taken as

$$K_L = (F_b + F_p) / \delta \tag{2-11}$$

where δ is the displacement of the abutment. According to ATC-32 (1996), the acceptable displacement for concrete piles in loose granular soils is 2 inches; thus, δ= 2 inches.

The equivalent stiffness of the abutment in the transverse direction is taken as

$$K_T = (F_w + F_p) / \delta \tag{2-12}$$

The longitudinal and transverse stiffness of the abutment are obtained as

$$K_L = (F_b + F_p) / \delta = (2607 + 400) / 2 = 1503.5 \; kips/in = 18042 \; kips/ft$$

$$K_T = (F_w + F_p) / \delta = (380 + 400) / 2 = 390 \; kips/in = 4680 \; kips/ft$$

The longitudinal and transverse capacity of abutment are $F_L = F_b + F_p = 2607 + 400 = 3007$ kips and $F_T = F_w + F_p = 380 + 400 = 780$ kips.

For one abutment, 11 sub-springs are used; thus, the stiffness of each sub-spring is $K_{LM} = K_L / 11 = 1640$ kips/ft and $K_{TM} = K_T / 11 = 425$ kips/ft.

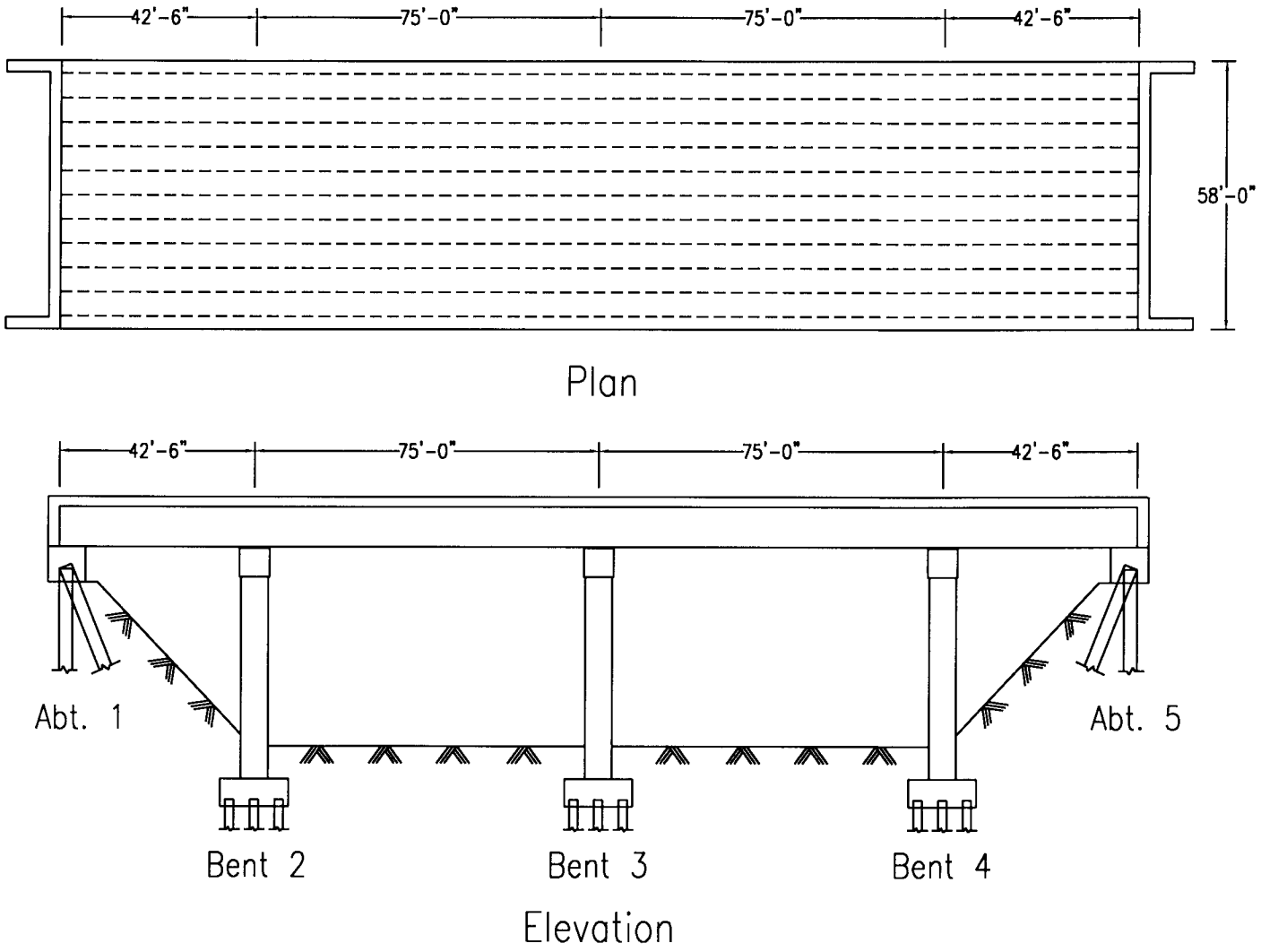

Figure 2-1 Plan and Elevation of a 602-11 Bridge

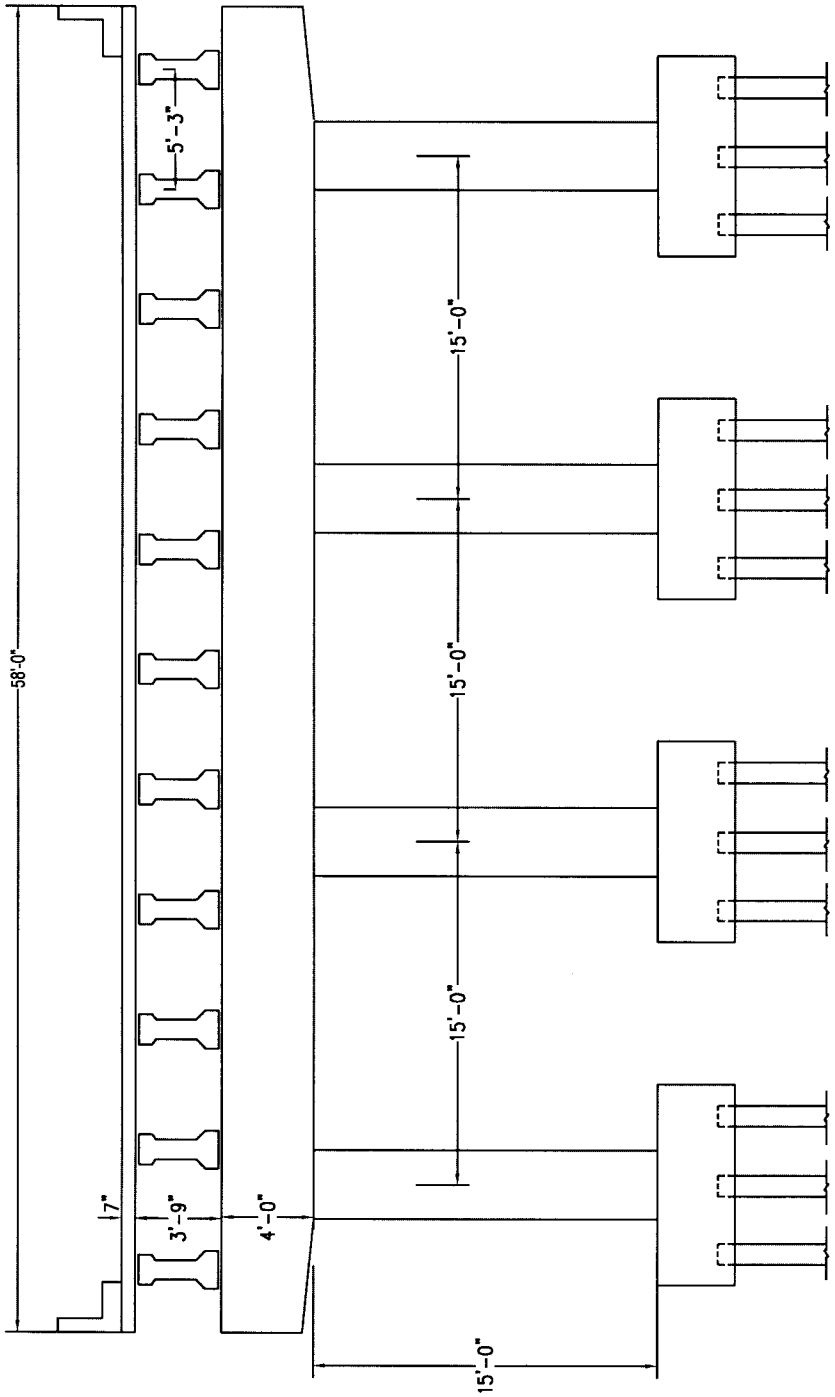

Figure 2-2 Transverse Section of a 602-11 Bridge

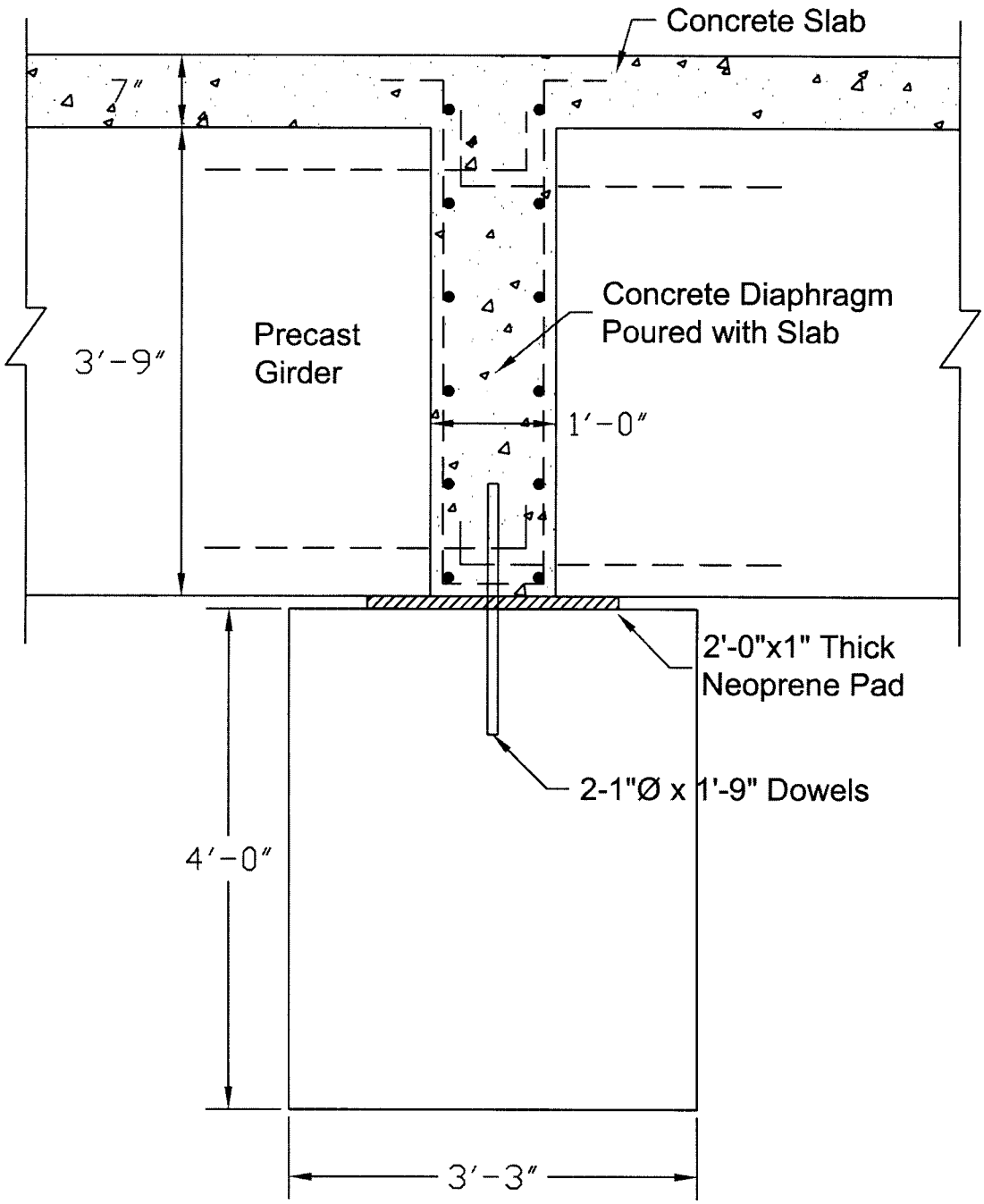

Figure 2-3 Connection of Girders and Cap Beams

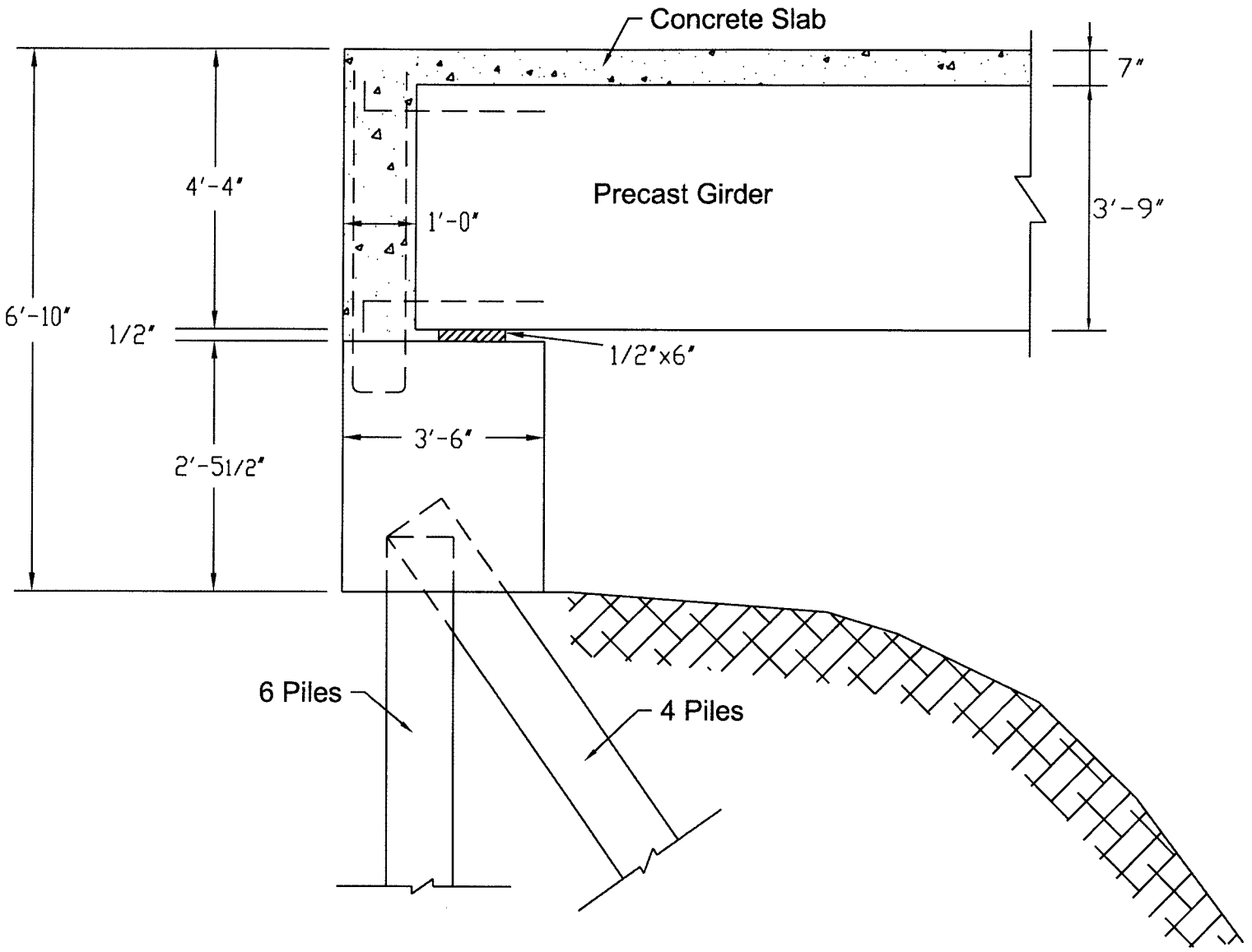

Figure 2-4 Detail of Abutment

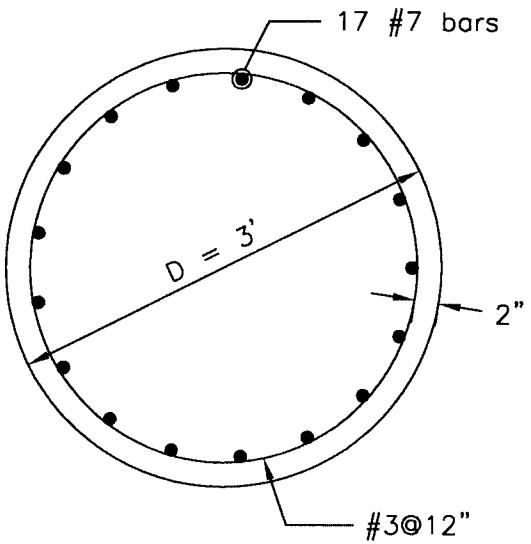

Cross Section of Columns

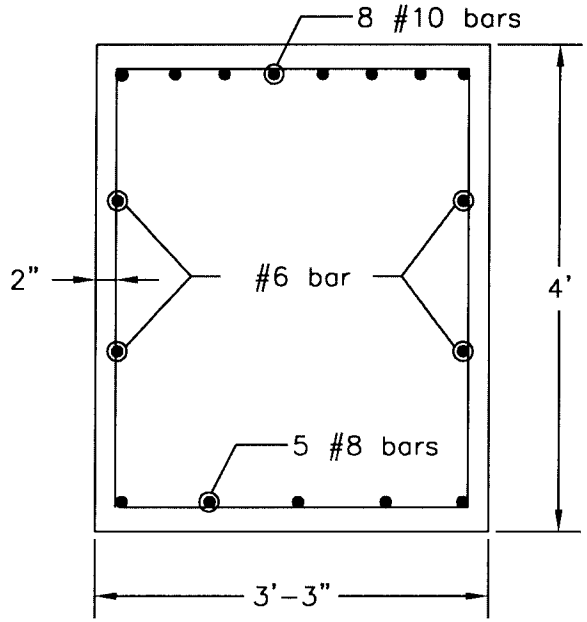

Cross Section of Cap Beams

Figure 2-5 Cross Sections of Columns and Cap Beams

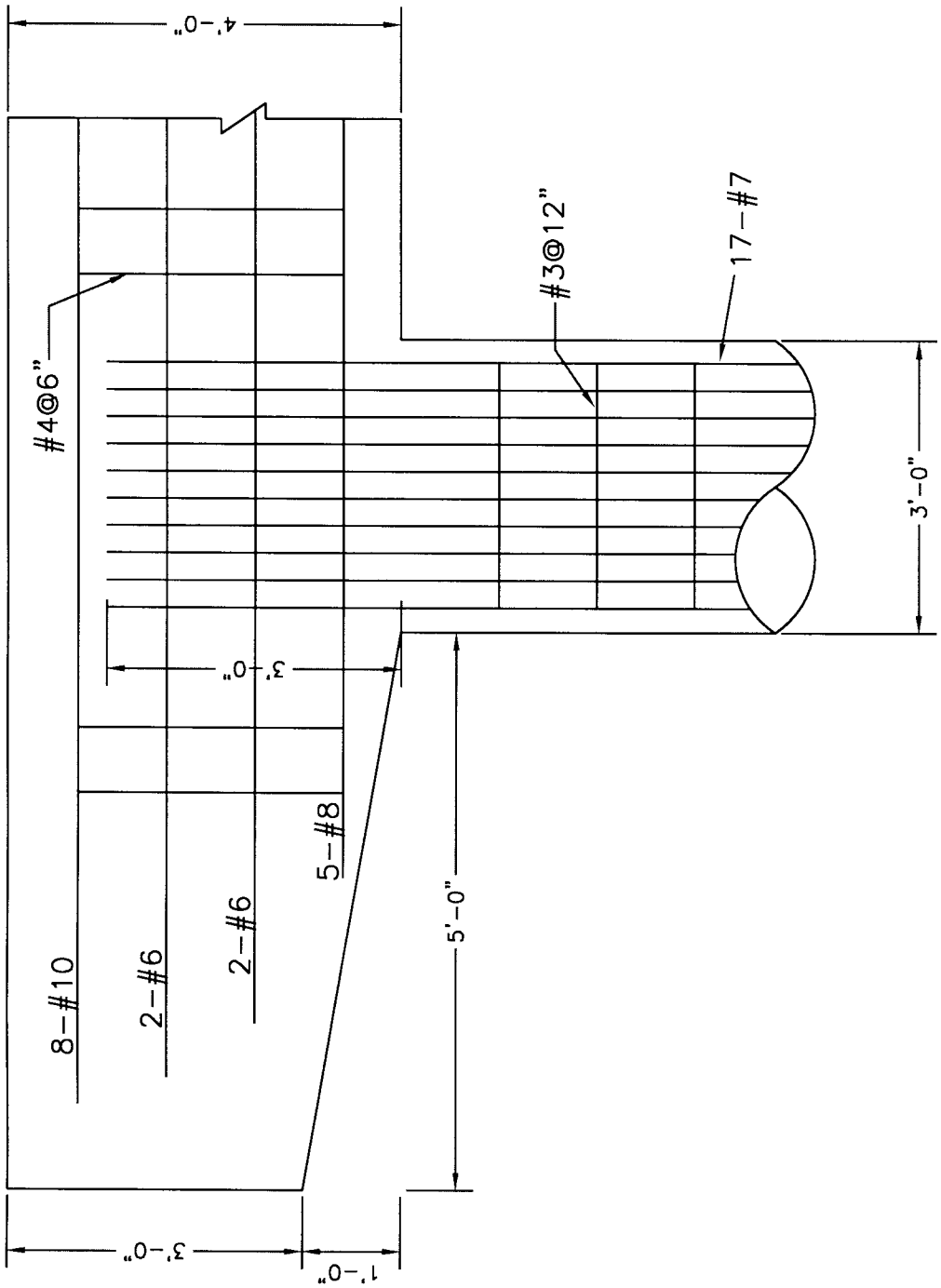

Figure 2-6 Joint Reinforcement of Column and Cap Beam

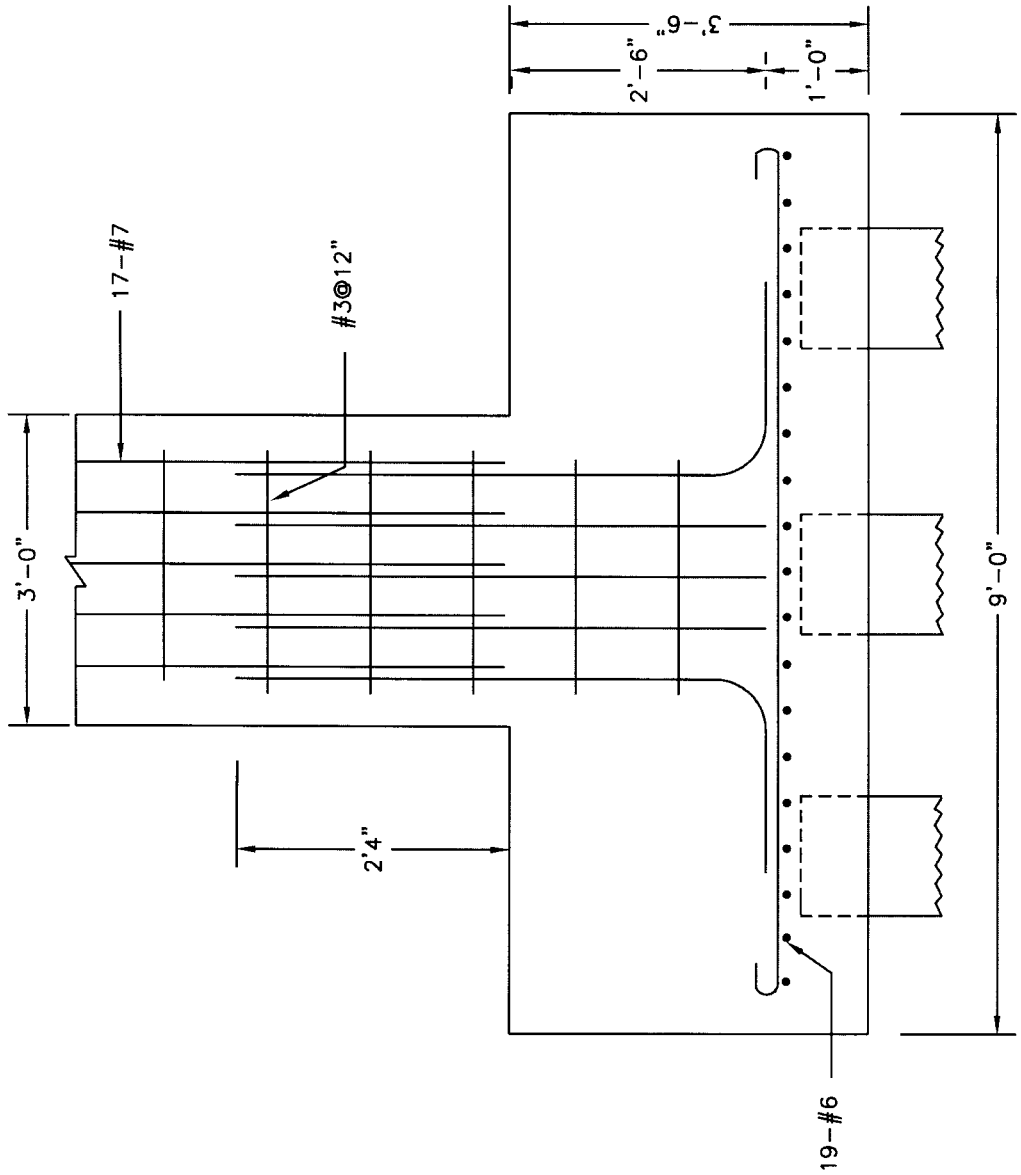

Figure 2-7 Detail of Column Splice at the Bottom of Column

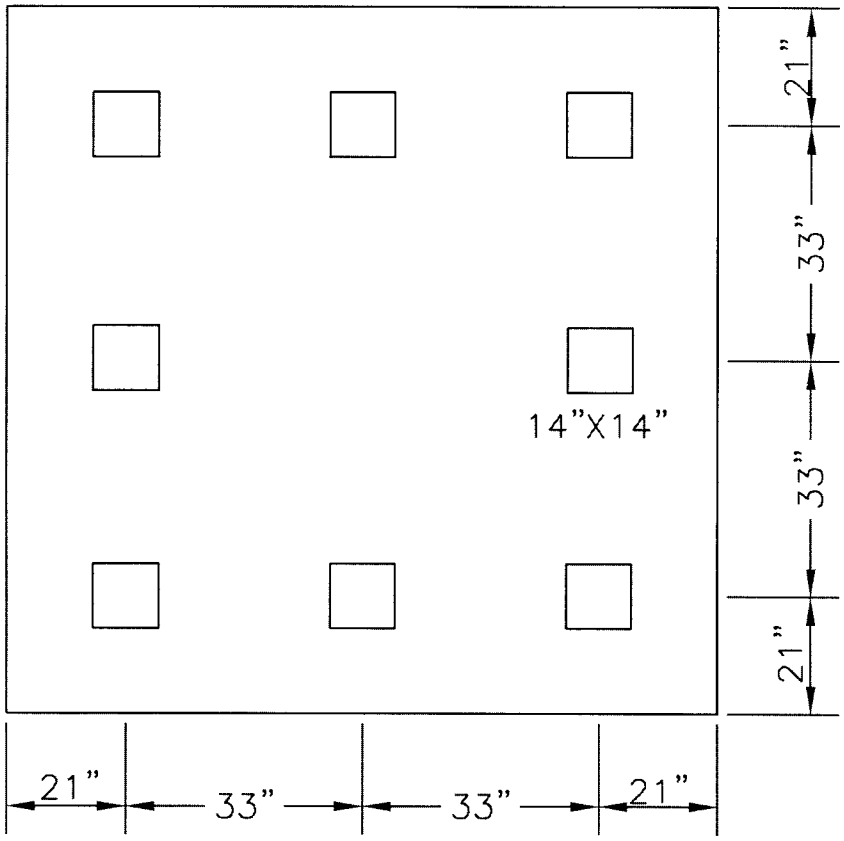

Figure 2-8 Plan of Pile Footing

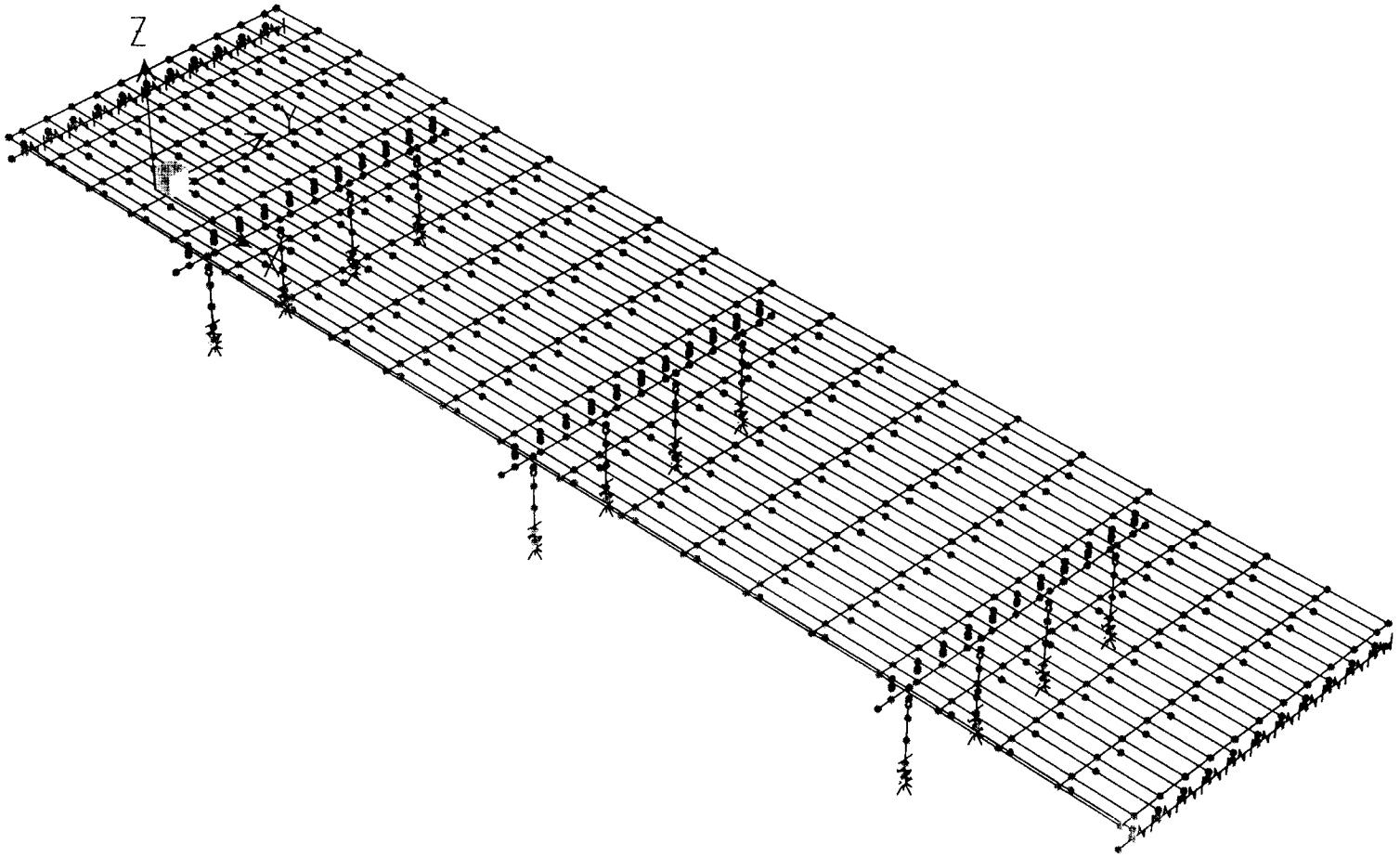

Figure 2-9 Three Dimensional View of the Bridge Finite Element Model

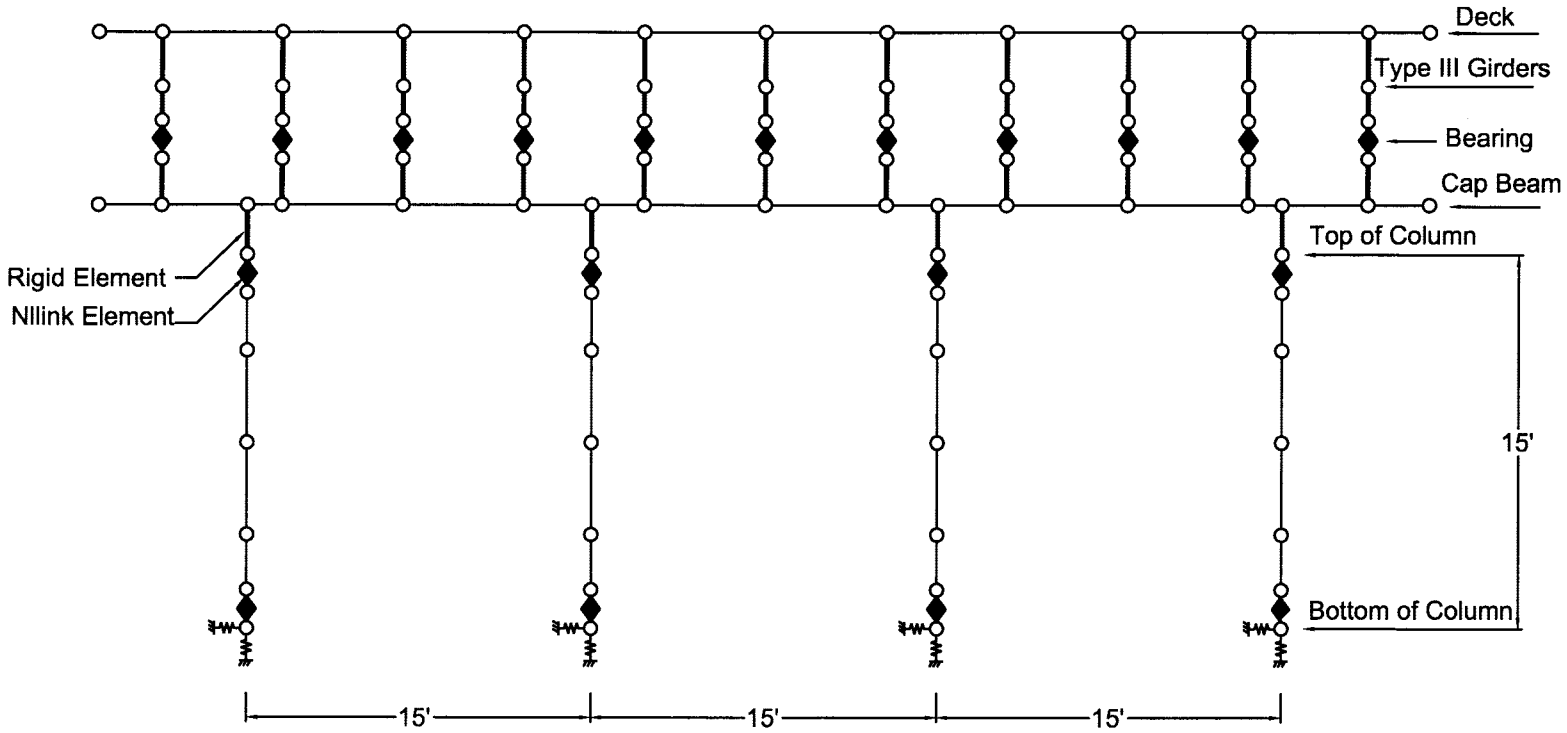

Figure 2-10 Transverse View of the Bridge Finite Element Model

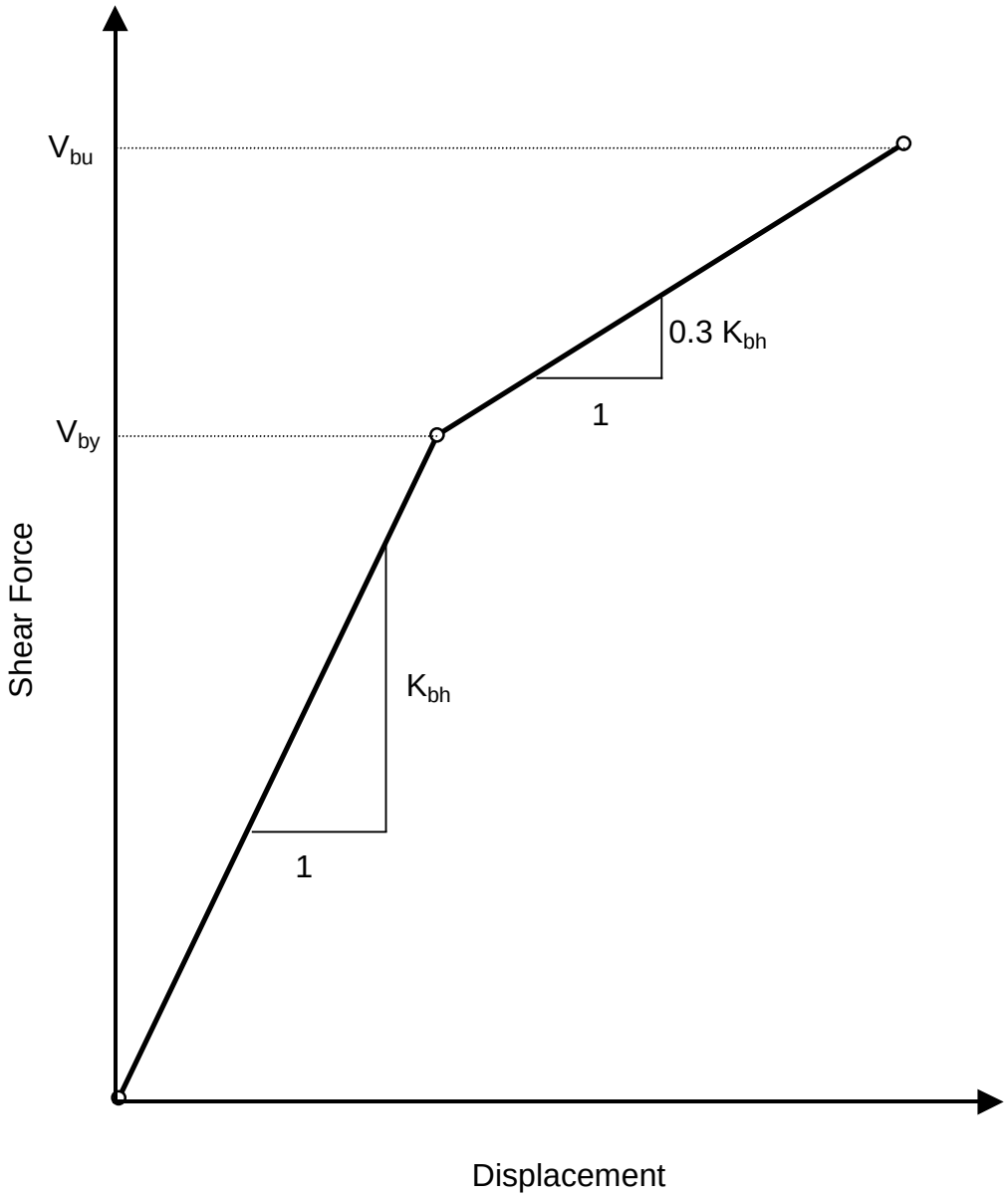

Figure 2-11 Shear Force - Displacement Diagram of a Bridge Bearing

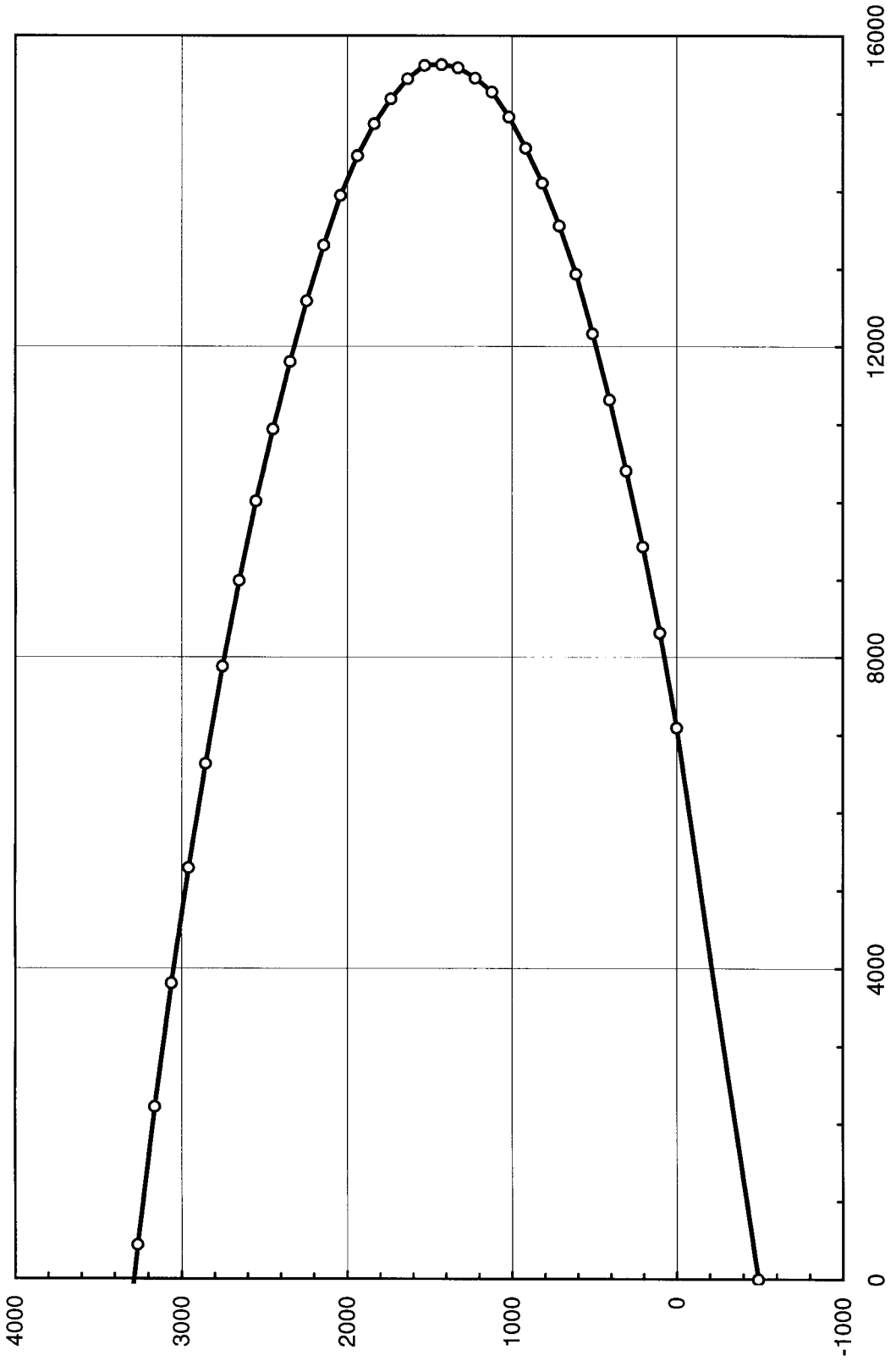

Figure 2-12 Column Interaction Diagram of a Bridge Column Section

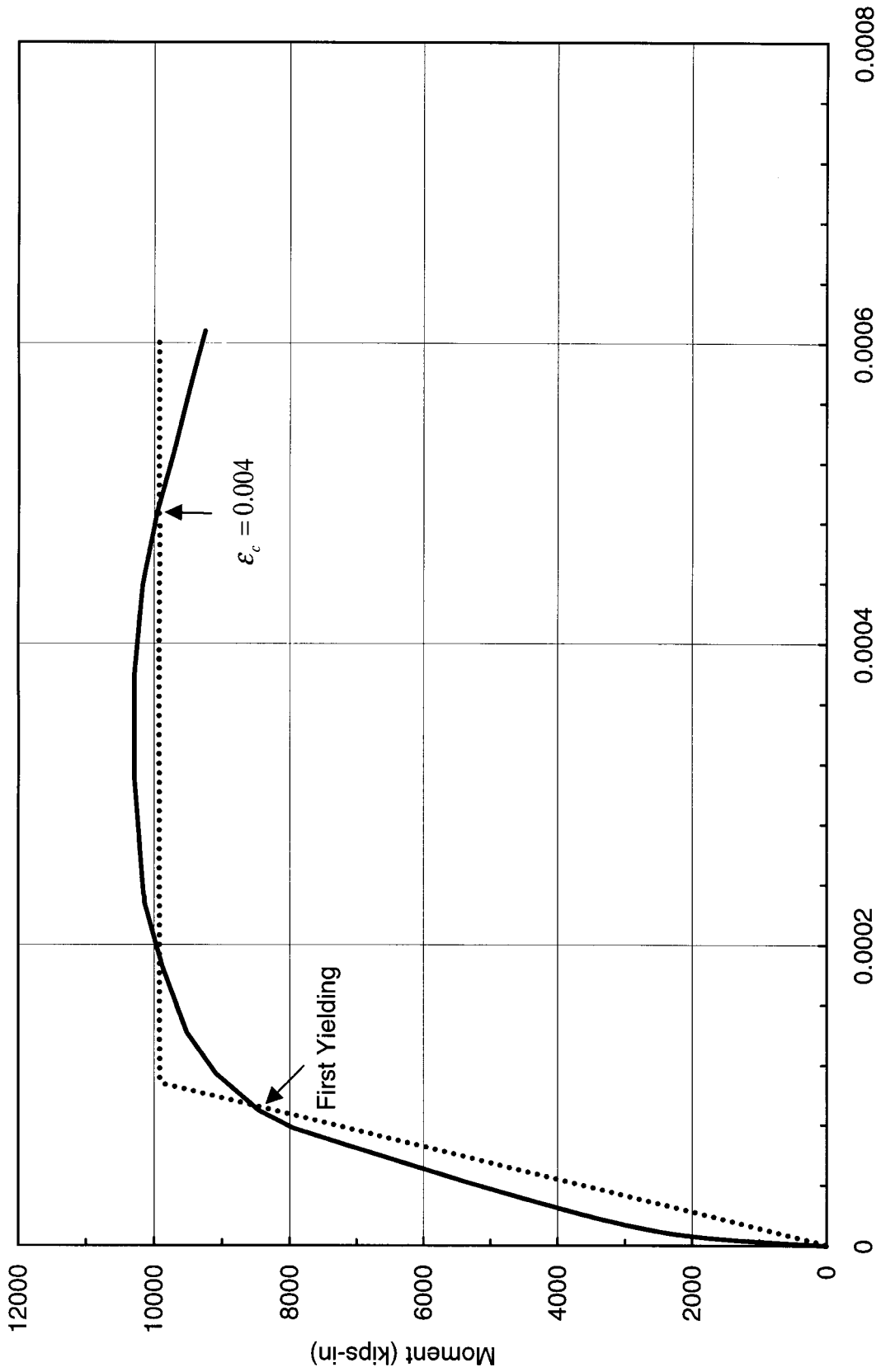

Figure 2-13 Moment-Curvature Diagram (P = 249 kips)

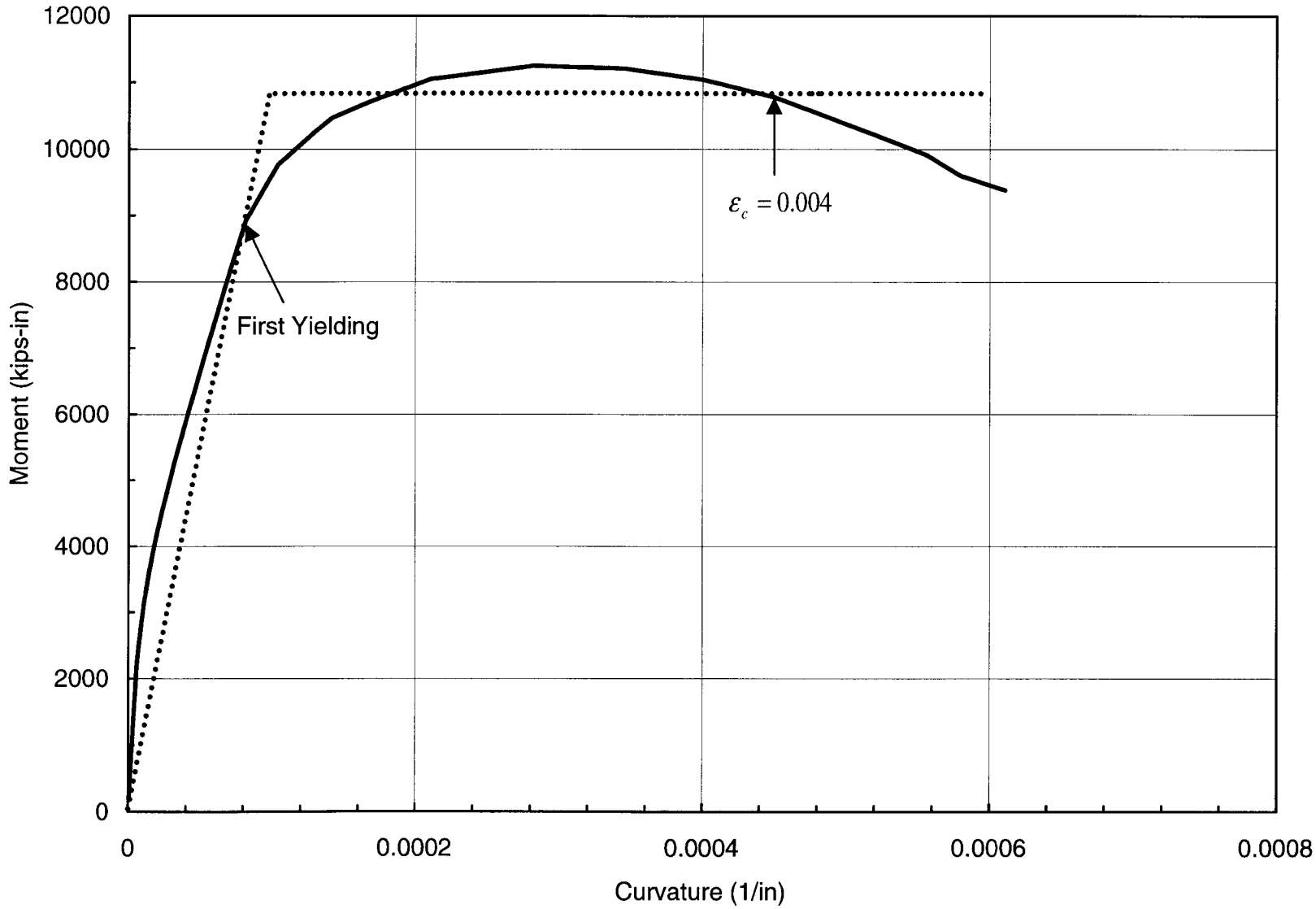

Figure 2-14 Moment-Curvature Diagram (P = 338 kips)

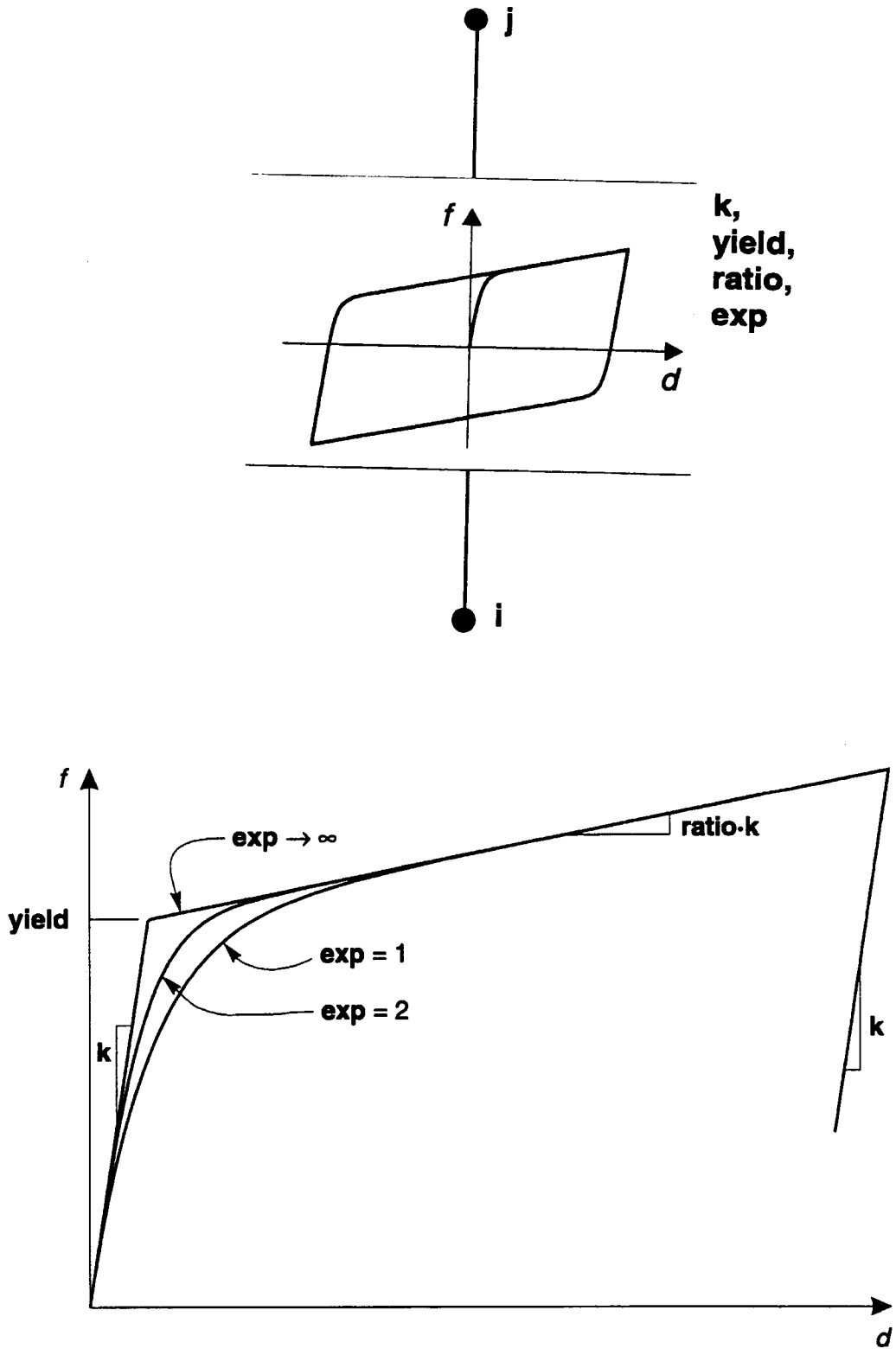

Figure 2-15 Bilinear Model of SAP2000 Nonlinear Element

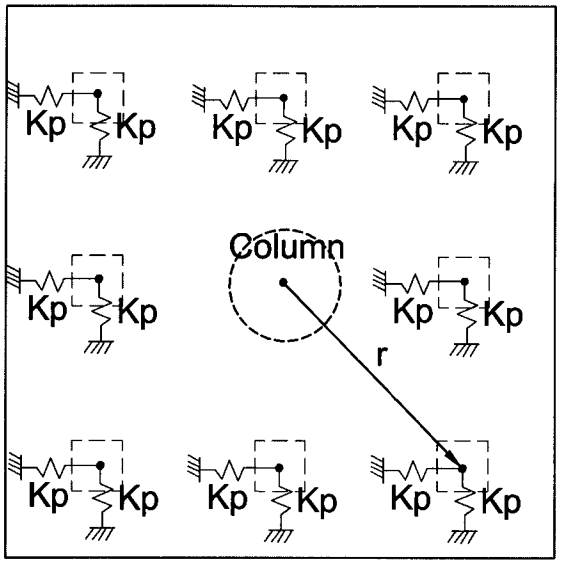

(a) Stiffness of Piles

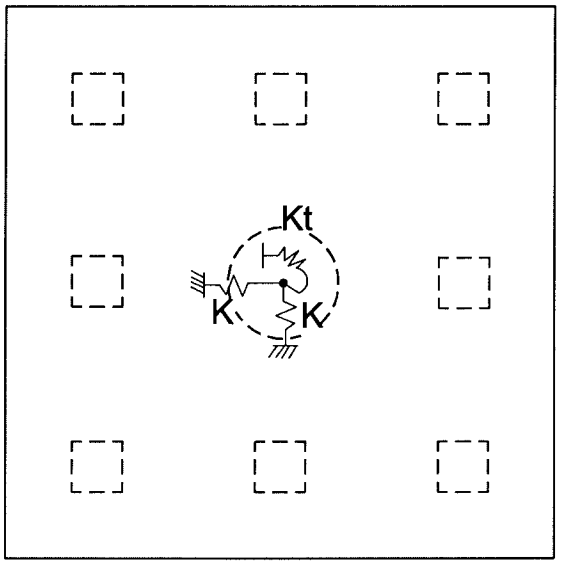

(b) Equivalent Stiffness of Pile Footing

Figure 2-16 Equivalent Stiffness of Pile Footing

SECTION 3
GENERATION OF EARTHQUAKE ACCELERATION TIME HISTORIES

In the central and eastern United States (CEUS), ground motion records are sparse; thus, synthetic acceleration time histories are utilized in the seismic response analysis of bridges. To generate synthetic ground motions, the characteristics of seismic source, path attenuation, and local soil conditions must be taken into consideration. In this section, the method of generating synthetic ground motions is presented. Uncertainties in modeling of seismic source, path attenuation, and local soil conditions are discussed in Section 5.

The generation of synthetic ground motions is illustrated in Figure 3-1. First, a synthetic ground motion at the outcrop of a rock site is generated using a seismological model (Hanks and McGuire, 1981; Boore, 1983; Hwang and Huo, 1994). Then, an acceleration time history at the ground surface is generated from a nonlinear site response analysis. In this study, the first step is performed using the computer program SMSIM (Boore, 1996) and the second step is carried out using the computer program SHAKE91 (Idriss and Sun, 1992).

3.1 Generation of Ground Motion at the Outcrop of a Rock Site

The Fourier acceleration amplitude spectrum at the outcrop of a rock site can be expressed as follows:

$$A(f) = C \cdot S(f) \cdot G(r) \cdot D(f) \cdot AF(f) \cdot P(f) \tag{3-1}$$

where C is the scaling factor, $S(f)$ is the source spectral function, $G(r)$ is the geometric attenuation function, $D(f)$ is the diminution function, $AF(f)$ is the amplification function of rock layers above the bedrock, and $P(f)$ is the high-cut filter.

The scaling factor C is expressed as (Boore, 1983)

$$C = \frac{< R_{\theta\phi} > FV}{4\pi\rho_0 {\beta_0}^3} \tag{3-2}$$

where F is the factor for free surface effect (2 for free surface), V is the partition of a vector into horizontal components $\left(1/\sqrt{2}\right)$, ρ_0 is the crustal density, β_0 is the shear wave velocity of continental crust at the seismic source region, and $< R_{\theta\phi} >$ is the radiation coefficient averaged over a range of azimuths θ and take-off angles ϕ. For θ and ϕ averaged over the whole focal sphere, $< R_{\theta\phi} >$ is taken as 0.55 (Boore and Boatwright, 1984).

The source spectral function *S(f)* used in this study is the source acceleration spectrum proposed by Brune (1970, 1971)

$$S(f) = (2\pi f)^2 \frac{M_0}{1 + (f / f_c)^2} \tag{3-3}$$

where M_0 is the seismic moment and f_c is the corner frequency. For a given moment magnitude $\boldsymbol{M}$, the corresponding seismic moment can be determined (Hanks and Kanamori, 1979). The corner frequency f_c is related to the seismic moment M_0, shear wave velocity at the source region β_0 and stress parameter $\Delta\sigma$ as follows

$$f_c = 4.9 \times 10^6 \beta_0 \left(\frac{\Delta\sigma}{M_0} \right)^{1/3} \tag{3-4}$$

The geometric attenuation function *G(r)* is expressed as follows (Atkinson and Mereu, 1992)

$$G(r) = \begin{cases} 1/r & 1 < r \leq 70\ km \\ 1/70 & 70 < r \leq 130\ km \\ \sqrt{130/r}/70 & r \geq 130\ km \end{cases} \tag{3-5}$$

where r is the hypocentral distance.

The diminution function *D(f)* represents the anelastic attenuation of seismic waves passing through the earth crust.

$$D(f) = \exp\left[\frac{-\pi f r}{Q(f)\beta_0}\right] \tag{3-6}$$

where *Q(f)* is the frequency-dependent quality factor for the study region. The quality factor *Q(f)* is expressed as

$$Q(f) = Q_0 f^{\eta} \tag{3-7}$$

The amplification function *AF(f)* represents the amplification of ground-motion amplitude when seismic waves travel through the rock layers with decreasing shear wave velocity above the bedrock. The amplification function *AF(f)* is expressed as (Boore and Joyner, 1991)

$$AF(f) = \sqrt{\rho_0 \beta_0 / \rho_e \beta_e} \tag{3-8}$$

where ρ_e and β_e are the frequency-dependent effective density and effective shear wave velocity of the rock layers from the surface to the depth of a quarter wavelength.

The high-cut filter *P(f)* represents a sharp decrease of acceleration spectra above a cut-off frequency f_m and the effect of increasing damping of rock layers near the ground surface (Boore and Joyner, 1991).

$$P(f, f_m) = \left[1 + (f / f_m)^8\right]^{-1/2} \exp(-\kappa \pi f) \tag{3-9}$$

where f_m is the high-cut frequency, and κ is the site dependent attenuation parameter, which can be determined based on the thickness, quality factor, and shear wave velocity of the rock layers.

To produce a synthetic ground motion, a time series of random band-limited white Gaussian noise is first generated and then multiplied by an exponential window. The normalized Fourier spectrum of the windowed time series is multiplied by Fourier acceleration amplitude spectrum as expressed in Equation (3-1). The resulting spectrum is then transformed back to the time domain to yield a sample of synthetic earthquake ground motion.

The normalized exponential window is expressed as follows (Boore, 1996):

$$w(t) = at^b \exp(-ct) \tag{3-10}$$

where *a*, *b*, and *c* are the parameters for determining the shape of the window. The duration of the window is equivalent to the duration of ground motion T and is taken as twice the strong motion duration T_e. In this study, the strong motion duration is determined as follows:

$$T_e = 1 / f_c + 0.05\, r \tag{3-11}$$

where $1/f_c$ is the source duration, and *r* is the hypercentral distance. The time at the peak of the exponential window t_p is determined as

$$t_p = \tau_p \times T_e \tag{3-12}$$

where τ_p is a parameter to locate the peak in the exponential window.

3.2 Generation of Ground Motion at the Ground Surface of a Soil Site

The local soil conditions at a site have significant effects on the characteristics of earthquake ground motion. Earthquake motions at the base of a soil profile can be drastically modified in frequency content and amplitude as seismic waves transmit through the soil deposits. Furthermore, soils exhibit significantly nonlinear behavior under strong ground shaking. In this study, the nonlinear site response analysis is performed using SHAKE91 (Idriss and Sun, 1992). In the SHAKE91 program, the soil profile consists of horizontal soil layers. For each soil layer, the required soil parameters include the thickness, unit weight, and shear wave velocity or low-strain shear modulus. In addition, a shear modulus reduction curve and a damping ratio curve also need to be specified.

The low-strain shear modulus $G_{\max}$ of a soil layer can be estimated from empirical formulas. For sands, the low-strain shear modulus is expressed as

$$G_{\max} = 6100[1 + 0.01(D_r - 75)]\sqrt{\bar{\sigma}} \tag{3-13}$$

where $\bar{\sigma}$ is the average effective confining pressure in psf and D_r is the relative density in percentage. For clays, the low-strain shear modulus is expressed as

$$G_{\max} = 2500 S_u \tag{3-14}$$

where S_u is the undrained shear strength of clay.

For sandy layers, the shear modulus reduction curve and the damping ratio curve used in this study are shown in Figure 3-2. The shear modulus reduction curve is the one suggested by Hwang and Lee (1991), and the damping ratio curve is the one suggested by Idriss (1990). It is noted that the shear modulus reduction curve shown in this figure is expressed as a function of the shear strain ratio γ/γ_0, where γ_0 is the reference strain, which can be computed using an empirical formula (Hwang and Lee, 1991). As shown in Figure 3-3, the shear modulus reduction

curves vary as a function of the average effective confining pressure $\bar{\sigma}$ of the sandy layer. The curve gradually shifts to the right with increasing confining pressure. In general, the confining pressure increases with the depth of the soil profile. Thus, the shear modulus reduction curves are different for the sandy layers at various depths. For clayey layers, the shear modulus reduction curves and damping ratio curves used in this study are those suggested by Vucetic and Dobry (1991). These curves vary as a function of the plasticity index PI of a clay layer, but they are independent of the depth of the layer. Figure 3-4 and Figure 3-5 show the shear modulus reduction curves and damping ratio curves for clays with PI = 15 and PI = 50, respectively.

3.3 Illustration of Generation of Acceleration Time Histories

As an illustration, a sample of synthetic ground motion is generated. The profile of rock layers of the study site is shown in Figure 3-6. This profile is established based on the study by Chiu et al. (1992), but the shear wave velocity of the top layer is set as 1 km/sec. The selection of this shear wave velocity, that is, 1 km/sec, is to ensure that there is no need to consider the nonlinear effect of soils in the first step of generating of ground motions. The earthquake moment magnitude M is set as 7.5 and the epicentral distance R is taken as 43 km. The seismic parameters used to generate the synthetic ground motion are summarized in Table 3-1. Following the method described in Section 3.1, an acceleration time history at the outcrop of a rock site is generated and shown Figure 3-7.

The soil profile of the selected site is shown Figure 3-8. It is noted that the base of the soil profile is a rock layer with the shear wave velocity of 1 km/sec, which is the same as the top layer of the rock profile shown in Figure 3-6. The shear modulus and damping ratio for sand layers are given in Figure 3-2. The shear modulus and damping ratio for clay layers are given in Figure 3-4 and 3-5. Using the program SHAKE91 and generated ground motion at the rock outcrop as the input motion, a nonlinear site response analysis is carried out, and the resulting acceleration time history at the ground surface is shown in Figure 3-9. The response spectra at the rock outcrop and at the ground surface are shown in Figure 3-10. As shown in the figure, the frequency contents of the ground motions at the rock outcrop and at the ground surface have significant difference.

Table 3-1 Summary of Seismic Parameters

Description	Value
Moment magnitude, M	7.5
Epicentral distance, R	43 km
Focal depth, H	10 km
Stress parameter, $\Delta\sigma$	172 bars
Crustal density , ρ_0	2.7 g/cm^3
Crustal shear wave velocity, β_0	3.5 km/sec
High-cut frequency, f_m	50 Hz
Quality factor, $Q(f)$	$600\ f^{0.37}$
Site dependent attenuation parameter, κ	0.0095
Parameter for peak time, τ_p	0.27

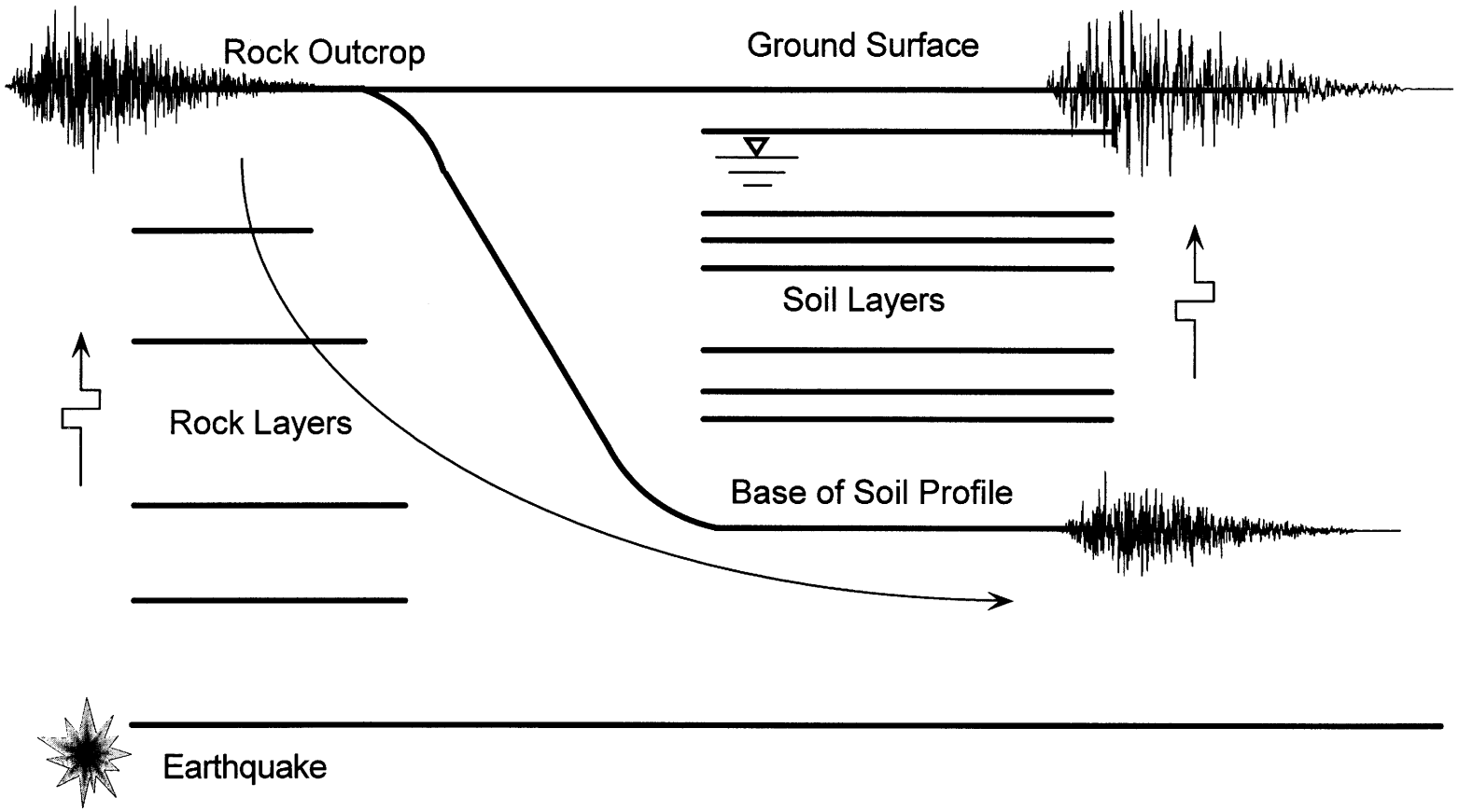

Figure 3-1 Illustration of Generating Synthetic Ground Motion

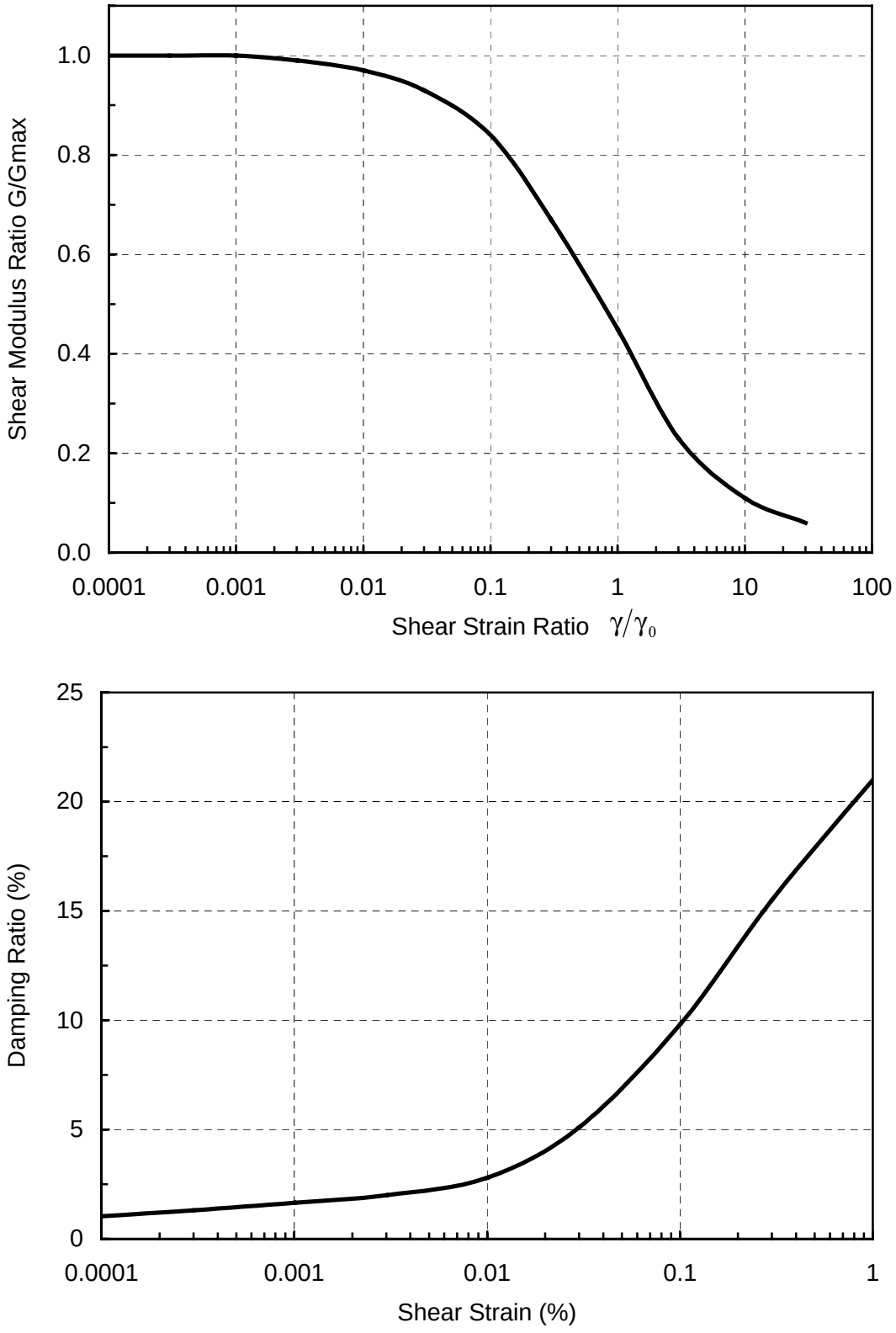

Figure 3-2 Shear Modulus Reduction and Damping Ratio Curves for Sandy Layer

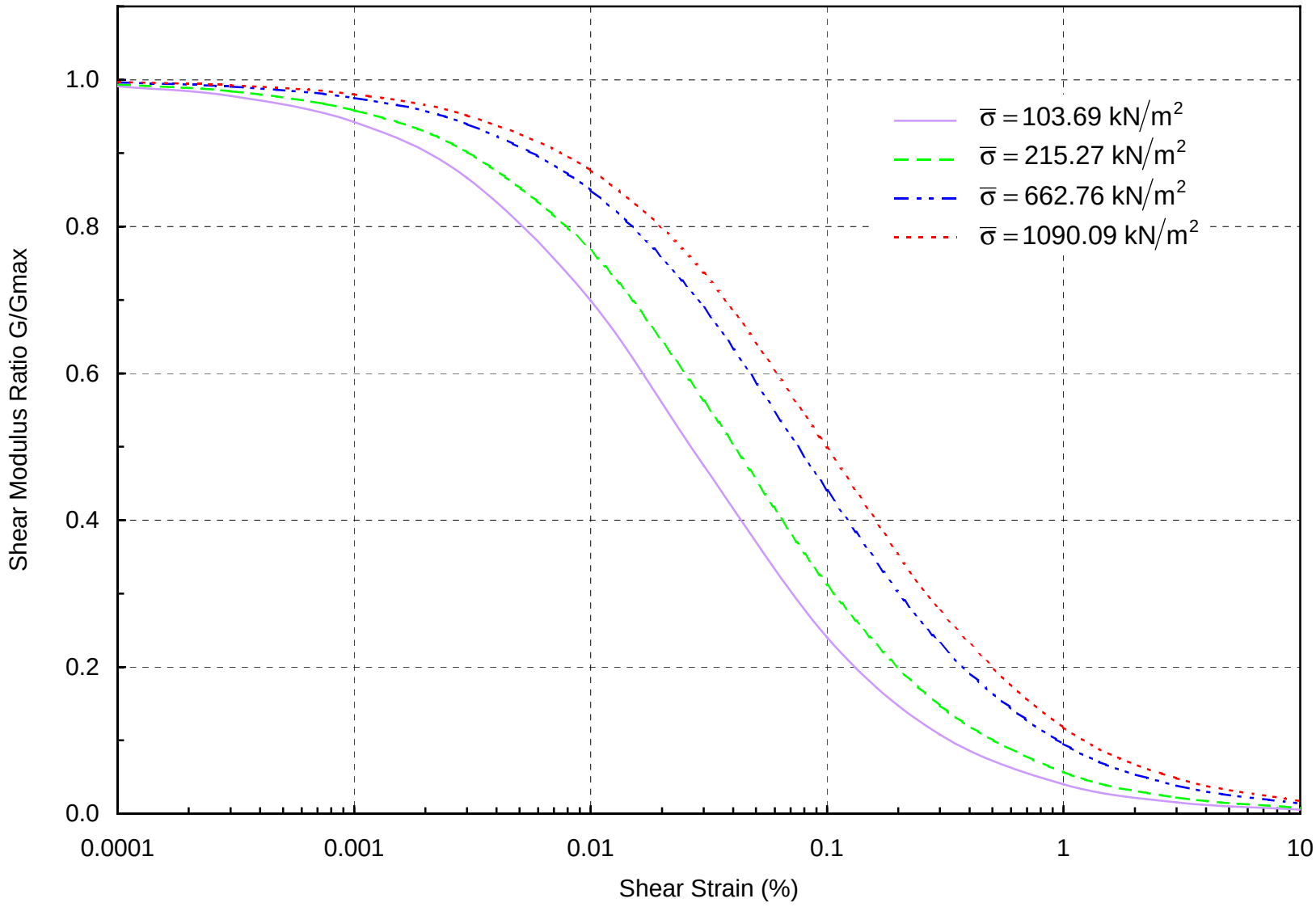

Figure 3-3 Average Effect of Confining Pressure on Shear Modulus Reduction Curves for Sands

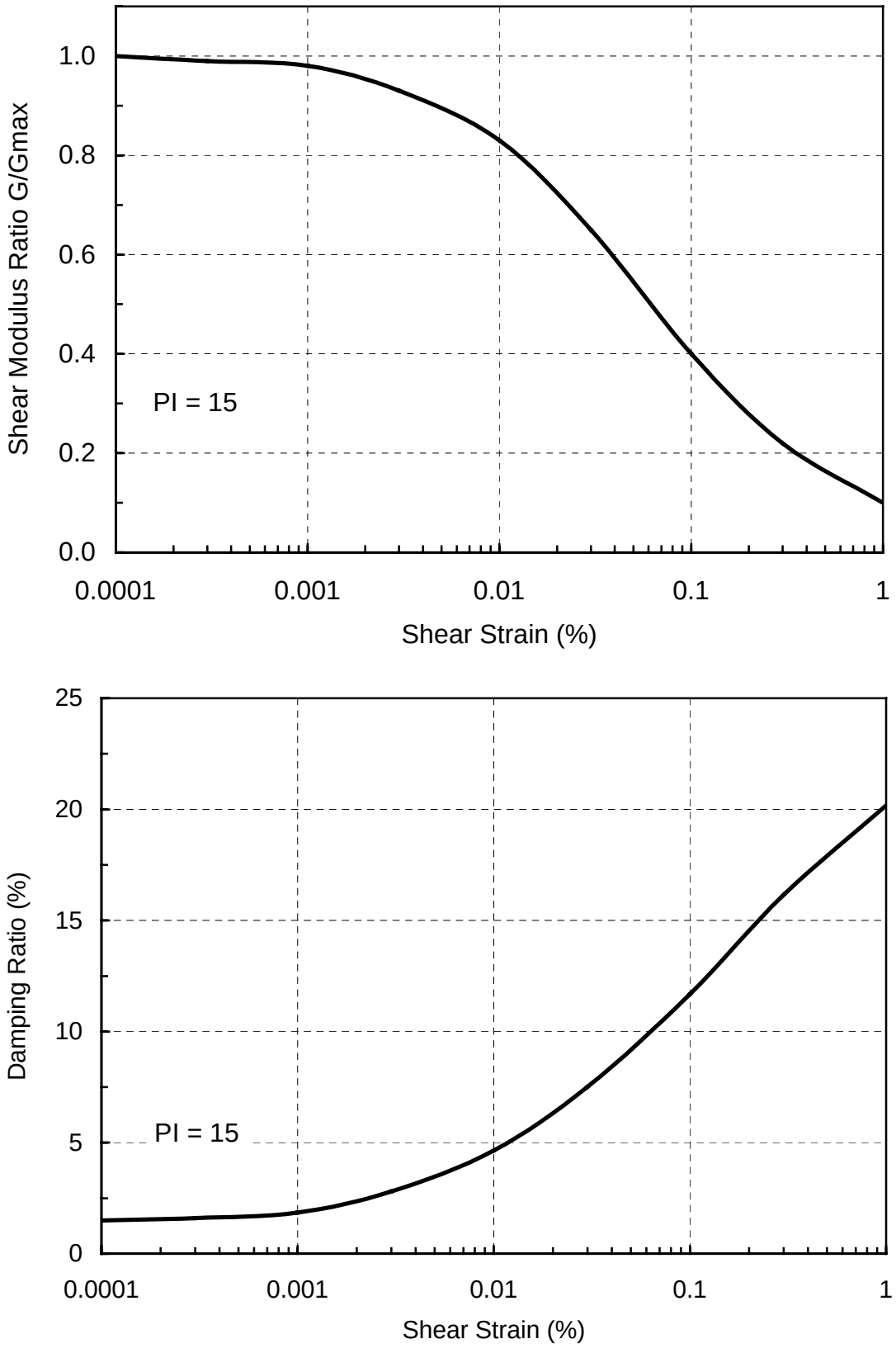

Figure 3-4 Shear Modulus Reduction and Damping Ratio Curves for Clays with PI=15

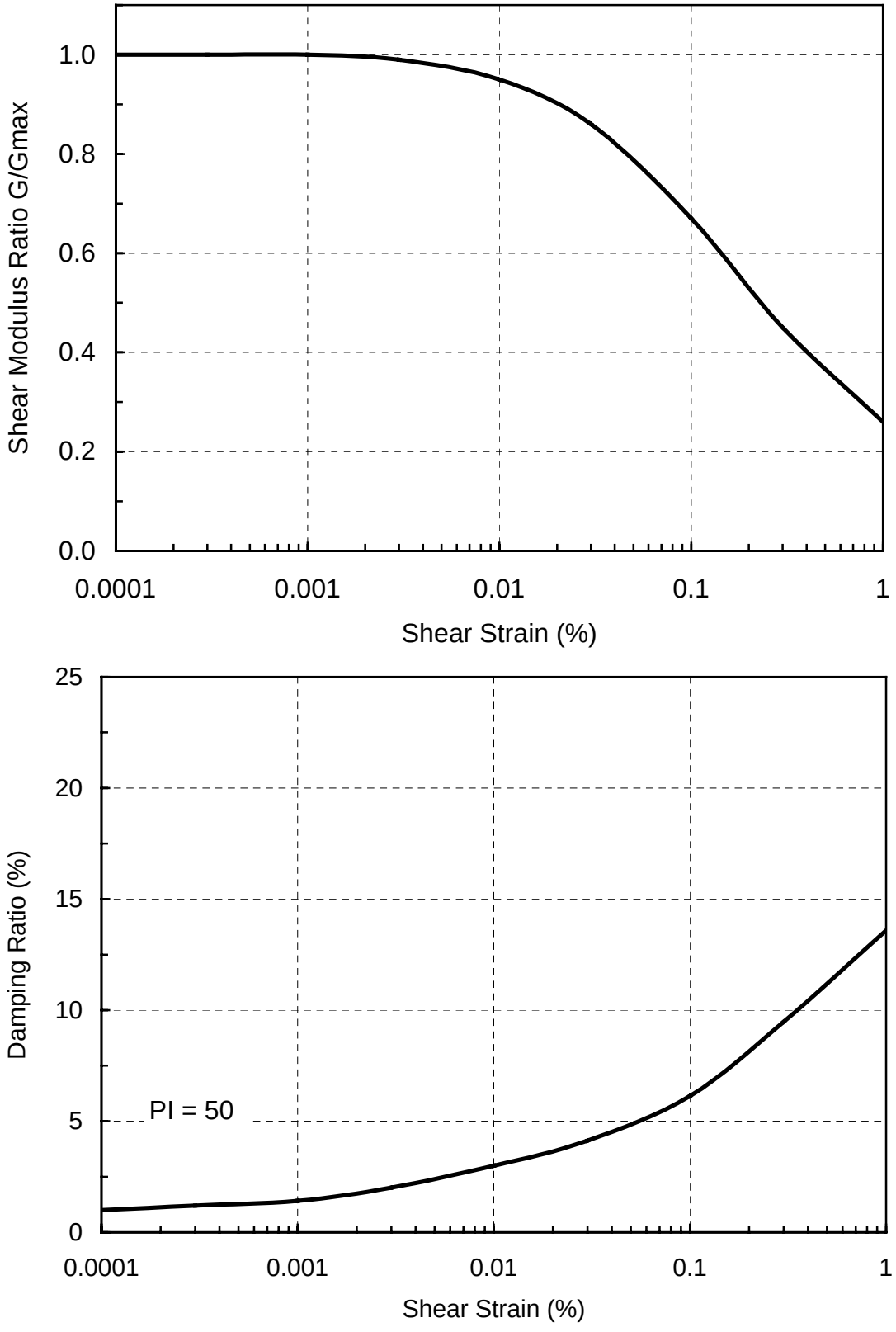

Figure 3-5 Shear Modulus Reduction and Damping Ratio Curves for Clay with PI=50

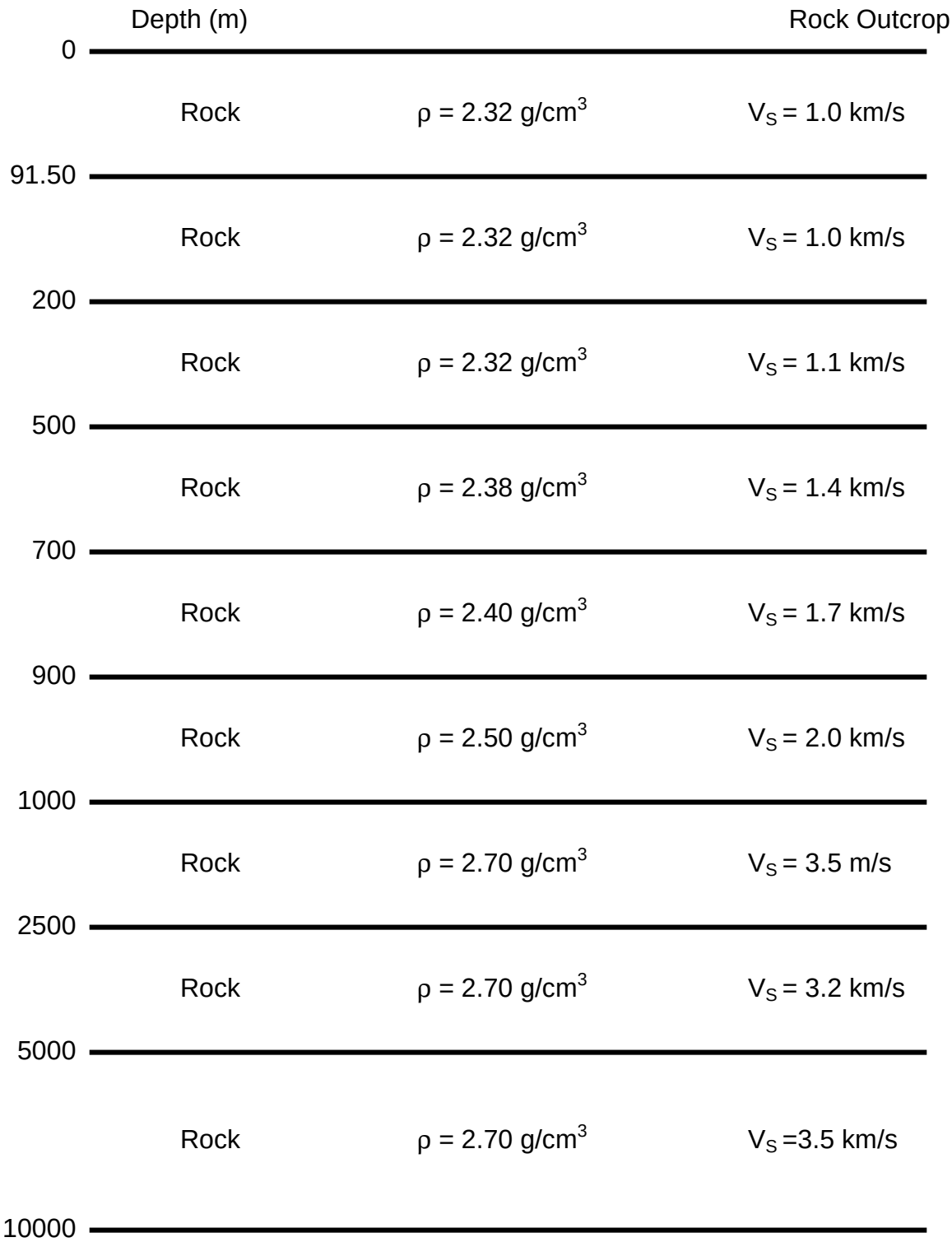

Figure 3-6 A Profile of Rock Layers

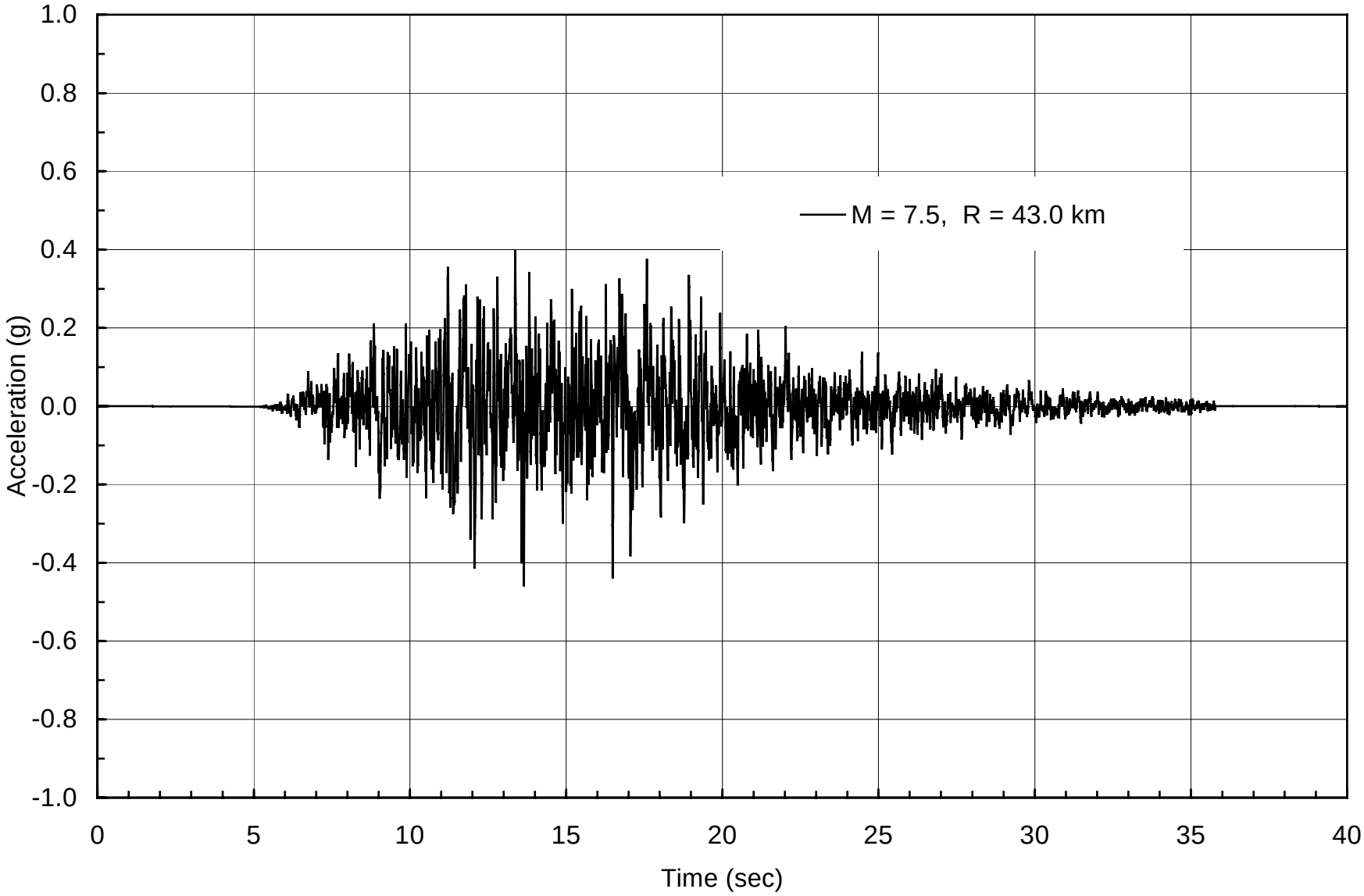

Figure 3-7 Acceleration Time History at the Rock Outcrop

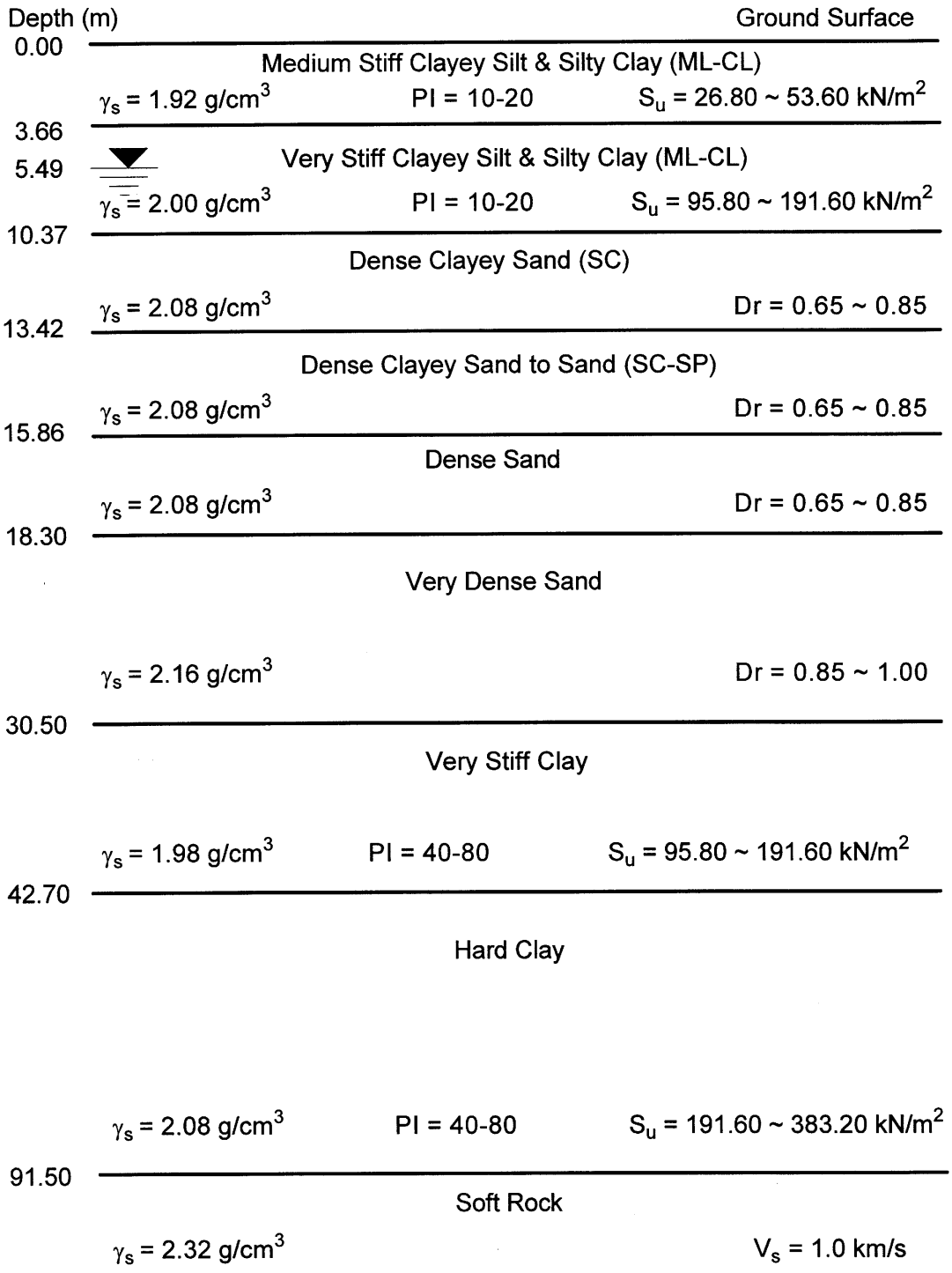

Figure 3-8 A Profile of Soil Layers

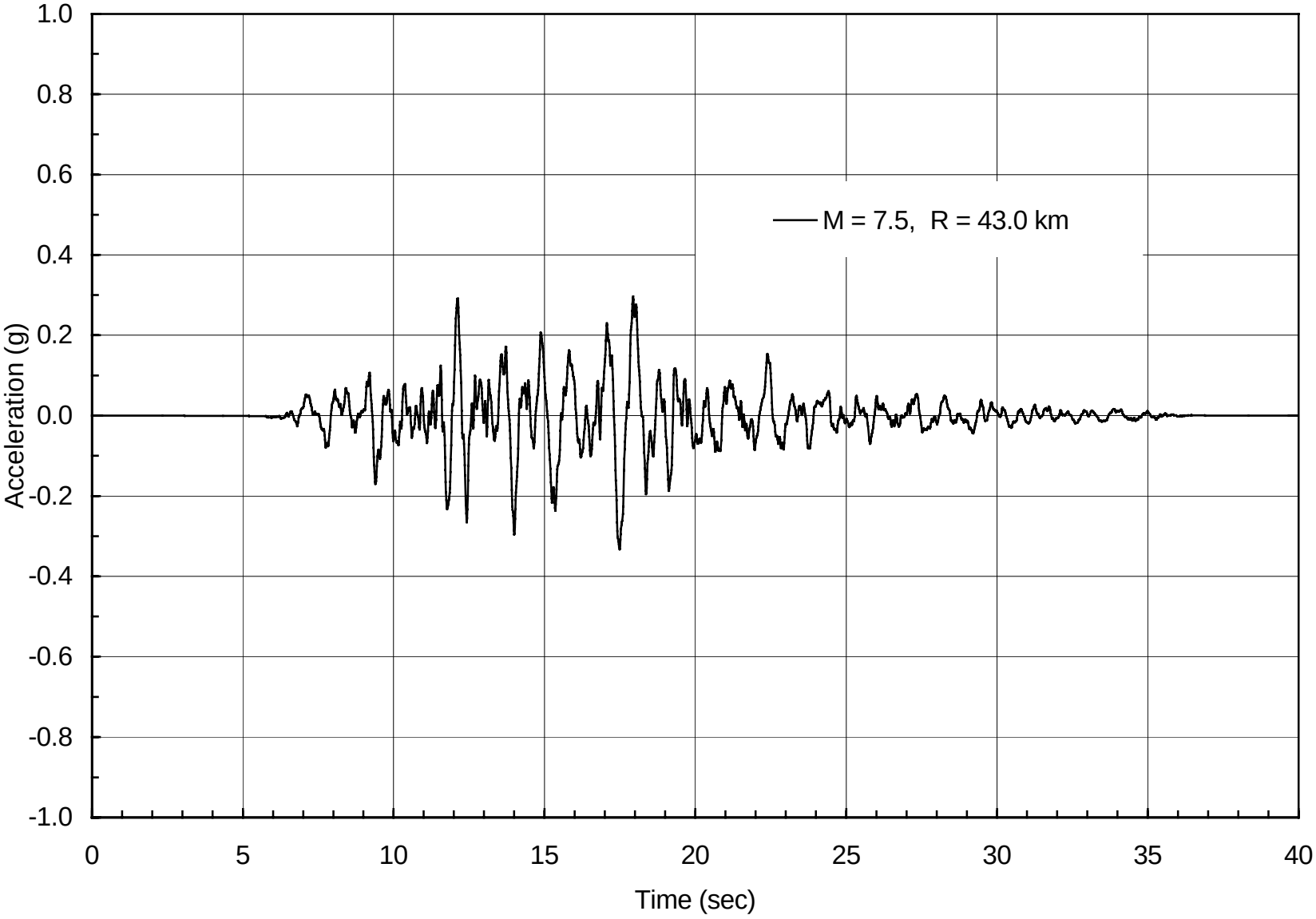

Figure 3-9 Acceleration Time History at the Ground Surface

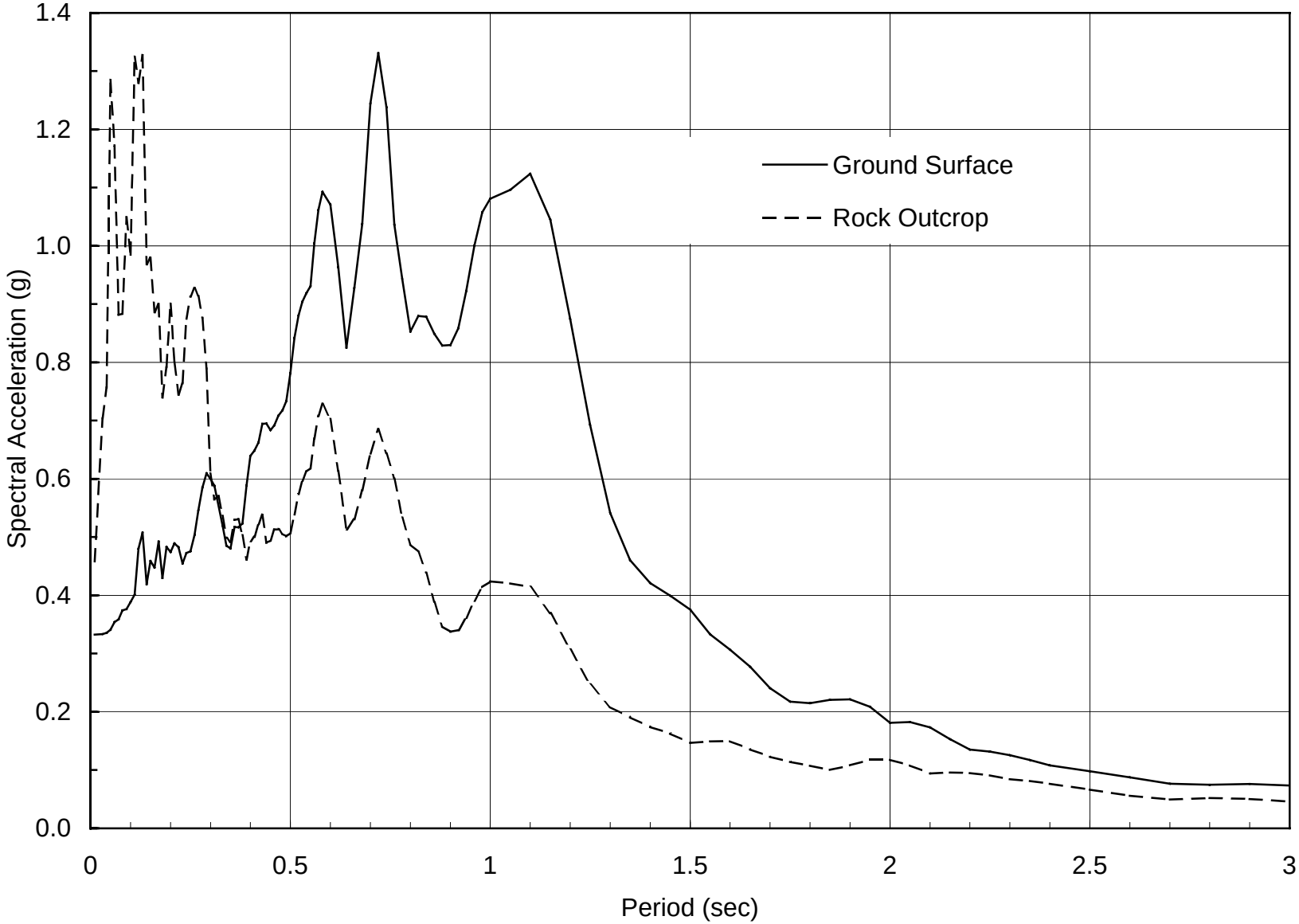

Figure 3-10 Acceleration Response Spectrums at the Ground Surface and Rock Outcrop

SECTION 4
SEISMIC DAMAGE ASSESSMENT OF BRIDGE

4.1 Nonlinear Seismic Response Analysis of Bridge

A free vibration analysis of the bridge is performed to identify the significant modes of the bridge. Figure 4-1 shows the fundamental mode of the bridge in the transverse direction, and the corresponding fundamental period is 0.48 second. Similarly, Figure 4-2 shows the fundamental mode of the bridge in the longitudinal direction, and the corresponding fundamental period is 0.35 second. The nonlinear seismic response analysis of the bridge is carried out using SAP2000. First, a static analysis of the bridge under dead load is performed, and then a nonlinear time history analysis of the bridge subject to earthquake loading in the transverse direction is carried out. Thus, the response results include both the effects of dead load and earthquake loading.

The acceleration time history as shown in Figure 3-9 is used as input motion in the transverse direction. The peak ground acceleration PGA of the input motion is 0.33 g, and the spectral acceleration SA at the fundamental period T_S corresponding to fundamental mode in the transverse direction is 0.72 g. The nonlinear seismic response analysis of the bridge is carried out in the time domain, and the Ritz-vector analysis and an iterative scheme are employed in each time step. The iteration is carried out until the solution converges. The maximum number of iterations is 100 in each iteration. If the convergence cannot be achieved, the program divides the time step into smaller sub-steps and tries again. In this study, the time step is 0.01 second; the number of Ritz-vector modes used in the analysis is 100; and the modal damping is selected as 0.05.

For the convenience of describing the seismic response results, the columns and bearings in bent 2 through bent 4 are re-numbered as shown in Figure 4-3. The displacement time history at the top and bottom of column 5 in bent 3 is shown in Figures 4-4 and 4-5, respectively. The moment, shear force, and axial force time histories at the bottom of column 5 are shown in Figure 4-6 through Figure 4-8. Table 4-1 shows the maximum displacements at various parts of

the bridge. In the table, the displacements of the super structure and the cap beam are measured at bent 3. Table 4-2 shows the maximum moment, shear force and axial force at the bottom of the columns. From evaluations of this type of bridge, it is found that damage may occur in bearings and columns; thus, only bearings and columns are considered in the seismic damage assessment.

4.2 Seismic Damage Assessment of Bearings

As shown in Figure 2-3, the bridge bearing consists mainly of two one-inch diameter bolts. The yield shear capacity V_{by} and ultimate shear capacity V_{bu} of the bearing are determined in Section 2.3. When the shear force acting on the bearing is less than the yield shear capacity of the bearing, the bolts in the bearing are within the elastic limit, and the bearing sustains no damage. When the shear force is greater than the yield shear capacity but less than the ultimate shear capacity, the bolts are yielding. When the shear force is greater than the ultimate shear capacity, the bolts are broken and bearing failure occurs. The criteria for the damage assessment of the bearing are summarized in Table 4-3.

The shear forces of all the bearings resulting from the seismic response analysis of the bridge are shown in Table 4-4. For bent 2, the shear force of bearing 6 is greater than the shear yield strength of bearing V_{by} (50 kips) but less than the ultimate shear strength V_{bu} (72 kips); therefore, the bearing is in the yielding damage state. For bent 3, the shear forces of a few bearings (bearings 15, 17-19) are greater than V_{by} but less than V_{bu}, so these bearings are yielding. The shear forces of all other bearings are less than the shear yield strength V_{by}; thus, these bearings do not sustain any damage. The damage states of all the bearings are summarized in Table 4-4.

4.3 Seismic Damage Assessment of Columns in Shear

Following *Seismic Retrofitting Manual for Highway Bridges* (1995), the criteria for assessing column shear failure are illustrated in Figure 4-9. In the figure, V_{di} is the initial shear strength and V_{dd} is the ductile shear strength.

The shear strength of columns can be expressed as (Priestley et al., 1996)

$$V_{di}(V_{dd}) = V_c + V_s + V_p \tag{4-1}$$

where V_c is the shear carried by concrete shear-resisting mechanism; V_s is the shear carried by transverse reinforcement shear resisting mechanisms, and V_p is the shear carried by axial compression.

The shear strength carried by concrete V_c is determined as

$$V_c = 0.8 A_g k \sqrt{f_c'} \tag{4-2}$$

where A_g is the column gross cross section area and k is the concrete shear resistance factor (3.5 for initial shear strength and 1.2 for ductile shear strength).

For initial shear failure, the shear strength carried by concrete V_{ci} is computed as

$$V_{ci} = 0.8 \frac{\pi \times 36^2}{4} k \sqrt{4500}/1000 = 55 \times 3.5 = 193 \ \ kips$$

For ductile shear failure, the shear strength carried by concrete V_{cd} is computed as

$$V_{cd} = 0.8\frac{\pi\times 36^2}{4}k\sqrt{4500}/1000 = 55\times 1.2 = 66 \quad kips$$

The shear strength carried by transverse reinforcement is

$$V_s = \frac{\pi}{2}\frac{A_{sp}f_{yh}D'}{s}\cot\theta \tag{4-3}$$

where D' is the core dimension from center to center of peripheral hoop, s is the space of peripheral hoop, A_{sp} is the area of spiral reinforcement, and θ is the angle of cracking. In this study, θ is taken as 30° as recommended by Priestley et al. (1996).

For the columns used in this study,

$$V_s = \frac{\pi}{2}\times\frac{0.11\times 48.8\times 32}{12}\times\cot 30^\circ = 44.13 \quad kips$$

The shear strength from axial compression is given by

$$V_p = P\tan\alpha \tag{4-4}$$

where α is the angle between the column axis and the line joining the centers of flexural compression at the top and bottom of the column. The following approximation is used to compute $\tan\alpha$.

$$\tan\alpha = \frac{D - 0.5\,(C_t + C_b)}{L_c} \tag{4-5}$$

where C_t is the depth of compressive stress block at the top of column, C_b is the depth of compressive stress block at the bottom of column, P is the axial force in the column and L_c is

the length of column. The determination of $\tan\alpha$ for all the columns is given in Table 4-5. The shear strength of all the columns is summarized in Table 4-6. As shown in Table 4-2, the maximum shear force in the columns is 122 kips, which is less than the ductile shear strength V_{dd} of the column (147.10 kips to 155.85 kips) listed in Table 4-6; therefore, all of the columns do not sustain any shear damage.

4.4 Seismic Damage Assessment of Columns in Flexure

From the results of the seismic response analysis, if the column moment is less than M_1, the reinforcement is in the elastic stage and the concrete may have minor cracking. Under this condition, the column is considered as no damage. When the column moment is larger than M_1 and less than M_y, the tensile reinforcement reaches yielding already and the concrete may have visible minor cracking; thus, the column is considered in the stage of cracking. When the column moment is larger than M_y, the plastic hinge begins to form at the column. For the column with lap splices at the bottom of the column, θ_{p2} is the plastic hinge rotation with ε_c equal to 0.002. If the column plastic hinge rotation is larger than θ_{p2}, the column core starts to disintegrate and the column is considered to fail in flexure. For the column without lap splices at the bottom of the column, θ_{p4} is the plastic hinge rotation with ε_c equal to 0.004. If the column plastic hinge rotation is larger than θ_{p4}, the column core starts to disintegrate and the column is considered to fail in flexure. The criteria for seismic damage assessment of columns with or without lap splices in flexure are shown in Tables 4-7 and 4-8.

As described in Section 2, the moment-curvature relation of a column section is determined using the program BIAX. From the moment-curvature curve, the characteristic moments and curvatures at the top and bottom of all the columns are determined and shown in Tables 4-9 and 4-10. According to Priestley et al. (1996), the plastic hinge length of column when the plastic hinge forms against a supporting member, such as the footing, is given by

$$L_p = 0.08L + 0.15 f_y d_{bl} \quad (f_y \text{ in ksi}) \tag{4-6}$$

Where, L is the distance from the critical section of the plastic hinge to the point of contraflexure, and d_{bl} is the diameter of the longitudinal reinforcement. In this study, $L = 15\ /2 = 7.5\,\text{ft} = 90\,\text{in}$, $d_{bl} = 0.875$ in, $f_y = 48.8$ kips. Therefore, the plastic hinge length is

$$L_p = 0.08 \times 90 + 0.15 \times 48.8 \times 0.875 = 13.6\ in \approx 1.1\ ft$$

The plastic hinge rotation θ_{p2} is computed as follows (*Seismic, 1995)*:

$$\theta_{p2} = (\phi_2 - \phi_y) L_p \tag{4-7}$$

where θ_{p2} is the plastic hinge rotation at $\varepsilon_c = 0.002$, and ϕ_2 is the curvature at $\varepsilon_c = 0.002$. Table 4-11 displays the determination of θ_{p2}. Similarly, the determination of θ_{p4} is shown in Table 4-12. From the seismic response analysis of the bridge, the maximum displacements and maximum forces at the top and bottom of all the columns are obtained and shown in Tables 4-13 through 4-16. The damage to the top and bottom of all the columns are determined and shown in Tables 4-17 and 4-18.

The damage patterns of bents 2 and 3 caused by the earthquake are displayed in Figures 4-10 and 4-11. It is noted that the damage pattern of bent 4 is the same as that of bent 2. As shown in the figures, this earthquake causes damage to columns and bearings. At the bottom of the column, all the outer columns fail in flexure, but the inner columns only form plastic hinges. At the top of the columns, all the columns form plastic hinges without the failure in flexure. The bearings also are yielding at several locations as shown in Figures 4-10 and 4-11. It is concluded that the bridge sustains extensive damage by this earthquake.

4.5 Alternative Approach for Seismic Damage Assessment of Bridge

The component-by-component assessment of seismic damage to a bridge as described in previous sections is appropriate when detailed seismic damage assessment is required, for example, the assessment of a bridge for seismic retrofit. For other purposes, for example, seismic fragility analysis, an alternative approach is desirable to assess the overall seismic damage to a bridge. For the bridge selected for this study, the bridge columns with the lap splices at the bottom of the columns are most vulnerable to earthquakes. When the bridge is subject to ground motion in the transverse direction, the vibration of the bridge is dominant by the fundamental mode in the transverse direction. As a result, the seismic responses of all columns in all the bents are similar, and the response of column 5 of bent 3 is selected to represent the responses of all the columns. In this study, damage to a column is determined using the relative displacement ductility ratio of a column, which is defined as

$$\mu_d = \frac{\Delta}{\Delta_{cy1}} \tag{4-8}$$

where Δ is the relative displacement at the top of a column obtained from seismic response analysis of the bridge, and Δ_{cy1} is the relative displacement of a column when the vertical reinforcing bars at the bottom of the column reaches the first yield.

In this study, seismic damage to a bridge is classified into five damage states as defined in the HAZUS99 (1999). These five damage states range from no damage to complete damage, and are described in Table 4-19. Furthermore, the five damage states are quantified in terms of the relative displacement ductility ratios as shown in Table 4-20. In the table, μ_{cy1} is the first yield displacement ductility ratio, μ_{cy} is the yield displacement ductility ratio, μ_{c2} is the displacement ductility ratio with $\varepsilon_c = 0.002$, and $\mu_{c\max}$ is the maximum displacement ductility ratio. It is noted that the displacement ductility ratio is defined in terms of the first yield displacement; thus, μ_{cy1} is equal to 1.

Under seismic loading, column 5 is deformed in double curvature. At the first yielding, the relative displacement at the top of the column 5 is computed as

$$\Delta_{cy1} = 2 \times \Delta_1^{'} \tag{4-9}$$

and $\Delta_1^{'}$ is determined as (*Seismic*, 1995)

$$\Delta_1^{'} = \frac{\phi_1 L^2}{3} \tag{4-10}$$

Substituting $\phi_1 = 1.002 \times 10^{-3}\, 1/\text{ft}$ (Table 4-9), and L = 7.5 ft into equation 4-10, $\Delta_1^{'}$ is obtained as

$$\Delta_1^{'} = \frac{\phi_1 L^2}{3} = \frac{1.002 \times 10^{-3} \times (15/2)^2}{3} = 1.88 \times 10^{-2} \ \ ft$$

and

$$\Delta_{cy1} = 2 \times \Delta_1^{'} = 0.0376 \ \ ft$$

The yield displacement of the column is computed in a similar way:

$$\Delta_y^{'} = \frac{\phi_y L^2}{3} = \frac{1.2 \times 10^{-3} \times (15/2)^2}{3} = 2.25 \times 10^{-2} \ \ ft$$

and

$$\Delta_{cy} = 2 \times \Delta_y^{'} = 0.045 \ \ ft$$

The yield displacement ductility ratio is

$$\mu_{cy} = \frac{\Delta cy}{\Delta_{cy1}} = \frac{0.045}{0.0376} = 1.20$$

Given the plastic hinge length and the plastic hinge rotation of a column with $\varepsilon_c = 0.002$, the plastic hinge displacement Δ_{p2} is computed as

$$\Delta_{p2} = \theta_{p2}(L - \frac{L_p}{2}) \tag{4-11}$$

For column 5, the plastic hinge displacement Δ_{p2} is

$$\begin{aligned}\Delta_{p2} &= \theta_{p2}(L - \frac{L_p}{2}) \\ &= 1.53\times10^{-3}(15 - \frac{1.1}{2}) \\ &= 2.211\times10^{-2}\ \ ft\end{aligned}$$

The total displacement of the column is

$$\Delta_{c2} = \Delta_{cy} + \Delta_{p2} \tag{4-12}$$

$$\Delta_{c2} = \Delta_{cy} + \Delta_{p2} = 4.5\times10^{-2} + 2.4987\times10^{-2} = 0.0661\ \ ft$$

The displacement ductility ratio at $\varepsilon_c = 0.002$ is

$$\mu_{c2} = \frac{\Delta_{c2}}{\Delta_{cy1}} = \frac{0.0661}{0.0376} = 1.76$$

Following *Seismic Retrofitting Manual for Highway Bridges* (1995), the maximum displacement ductility ratio is computed as $\mu_{c\max} = \mu_{c2} + 3$. The maximum ductility ratio of column 5 is

$$\mu_{c\max} = \mu_{c2} + 3 = 4.76$$

From the SAP2000 analysis result, the displacements at the top and bottom of column 5 are as follows:

$$\Delta_{top} = 0.1325\ ft$$

$$\Delta_{bottom} = 0.06373\ ft$$

The relative displacement between the top and bottom of the column is

$$\Delta = \Delta_{top} - \Delta_{bottom} = 0.1325 - 0.06373 = 0.06877\ ft$$

The displacement ductility ratio is

$$\mu_d = \frac{\Delta}{\Delta_{cy1}} = \frac{0.06877}{0.0376} = 1.83$$

The displacement ductility ratio of the column is

$$\mu_{c\max} > \mu_d > \mu_{c2}$$

According to the criteria shown in Table 4-20, the bridge sustains extensive damage from the earthquake.

The evaluation of bridge damage in terms of the column ductility ratio in Section 4.5 reaches the same damage state as the bridge is evaluated using detailed component-by-component approach as shown in the previous sections. Thus, the column ductility ratio can be used to express the overall damage to the entire bridge.

Table 4-1 Maximum Displacements Resulting From Earthquake

Location		Maximum displacement (ft)
Super structure		0.1345
Cap beam		0.1334
Column 1	Top	0.1254
	Bottom	0.0609
Column 5	Top	0.1325
	Bottom	0.0637
Abutment		0.1175

Table 4-2 Maximum Forces at the Bottom of Columns

Columns	Axial force (kips)	Moment (kips-ft)	Shear force (kips)
1	392	-842	-115
2	302	857	117
3	302	-854	-115
4	395	843	116
5	445	-881	-120
6	358	900	122
7	357	-900	-122
8	449	883	122

Table 4-3 Damage Assessment Criteria for Bearings

Criteria	Description of damage	Bearing status
$V < V_{by}$	No damage to A307 Swedge bolts	No Damage (OK)
$V_{by} \le V < V_{bu}$	A307 Swedge bolts yielding	Yielding (Y)
$V \ge V_{bu}$	A307 Swedge bolts broken	Failure (F)

Table 4-4 Damage Assessment of Bearings

Bearings	Shear force (kips)	Bearing status
1	11.9	OK
2	13.5	OK
3	46.7	OK
4	49.7	OK
5	47.6	OK
6	51.3	Y
7	48.4	OK
8	49.0	OK
9	47.9	OK
10	13.7	OK
11	12.1	OK
12	14.1	OK
13	14.2	OK
14	48.9	OK
15	51.9	Y
16	49.9	OK
17	52.8	Y
18	50.6	Y
19	51.3	Y
20	49.5	OK
21	14.1	OK
22	14.2	OK

Table 4-5 Determination of $\tan\alpha$

Columns	P *(kips)*	C_t (in)	C_b (in)	L_c (in)	D (in)	$\tan\alpha$
1	263	10.6	10.8	180	36	0.141
2	282	10.8	11	180	36	0.139
3	282	10.8	11	180	36	0.139
4	263	10.6	10.8	180	36	0.141
5	313	11.1	11.4	180	36	0.138
6	338	11.6	11.7	180	36	0.135
7	338	11.6	11.7	180	36	0.135
8	313	11.1	11.4	180	36	0.138

Table 4-6 Summary of Column Shear Strength

Columns	V_p (kips)	V_s (kips)	V_{ci} (kips)	V_{cd} (kips)	V_{di} (kips)	V_{dd} (kips)
1	36.97	44.13	193	66	274.10	147.10
2	39.32	44.13	193	66	276.45	149.45
3	39.32	44.13	193	66	276.45	149.45
4	36.97	44.13	193	66	274.10	147.10
5	43.04	44.13	193	66	280.17	153.17
6	45.72	44.13	193	66	282.85	155.85
7	45.72	44.13	193	66	282.85	155.85
8	43.04	44.13	193	66	280.17	153.17

Table 4-7 Seismic Damage Assessment Criteria for Columns with Splice in Flexure

Criteria	Description of damage	Column status
$M_1 > M$	No reinforcing steel yielding, minor cracking in concrete	No Damage (OK)
$M_y > M \geq M_1$	Tensional reinforcement yielding and extensive cracking in concrete	Cracking (C)
$M \geq M_y, \theta < \theta_{p2}$	Hinging in column, but no failure of column	Hinging (H)
$M \geq M_y, \theta > \theta_{p2}$	Flexural failure of column	Flexural failure (F)

Table 4-8 Seismic Damage Assessment Criteria for Columns without Splice in Flexure

Criteria	Description of damage	Column status
$M_1 > M$	No reinforcing steel yielding, minor cracking in concrete	No Damage (OK)
$M_y > M \geq M_1$	Tensional reinforcement yielding and extensive cracking in concrete	Cracking (C)
$M \geq M_y, \theta < \theta_{p4}$	Hinging in column, but no failure of column	Hinging (H)
$M \geq M_y, \theta > \theta_{p4}$	Flexural failure of column	Flexural failure (F)

Table 4-9 Characteristic Moments and Curvatures at the Top of Columns

Columns	Position	P (kips)	ϕ_1 (1/ft)	M_1 (kips-ft)	ϕ_y (1/ft)	M_y (kips-ft)
1	Top	249	1.07E-03	705	1.26E-03	830
2	Top	267	1.05E-03	714	1.24E-03	844
3	Top	267	1.05E-03	714	1.24E-03	844
4	Top	249	1.07E-03	705	1.26E-03	830
5	Top	298	1.02E-03	728	1.21E-03	869
6	Top	323	9.92E-04	738	1.20E-03	888
7	Top	323	9.92E-04	738	1.20E-03	888
8	Top	298	1.02E-03	728	1.21E-03	869

Table 4-10 Characteristic Moments and Curvatures at the Bottom of Columns

Columns	Position	P (kips)	ϕ_1 (1/ft)	M_1 (kips-ft)	ϕ_y (1/ft)	M_y (kips-ft)
1	Bottom	263	1.06E-03	712	1.25E-03	841
2	Bottom	282	1.03E-03	722	1.22E-03	856
3	Bottom	282	1.03E-03	722	1.22E-03	856
4	Bottom	263	1.06E-03	712	1.25E-03	841
5	Bottom	313	1.00E-03	734	1.20E-03	881
6	Bottom	338	9.77E-04	743	1.19E-03	899
7	Bottom	338	9.77E-04	743	1.19E-03	899
8	Bottom	313	1.00E-03	734	1.20E-03	881

Table 4-11 Determination of θ_{p2}

Columns	Position	ϕ_2 (1/ft)	ϕ_y (1/ft)	$\phi_2 - \phi_y$ (1/ft)	L_p (ft)	θ_{p2} (rad)
1	Bottom	2.73E-03	1.25E-03	1.48E-03	1.1	1.63E-03
2	Bottom	2.67E-03	1.22E-03	1.45E-03	1.1	1.59E-03
3	Bottom	2.67E-03	1.22E-03	1.45E-03	1.1	1.59E-03
4	Bottom	2.73E-03	1.25E-03	1.48E-03	1.1	1.63E-03
5	Bottom	2.59E-03	1.20E-03	1.39E-03	1.1	1.53E-03
6	Bottom	2.52E-03	1.19E-03	1.33E-03	1.1	1.46E-03
7	Bottom	2.52E-03	1.19E-03	1.33E-03	1.1	1.46E-03
8	Bottom	2.59E-03	1.20E-03	1.39E-03	1.1	1.53E-03

Table 4-12 Determination of θ_{p4}

Columns	Position	ϕ_4 (1/ft)	ϕ_y (1/ft)	$\phi_4 - \phi_y$ (1/ft)	L_p (ft)	θ_{p4} (rad)
1	Top	5.84E-03	1.26E-03	4.58E-03	1.1	5.04E-03
2	Top	5.72E-03	1.24E-03	4.49E-03	1.1	4.94E-03
3	Top	5.72E-03	1.24E-03	4.49E-03	1.1	4.94E-03
4	Top	5.84E-03	1.26E-03	4.58E-03	1.1	5.04E-03
5	Top	5.56E-03	1.21E-03	4.34E-03	1.1	4.78E-03
6	Top	5.45E-03	1.20E-03	4.25E-03	1.1	4.67E-03
7	Top	5.45E-03	1.20E-03	4.25E-03	1.1	4.67E-03
8	Top	5.56E-03	1.21E-03	4.34E-03	1.1	4.78E-03

Table 4-13 Maximum Displacements at the Top of Columns

Column	Position	Vertical displacement (ft)	Horizontal displacement (ft)	θ (rad)
1	Top	-1.06E-04	-1.66E-05	1.62E-03
2	Top	-7.01E-05	-1.70E-05	1.81E-03
3	Top	-8.10E-05	-1.70E-05	1.80E-03
4	Top	-3.45E-05	-1.66E-05	1.60E-03
5	Top	-1.21E-04	-1.75E-05	1.82E-03
6	Top	-8.58E-05	-1.79E-05	1.95E-03
7	Top	-9.68E-05	-1.79E-05	1.94E-03
8	Top	-4.78E-05	-1.75E-05	1.79E-03

Table 4-14 Maximum Forces at the Top of Columns

Column	Position	Axial force (kips)	Shear force (kips)	Moment (kip-ft)
1	Top	-123.19	108.19	-828.50
2	Top	-287.28	110.61	-842.83
3	Top	-247.48	110.61	-842.83
4	Top	-374.68	108.19	-828.50
5	Top	-170.03	113.32	-867.33
6	Top	-342.92	116.47	-889.06
7	Top	-303.49	116.47	-889.06
8	Top	-425.98	113.32	-867.32

Table 4-15 Maximum Displacements at the Bottom of Columns

Column	Position	Vertical displacement (ft)	Horizontal displacement (ft)	θ (rad)
1	Bottom	-3.74E-05	1.80E-05	1.74E-03
2	Bottom	-8.49E-05	1.85E-05	1.18E-03
3	Bottom	-7.45E-05	1.85E-05	1.18E-03
4	Bottom	-1.12E-04	1.80E-05	1.74E-03
5	Bottom	-5.03E-05	1.88E-05	1.89E-03
6	Bottom	-1.01E-04	1.95E-05	1.27E-03
7	Bottom	-9.01E-05	1.95E-05	1.27E-03
8	Bottom	-1.26E-04	1.88E-05	1.89E-03

Table 4-16 Maximum Forces at the Bottom of Columns

Column	Position	Axial force (kips)	Shear force (kips)	Moment (kip-ft)
1	Bottom	-132.25	116.96	843.33
2	Bottom	-300.59	120.31	859.01
3	Bottom	-263.64	120.31	859.01
4	Bottom	-395.10	116.97	843.33
5	Bottom	-178.10	122.45	883.35
6	Bottom	-357.15	126.76	902.64
7	Bottom	-318.73	126.75	902.64
8	Bottom	-447.38	122.45	883.35

Table 4-17 Determination of Damage Status at the Top of Columns

Column	Position	Demand		Capacity			Column status
		Moment (kip-ft)	θ	M_1	M_y	θ_{p4}	
1	Top	828.50	1.62E-03	705	830	5.04E-03	H
2	Top	842.83	1.81E-03	714	844	4.94E-03	H
3	Top	842.83	1.80E-03	714	844	4.94E-03	H
4	Top	828.50	1.60E-03	705	830	5.04E-03	H
5	Top	867.33	1.82E-03	728	869	4.78E-03	H
6	Top	889.06	1.95E-03	738	888	4.67E-03	H
7	Top	889.06	1.94E-03	738	888	4.67E-03	H
8	Top	867.32	1.79E-03	728	869	4.78E-03	H

Table 4-18 Determination of Damage Status at the Bottom of Columns

Column	Position	Demand		Capacity			Column status
		Moment (kip-ft)	θ	M_1	M_y	θ_{p2}	
1	Bottom	843.33	1.74E-03	712	841	1.63E-03	F
2	Bottom	859.01	1.18E-03	722	856	1.59E-03	H
3	Bottom	859.01	1.18E-03	722	856	1.59E-03	H
4	Bottom	843.33	1.74E-03	712	841	1.63E-03	F
5	Bottom	883.35	1.89E-03	734	881	1.53E-03	F
6	Bottom	902.64	1.27E-03	743	899	1.46E-03	H
7	Bottom	902.64	1.27E-03	743	899	1.46E-03	H
8	Bottom	883.35	1.89E-03	734	881	1.53E-03	F

Table 4-19 Bridge Damage States (HAZUS99)

Damage states		Description
N	No damage	No damage to the structure.
S	Sight/Minor damage	Minor cracking and spalling to the abutment, cracks in shear keys at abutments, minor spalling and cracks at hinges, minor spalling at the column (damage requires no more than cosmetic repair) or minor cracking to the deck.
M	Moderate damage	Any column experiencing moderate (shear cracks) cracking and spalling (column structurally still sound), moderate movement of the abutment (<2"), extensive cracking and spalling of shear keys, any connection having cracked shear keys or bent bolts, keeper bar failure without unseating, rocker bearing failure or moderate settlement of the approach.
E	Extensive damage	Any column degrading without collapse – shear failure – (column structurally unsafe), significant residual movement at connections, or major settlement approach, vertical offset of the abutment, differential settlement at connections, shear key failure at abutments.
C	Complete damage	Any column collapsing and connection losing all bearing support, which may lead to imminent deck collapse, tilting of substructure due to foundation failure.

Table 4-20 Bridge Damage States Measured by Displacement Ductility Ratios

Damage states		Criteria
N	No damage	$\mu_{cy1} > \mu_d$
S	Slight/Minor damage	$\mu_{cy} > \mu_d > \mu_{cy1}$
M	Moderate damage	$\mu_{c2} > \mu_d > \mu_{cy}$
E	Extensive damage	$\mu_{c\max} > \mu_d > \mu_{c2}$
C	Complete damage	$\mu_d > \mu_{c\max}$

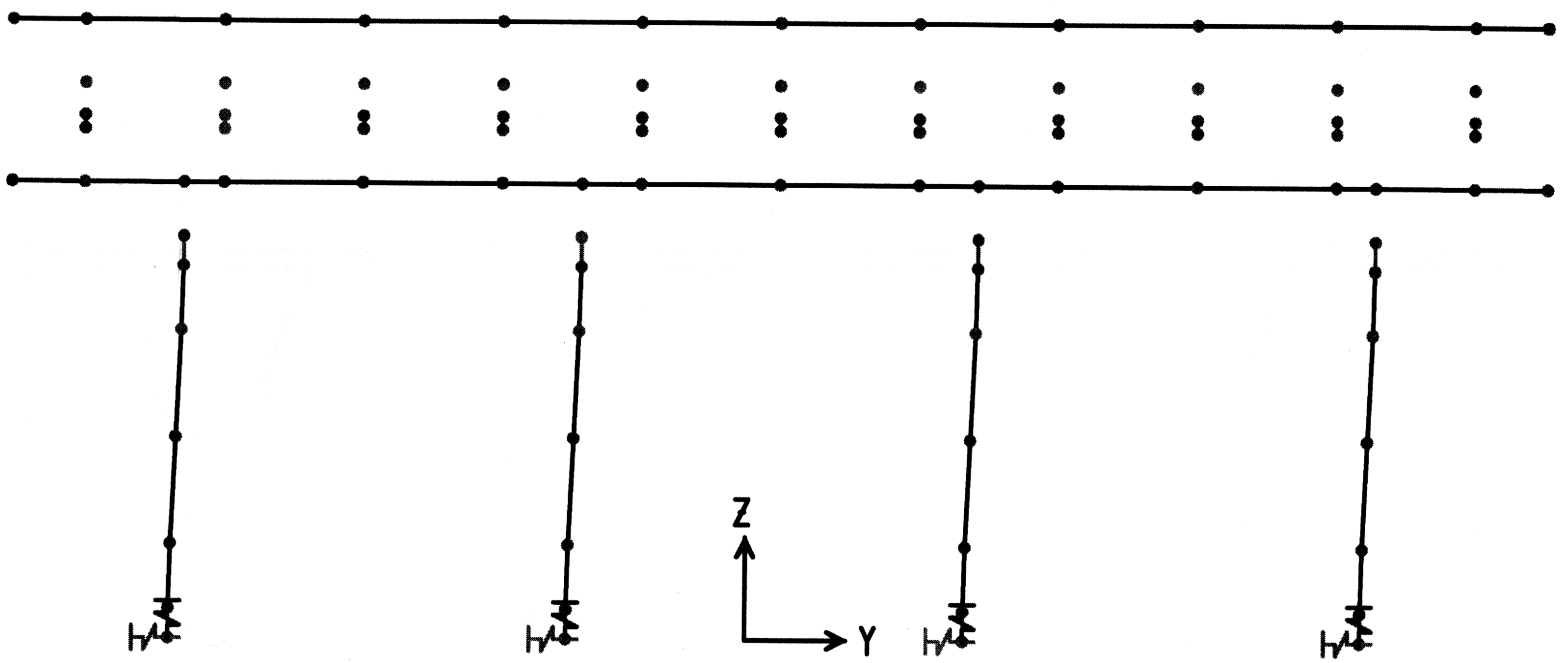

Figure 4-1 Fundamental Mode of the Bridge in the Transverse Direction

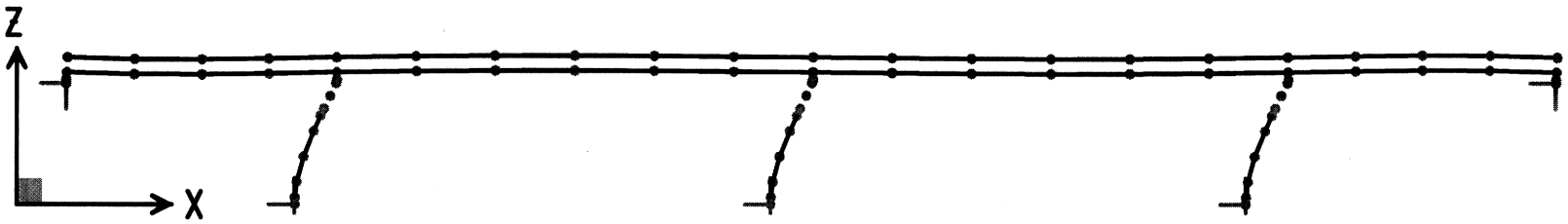

Figure 4-2 Fundamental Mode of the Bridge in the Longitudinal Direction

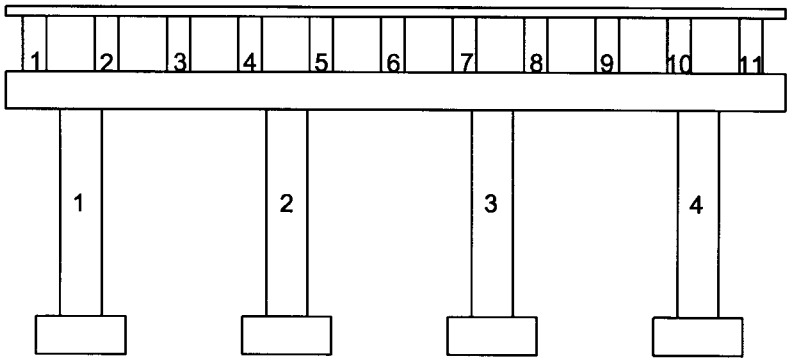

Bent 2

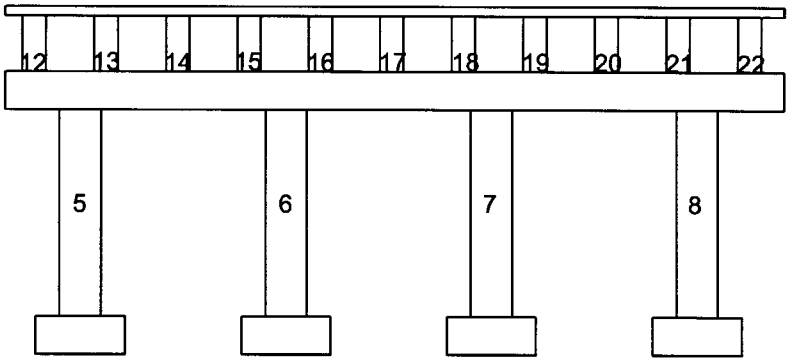

Bent 3

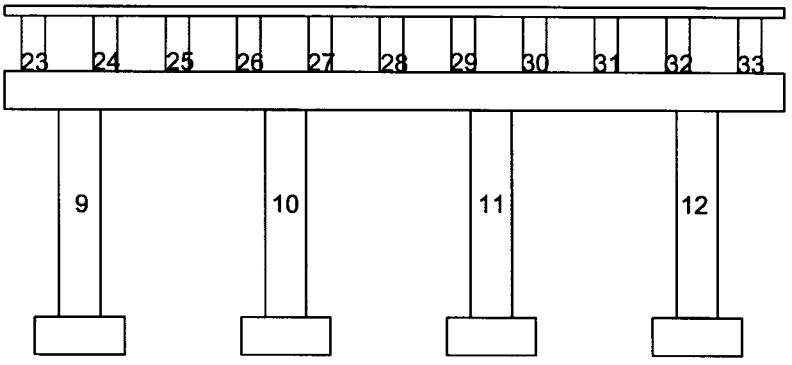

Bent 4

Figure 4-3 Column Numbers and Bearing Numbers

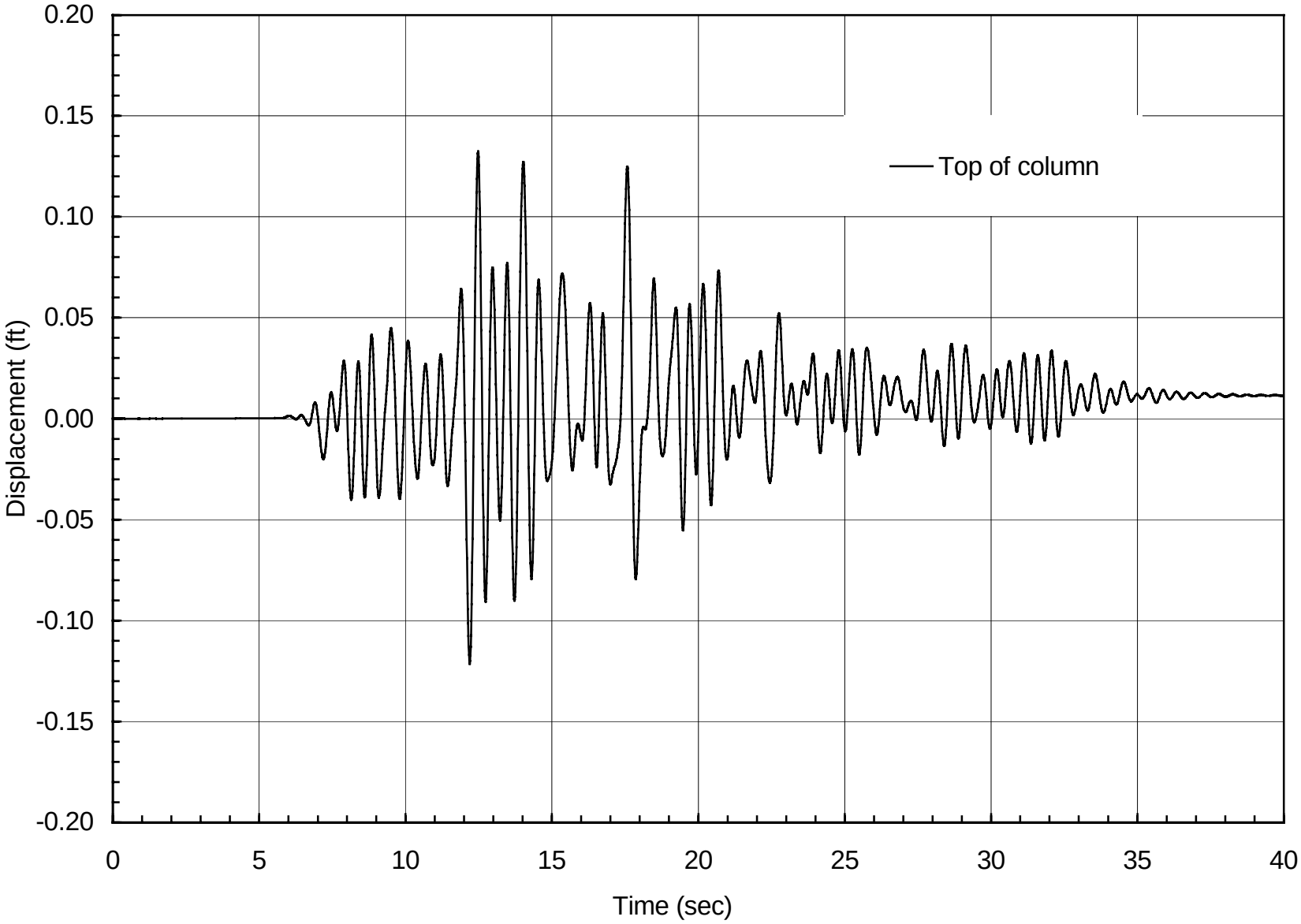

Figure 4-4 Displacement Time History at the Top of Column 5

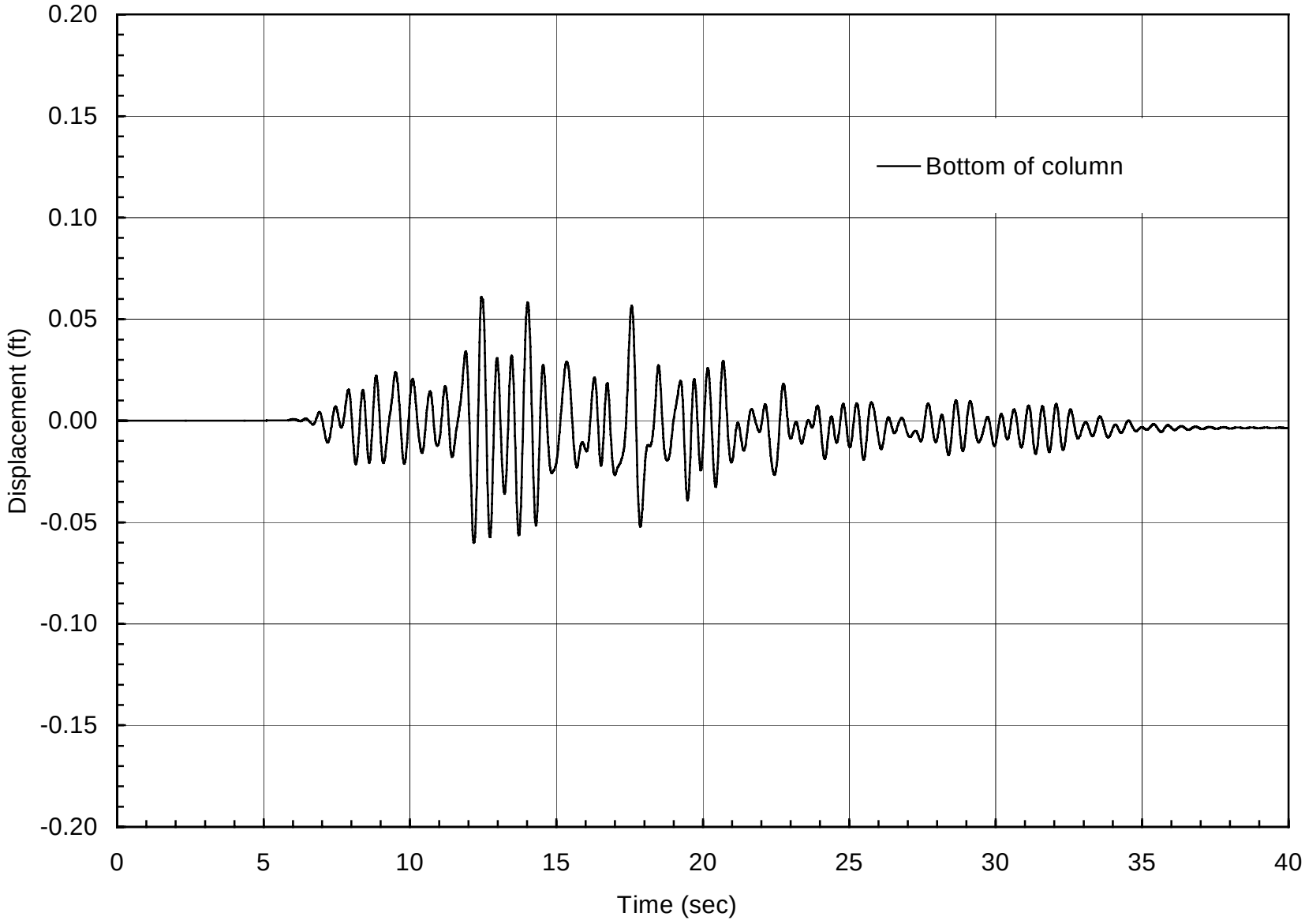

Figure 4-5 Displacement Time History at the Bottom of Column 5

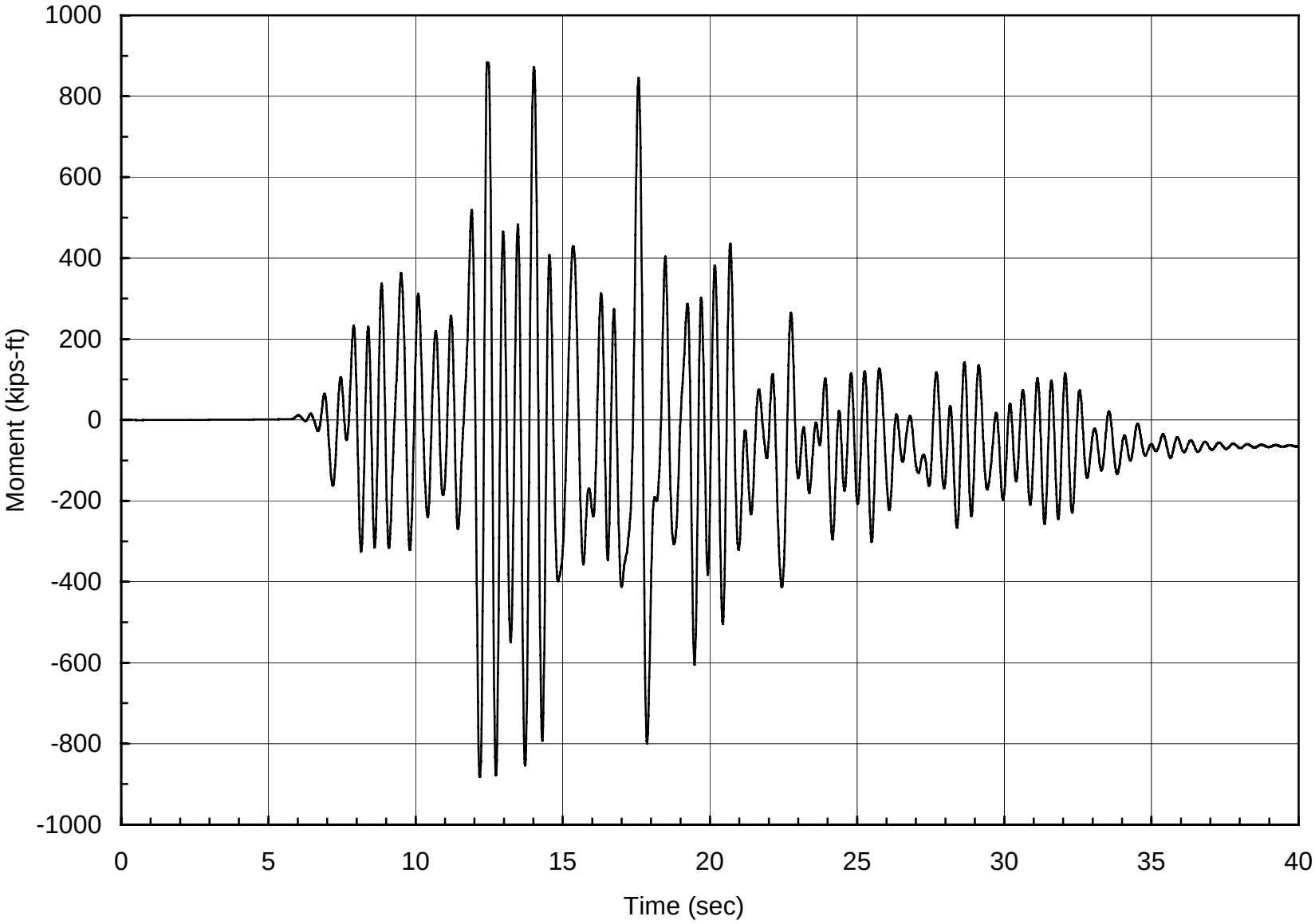

Figure 4-6 Moment Time History at the Bottom of Colume 5

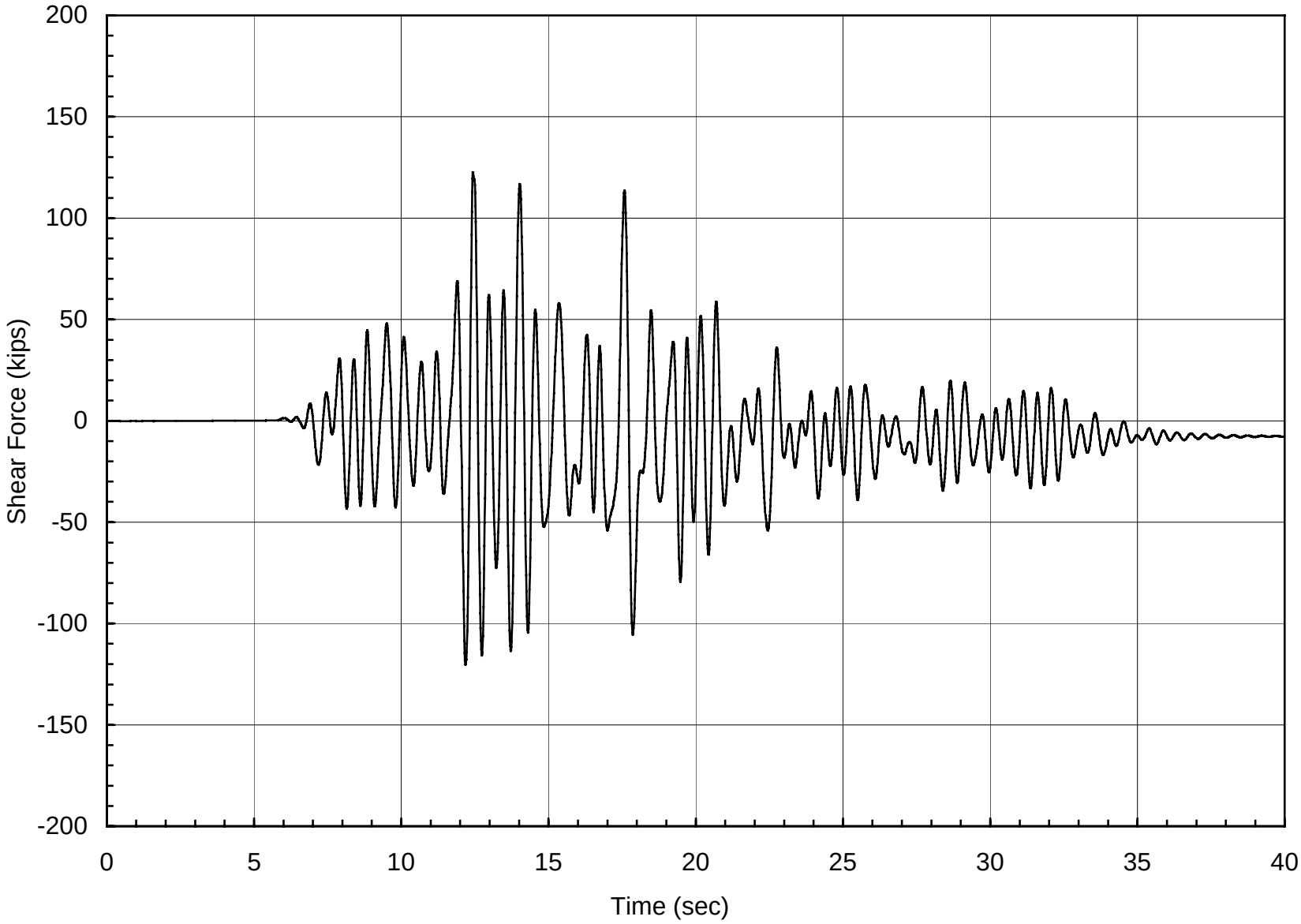

Figure 4-7 Shear Force Time History at the Bottom of Colume 5

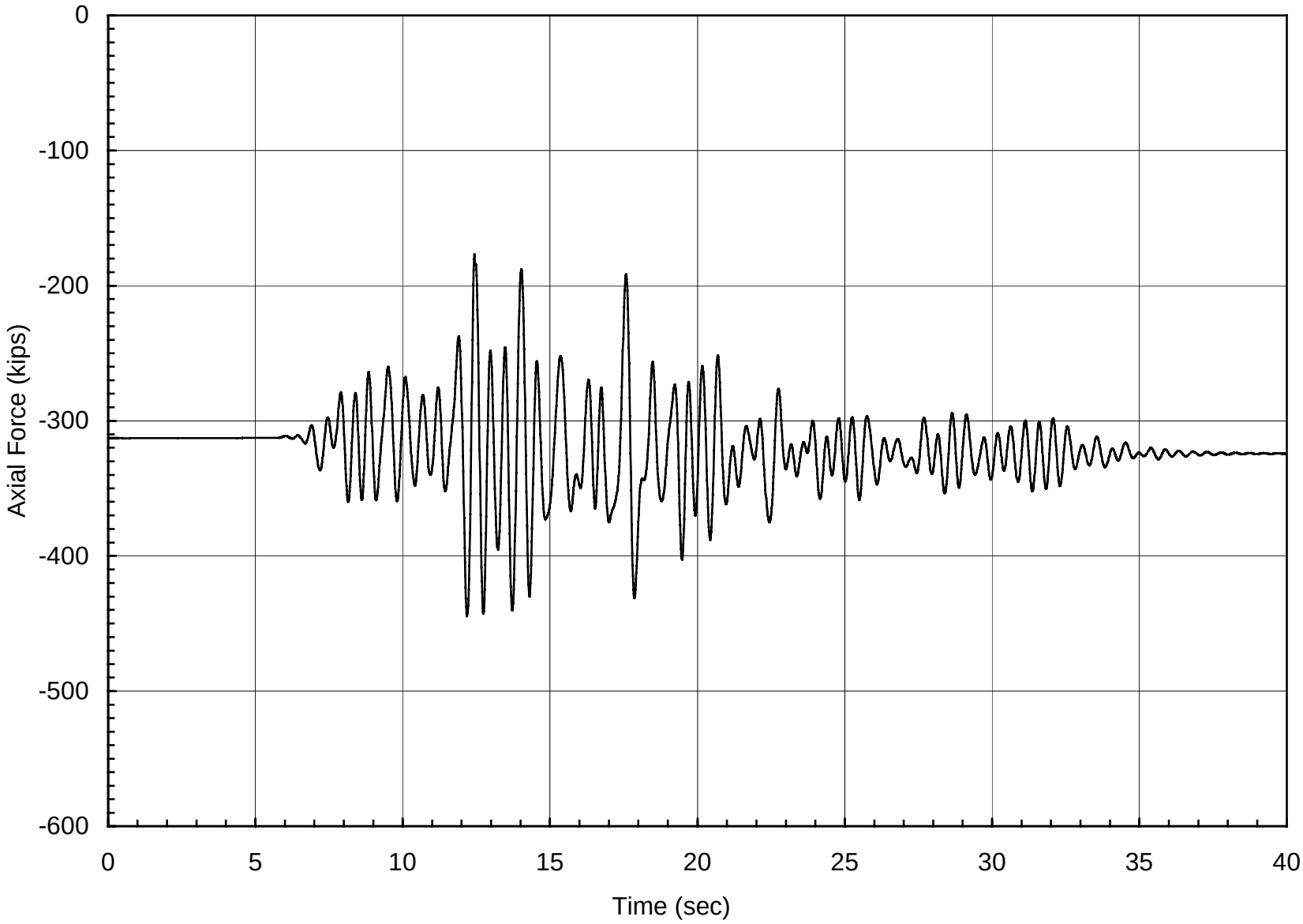

Figure 4-8 Axial Force Time History at the Bottom of Colume 5

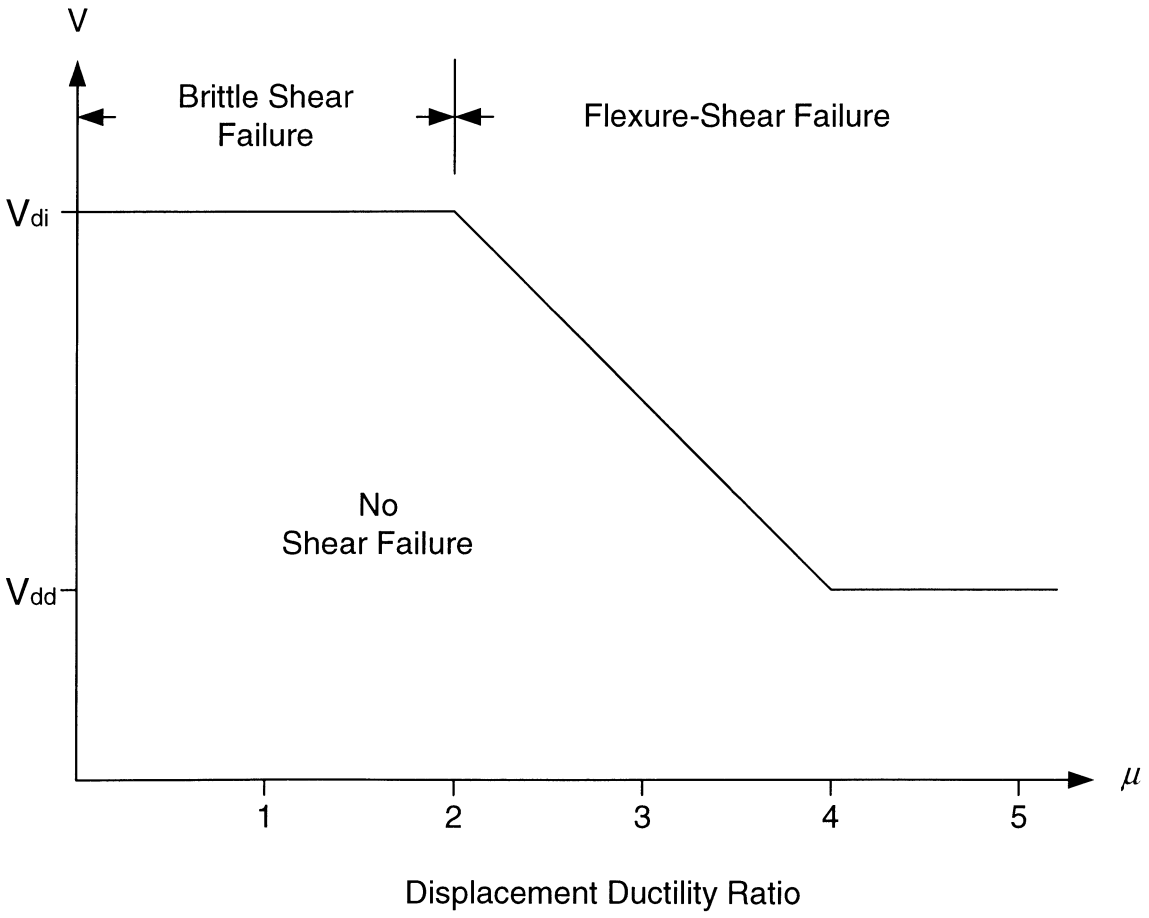

Figure 4-9 Relationship Between Displacement Ductility Ratio and Column Shear Strength

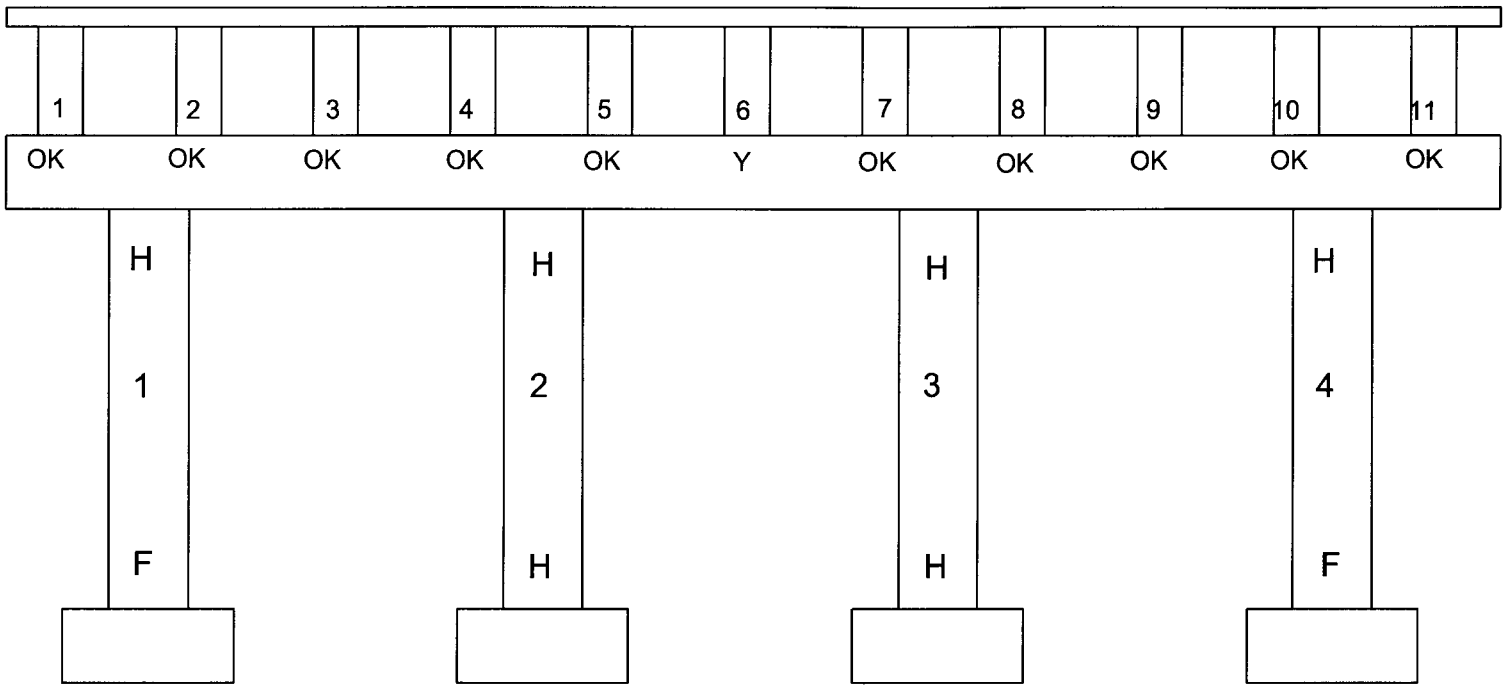

Figure 4-10 Damage Pattern of Bent 2

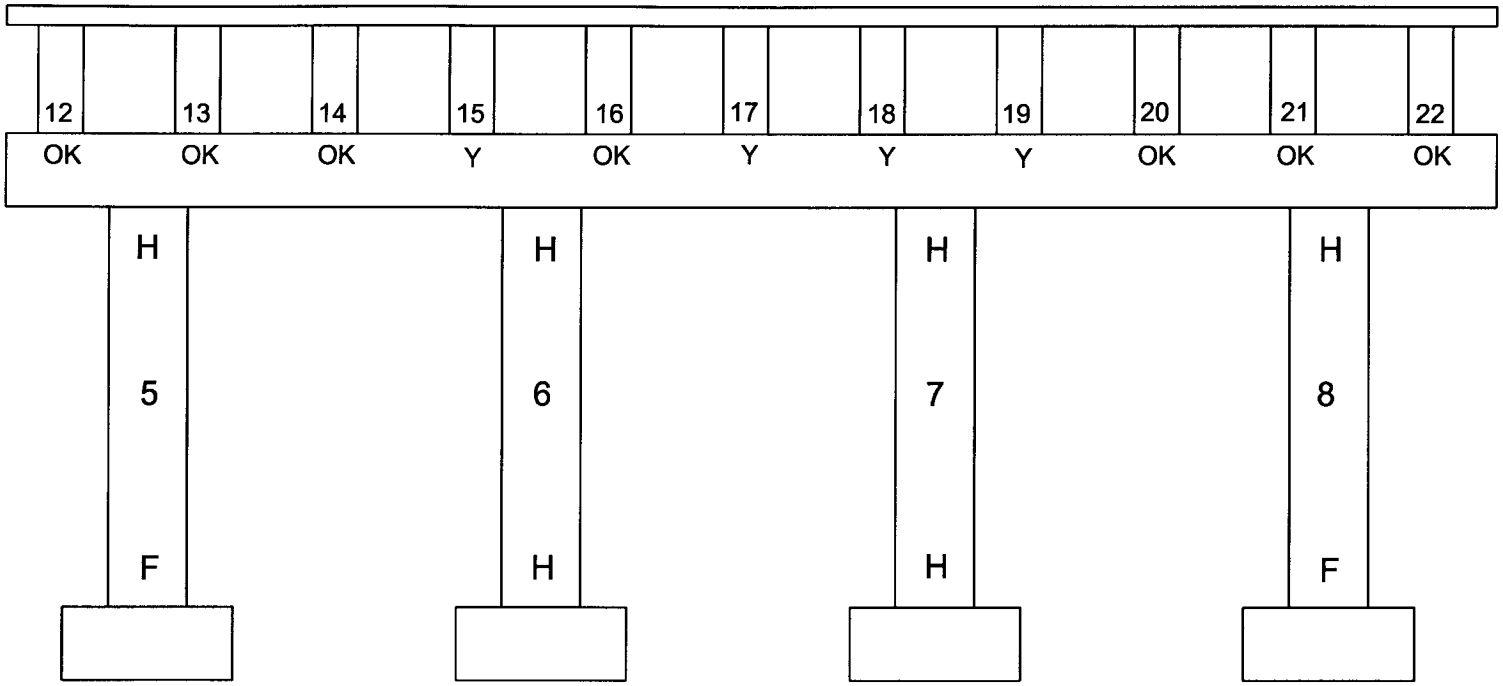

Figure 4-11 Damage Pattern of Bent 3

SECTION 5
UNCERTAINTIES IN THE EARTHQUAKE-SITE-BRIDGE SYSTEM

The uncertainties in parameters used in modeling earthquake, site condition, and bridge are considered in this section.

5.1 Uncertainty in Earthquake Modeling

In the generation of earthquake ground motion at the rock outcrop, uncertainties in earthquake source, seismic wave propagation, and rock condition near the ground surface are considered. The seismic parameters, such as the stress parameter $\Delta\sigma$, quality factor Q, and the attenuation parameter κ have significant effects on the resulting ground motion. From a literature review (*Guidelines*, 1993; Hwang and Huo, 1994), the random seismic parameters are identified and shown in Table 5-1. These parameters are considered to follow a uniform distribution. In Table 5-1, the parameter ϕ is the random phase angle, which is used to generate a time series of random band-limited white Gaussian noise. The time at which the peak of the acceleration occurs is also considered as a random variable. It is noted that the strong motion duration T_e is determined from the stress parameter and other seismic parameters; thus, the duration of ground motion will vary as different values are assigned to these seismic parameters.

For each random seismic parameter listed in Table 5-1, 100 samples are generated according to its distribution function. The exceptions are the two parameters defining the quality factors. For these two parameters, only 10 samples are established as shown in Table 5-2. These samples are then combined using the Latin Hypercube sampling technique to establish 100 sets of seismic parameters as shown in Table 5-3. For each set of seismic parameters, an acceleration time history at the rock outcrop is generated using the method described in Section 3. Thus, a total of 100 acceleration time histories at the rock outcrop are generated for this study.

5.2 Uncertainties in Soil Modeling

In this study, the computer program SHAKE91 is used to perform the nonlinear site response

analysis. The input soil parameters include the low strain shear modulus, shear modulus reduction curves and damping ratio curves. The uncertainties in these soil parameters established by Hwang and Huo (1994) are utilized in this study.

The low strain shear modulus of soils is estimated using empirical formulas. For sandy soils, the low strain shear modulus is a function of the relative density D_r (Equation 3-13) and for clayey soils, the low strain shear modulus is a function of the undrained shear strength S_u (Equation 3-14). The ranges of these two soil parameters are listed in Table 5-4, and these two soil parameters are assumed to follow a uniform distribution.

Figure 5-1 shows the shear modulus reduction curves and damping ratio curves for sandy soils. For clayey soils, the shear modulus reduction curves and damping ratio curves are a function of the plasticity index PI. The shear modulus reduction curves and damping ratio curves for clays with PI = 15 and 50 are shown in Figures 5-2 and 5-3, respectively. An upper bound curve and a lower bound curve are also shown in Figures 5-1 through 5-3. The upper bound curve corresponds to the mean value plus two standard deviations, while the lower bound curve corresponds to the mean value minus two standard deviations (Hwang and Huo, 1994).

The random soil parameters are the relative density of sand D_r, undrained shear strength of clay S_u, shear modulus reduction curves, and the corresponding damping ratio curves. For each soil parameter, 10 samples are generated. For example, Figures 5-4 and 5-5 show 10 samples of shear modulus reduction curves and corresponding damping ratio curves for clays with PI = 15. These samples of soil parameters are used to construct 10 samples of the soil profile, which are denoted as soil profile 1 to soil profile 10. Each sample of soil profile is matched with 10 samples of acceleration time history at the rock outcrop to establish 100 earthquake-site samples. For each earthquake-site sample, an acceleration time history at the ground surface is generated from a nonlinear site response analysis using SHAKE91.

5.3 Uncertainty in Bridge Modeling

The bridge model includes the bridge itself and supporting springs representing pile footings and abutments. The uncertainty in modeling the bridge itself is mainly due to the uncertainties associated with construction materials, namely, concrete and reinforcement. This uncertainty affects the strength and stiffness of structural members and the nonlinear behavior of columns. The uncertainties in supporting springs are mainly from surrounding soils. This uncertainty affects the stiffness of supporting springs.

Following Hwang and Huo (1998), the concrete compressive strength with design value of 3.0 ksi is assumed to have a normal distribution with a mean strength of 4.5 ksi and a coefficient of variation (COV) of 0.2. The yield strength of grade 40 reinforcement is described by a lognormal distribution with a mean value of 48.8 ksi and a COV of 0.11. Ten samples of concrete compressive strength and steel yield strength are generated with each sample in the one-tenth of the probability distributions. These samples are combined using the Latin Hypercube sampling technique to create 10 bridge samples, numbered from bridge sample 1 to bridge sample 10 as shown in Table 5-5. For all bridge samples, the moment-curvature relations of column sections are derived using BIAX. Based on these moment-curvature relationships, the nonlinear characteristics of column sections are determined and used in the nonlinear seismic response analyses of bridges. Thus, uncertainties in nonlinear behavior of columns are included in the seismic response analysis and seismic damage assessment of bridges.

The uncertainty in modeling spring stiffness of pile footings and abutments is taken into account in this study. Spring stiffness is considered to follow a uniform distribution. The mean values are determined as described in Section 2. The coefficient of variation is taken as 30%, since the uncertainties of random soil parameters listed in Table 5-4 are in the range of 20%~33%. Ten samples of spring stiffness are generated according to the distribution and are listed in Tables 5-6 (pile footings) and 5-7 (abutments). Each sample of spring stiffness is assigned to a bridge sample.

5.4 Generation of Earthquake-Site-Bridge Samples

In this study, each bridge sample is matched with a soil profile sample, and 10 earthquake samples as illustrated in Figure 5-6. Therefore, a total of 100 earthquake-site-bridge samples as listed in Table 5-8 are established for the seismic response analysis.

Table 5-1 Uncertainties in Seismic Parameters

Parameters	Range
Moment magnitude, M	6.0 ~ 8.0
Epicentral distance, R	40 ~ 100 km
Stress parameter, $\Delta\sigma$	100 ~ 200 bars
Q_0 in quality factor $Q=Q_0 f^{\eta}$	400 ~ 1000
η in quality factor $Q=Q_0 f^{\eta}$	0.30 ~ 0.40
Kappa, κ	0.006 ~ 0.01 sec
Focal depth, H	6 ~ 15 km
Peak parameter, τ_p	0.15 ~ 0.3
Phase angle, ϕ	0 ~ 2π

Table 5-2 Ten Samples of Quality Factor Parameters

Sample	Q_0	η
1	1000	0.30
2	930	0.31
3	870	0.32
4	800	0.33
5	730	0.34
6	680	0.36
7	600	0.37
8	530	0.38
9	470	0.39
10	400	0.4

Table 5-3 Summary of Seismic Parameters

Earthquake number	M	R *(km)*	$\Delta\sigma$ (bars)	Q_o	η	H (km)	κ (sec)	τ_p
1	6.3	50	161	1000	0.30	6.6	0.0077	0.27
2	6.7	89	153	930	0.31	7.8	0.0088	0.17
3	7.7	84	124	870	0.32	6.6	0.0068	0.24
4	6.7	65	160	800	0.33	14.8	0.0068	0.17
5	7.3	55	103	730	0.34	14.8	0.0081	0.25
6	6.4	85	154	680	0.36	8.1	0.0061	0.28
7	6.2	45	103	600	0.37	12.2	0.0062	0.27
8	6.5	89	109	530	0.38	9.0	0.0087	0.19
9	6.7	81	116	470	0.39	13.7	0.0095	0.16
10	6.3	95	153	400	0.40	10.7	0.0099	0.20
11	6.4	95	198	1000	0.30	9.3	0.0098	0.24
12	7.3	75	145	930	0.31	6.1	0.0079	0.19
13	6.5	100	113	870	0.32	9.6	0.0071	0.17
14	6.1	91	144	800	0.33	11.0	0.0082	0.18
15	6.0	56	116	730	0.34	8.6	0.0070	0.30
16	7.8	99	169	680	0.36	13.2	0.0071	0.24
17	7.5	43	172	600	0.37	10.1	0.0095	0.27
18	6.1	48	163	530	0.38	11.4	0.0078	0.15
19	7.3	63	147	470	0.39	12.4	0.0098	0.28
20	6.5	66	130	400	0.40	12.6	0.0061	0.29
21	6.7	65	106	1000	0.30	11.6	0.0067	0.21
22	7.4	73	178	930	0.31	10.9	0.0069	0.26
23	6.4	50	158	870	0.32	11.0	0.0067	0.26
24	7.0	48	170	800	0.33	7.1	0.0088	0.26
25	7.9	94	153	730	0.34	7.8	0.0099	0.22
26	6.1	81	198	680	0.36	12.2	0.0091	0.16
27	6.8	96	102	600	0.37	11.5	0.0061	0.21
28	7.6	97	143	530	0.38	14.3	0.0076	0.24
29	7.9	94	131	470	0.39	14.2	0.0070	0.26
30	7.2	55	120	400	0.40	10.8	0.0092	0.30
31	7.7	72	127	1000	0.30	13.2	0.0075	0.20
32	7.3	54	165	930	0.31	8.6	0.0061	0.25
33	8.0	99	143	870	0.32	13.1	0.0079	0.23
34	6.9	94	197	800	0.33	8.7	0.0067	0.27
35	6.6	90	183	730	0.34	13.1	0.0093	0.29
36	6.7	78	141	680	0.36	6.4	0.0084	0.28
37	7.0	90	180	600	0.37	13.7	0.0094	0.22
38	6.5	42	183	530	0.38	13.1	0.0067	0.25
39	7.6	98	199	470	0.39	8.6	0.0072	0.25
40	7.5	89	122	400	0.40	12.7	0.0084	0.21
41	7.2	70	136	1000	0.30	12.6	0.0097	0.16
42	7.2	92	179	930	0.31	8.2	0.0091	0.23
43	7.8	95	151	870	0.32	12.2	0.0089	0.19
44	8.0	48	164	800	0.33	14.8	0.0089	0.25
45	7.4	46	150	730	0.34	10.8	0.0093	0.25
46	7.2	55	109	680	0.36	7.7	0.0074	0.23
47	6.3	82	146	600	0.37	13.1	0.0076	0.29
48	7.9	61	176	530	0.38	9.7	0.0093	0.21
49	6.1	64	132	470	0.39	7.2	0.0074	0.16
50	7.3	48	186	400	0.40	7.1	0.0074	0.28

Table 5-3 Summary of Seismic Parameters (Continued)

Earthquake number	M	R *(km)*	$\Delta\sigma$ (bars)	Q_o	η	H (km)	κ (sec)	τ_p
51	6.3	79	170	1000	0.30	9.0	0.0081	0.23
52	7.6	64	120	930	0.31	9.4	0.0066	0.24
53	6.6	64	195	870	0.32	9.9	0.0093	0.18
54	6.8	92	146	800	0.33	13.0	0.0078	0.19
55	7.5	45	160	730	0.34	7.4	0.0091	0.18
56	7.6	41	157	680	0.36	7.9	0.0079	0.15
57	6.9	75	153	600	0.37	14.8	0.0080	0.29
58	6.2	90	135	530	0.38	9.7	0.0090	0.21
59	7.4	78	191	470	0.39	9.6	0.0090	0.27
60	7.2	74	196	400	0.40	12.8	0.0066	0.21
61	6.6	88	197	1000	0.30	9.5	0.0068	0.28
62	6.6	54	153	930	0.31	12.8	0.0069	0.27
63	7.8	79	134	870	0.32	11.4	0.0091	0.17
64	7.4	72	107	800	0.33	8.0	0.0092	0.18
65	6.4	66	125	730	0.34	13.6	0.0092	0.20
66	6.7	49	174	680	0.36	7.3	0.0083	0.29
67	6.4	41	129	600	0.37	8.3	0.0085	0.28
68	6.3	85	131	530	0.38	7.1	0.0097	0.25
69	6.2	45	167	470	0.39	14.0	0.0097	0.18
70	7.8	75	142	400	0.40	8.2	0.0072	0.25
71	7.3	83	197	1000	0.30	8.9	0.0095	0.19
72	7.9	43	124	930	0.31	9.0	0.0083	0.23
73	6.8	66	116	870	0.32	12.1	0.0095	0.26
74	7.0	99	200	800	0.33	9.5	0.0070	0.19
75	6.1	59	172	730	0.34	13.1	0.0084	0.23
76	7.8	62	126	680	0.36	13.1	0.0090	0.21
77	7.3	52	157	600	0.37	14.9	0.0063	0.30
78	7.5	65	127	530	0.38	11.3	0.0076	0.21
79	6.5	86	164	470	0.39	6.5	0.0061	0.20
80	7.4	75	136	400	0.40	14.4	0.0093	0.19
81	6.0	97	174	1000	0.30	12.6	0.0079	0.29
82	6.0	89	178	930	0.31	7.8	0.0071	0.15
83	7.2	86	108	870	0.32	7.1	0.0097	0.19
84	6.9	41	112	800	0.33	12.7	0.0095	0.26
85	6.3	66	191	730	0.34	6.1	0.0084	0.20
86	6.4	79	164	680	0.36	6.7	0.0070	0.21
87	7.6	52	120	600	0.37	10.9	0.0061	0.18
88	7.0	65	163	530	0.38	10.8	0.0095	0.21
89	7.6	82	188	470	0.39	13.2	0.0078	0.20
90	6.9	55	113	400	0.40	12.9	0.0092	0.20
91	6.0	65	106	1000	0.30	13.8	0.0089	0.21
92	7.4	98	194	930	0.31	11.4	0.0061	0.27
93	6.5	60	169	870	0.32	9.9	0.0061	0.25
94	6.8	51	108	800	0.33	13.2	0.0071	0.19
95	8.0	69	163	730	0.34	12.0	0.0095	0.30
96	7.7	84	157	680	0.36	11.4	0.0084	0.21
97	7.1	45	166	600	0.37	7.9	0.0064	0.28
98	7.0	73	162	530	0.38	9.9	0.0095	0.26
99	7.1	59	110	470	0.39	11.0	0.0096	0.26
100	7.4	93	138	400	0.40	12.2	0.0090	0.22

Table 5-4 Uncertainty in Soil Parameters

Soil classification		Random variable	Range
Sand	Very loose	D_r	0.00~0.15
	Loose		0.15~0.35
	Medium dense		0.35~0.65
	Dense		0.65~0.85
	Very dense		0.85~1.00
Clay	Very soft	S_u	0.00~11.98 (kN/m^2)
	Soft		11.98~23.95 (kN/m^2)
	Medium stiff		23.95~47.90 (kN/m^2)
	Stiff		47.90~95.80 (kN/m^2)
	Very stiff		95.80~191.60 (kN/m^2)
	Hard		191.60~383.20 (kN/m^2)

Table 5-5 Material Values of Ten Bridge Samples

Bridge sample	Concrete strength and elastic module			Reinforcing steel strength	
	f_c (ksi)	f_c (ksf)	E (ksf)	f_y (ksi)	f_y (ksf)
1	3.89	560.6	512126	40.49	5830.6
2	3.57	513.7	490232	43.29	6234.2
3	4.39	631.7	543646	49.20	7084.3
4	3.02	434.8	451039	46.51	6697.1
5	4.85	697.9	571432	52.26	7525.2
6	5.11	735.4	586573	45.05	6487.4
7	4.61	664.3	557485	58.14	8372.8
8	5.43	782.3	604991	47.86	6891.1
9	5.98	861.2	634748	50.62	7289.6
10	4.15	598.1	528968	54.38	7830.8

Table 5-6 Stiffness of Pile Footings

Bridge sample	Lateral stiffness (kips/ft)	Torsion stiffness (kips/rad)
1	1344	4462
2	1472	4887
3	1600	5312
4	1728	5737
5	1856	6162
6	1984	6586
7	2112	7011
8	2240	7436
9	2368	7861
10	2496	8286

Table 5-7 Spring Stiffness of Abutments

Bridge sample	Longitudinal (kips/ft)		Transverse (kips/ft)	
	Total spring	Sub-spring	Total spring	Sub-spring
1	12628	1148	3278	298
2	13827	1257	3586	326
3	15037	1367	3894	354
4	16236	1476	4213	383
5	17435	1585	4521	411
6	18645	1695	4829	439
7	19844	1804	5148	468
8	21043	1913	5456	496
9	22253	2023	5764	524
10	23452	2132	6083	553

Table 5-8 Earthquake-Site-Bridge Samples

Sample ID	Bridge	Site	Earthquake		Sample ID	Bridge	Site	Earthquake
BSE001	1	1	1		BSE051	6	6	51
BSE002	1	1	2		BSE052	6	6	52
BSE003	1	1	3		BSE053	6	6	53
BSE004	1	1	4		BSE054	6	6	54
BSE005	1	1	5		BSE055	6	6	55
BSE006	1	1	6		BSE056	6	6	56
BSE007	1	1	7		BSE057	6	6	57
BSE008	1	1	8		BSE058	6	6	58
BSE009	1	1	9		BSE059	6	6	59
BSE010	1	1	10		BSE060	6	6	60
BSE011	2	2	11		BSE061	7	7	61
BSE012	2	2	12		BSE062	7	7	62
BSE013	2	2	13		BSE063	7	7	63
BSE014	2	2	14		BSE064	7	7	64
BSE015	2	2	15		BSE065	7	7	65
BSE016	2	2	16		BSE066	7	7	66
BSE017	2	2	17		BSE067	7	7	67
BSE018	2	2	18		BSE068	7	7	68
BSE019	2	2	19		BSE069	7	7	69
BSE020	2	2	20		BSE070	7	7	70
BSE021	3	3	21		BSE071	8	8	71
BSE022	3	3	22		BSE072	8	8	72
BSE023	3	3	23		BSE073	8	8	73
BSE024	3	3	24		BSE074	8	8	74
BSE025	3	3	25		BSE075	8	8	75
BSE026	3	3	26		BSE076	8	8	76
BSE027	3	3	27		BSE077	8	8	77
BSE028	3	3	28		BSE078	8	8	78
BSE029	3	3	29		BSE079	8	8	79
BSE030	3	3	30		BSE080	8	8	80
BSE031	4	4	31		BSE081	9	9	81
BSE032	4	4	32		BSE082	9	9	82
BSE033	4	4	33		BSE083	9	9	83
BSE034	4	4	34		BSE084	9	9	84
BSE035	4	4	35		BSE085	9	9	85
BSE036	4	4	36		BSE086	9	9	86
BSE037	4	4	37		BSE087	9	9	87
BSE038	4	4	38		BSE088	9	9	88
BSE039	4	4	39		BSE089	9	9	89
BSE040	4	4	40		BSE090	9	9	90
BSE041	5	5	41		BSE091	10	10	91
BSE042	5	5	42		BSE092	10	10	92
BSE043	5	5	43		BSE093	10	10	93
BSE044	5	5	44		BSE094	10	10	94
BSE045	5	5	45		BSE095	10	10	95
BSE046	5	5	46		BSE096	10	10	96
BSE047	5	5	47		BSE097	10	10	97
BSE048	5	5	48		BSE098	10	10	98
BSE049	5	5	49		BSE099	10	10	99
BSE050	5	5	50		BSE100	10	10	100

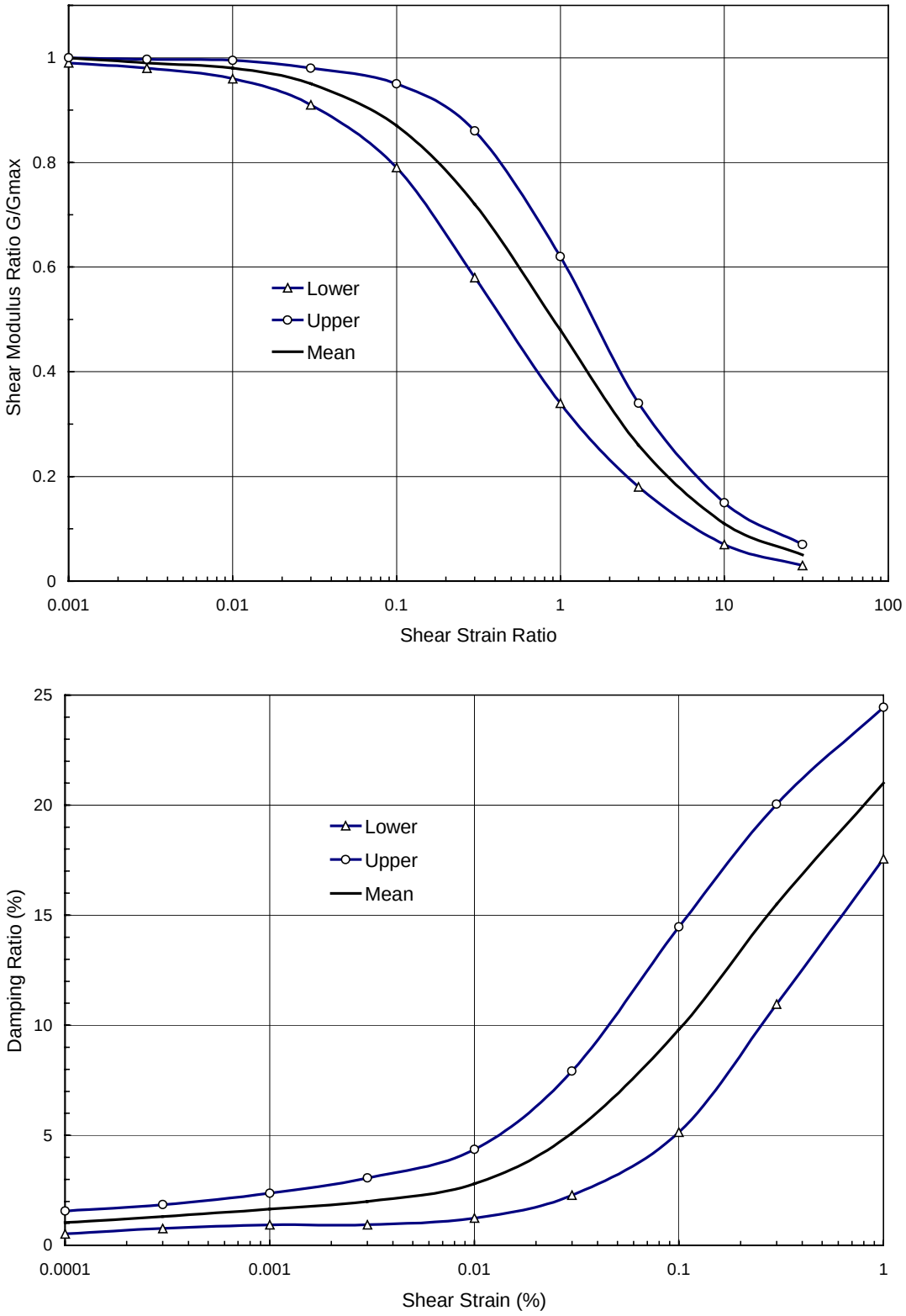

Figure 5-1 Shear Modulus Reduction and Damping Ratio Curves for Sand

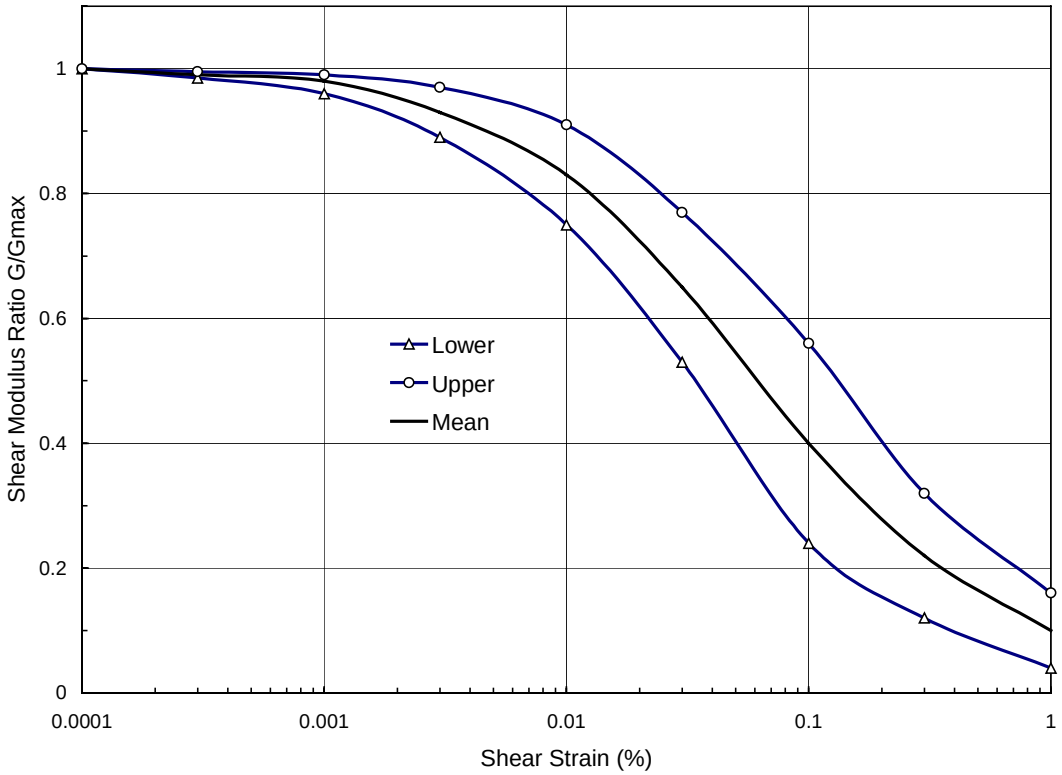

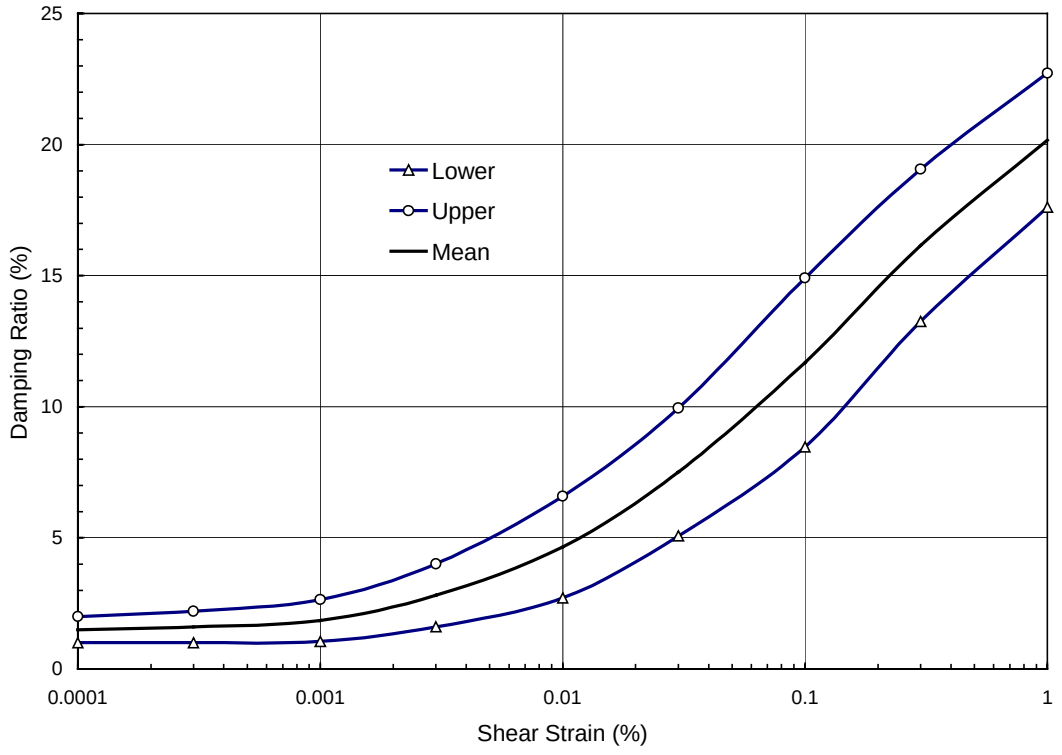

Figure 5-2 Shear Modulus Reduction and Damping Ratio Curves for Clays with PI = 15

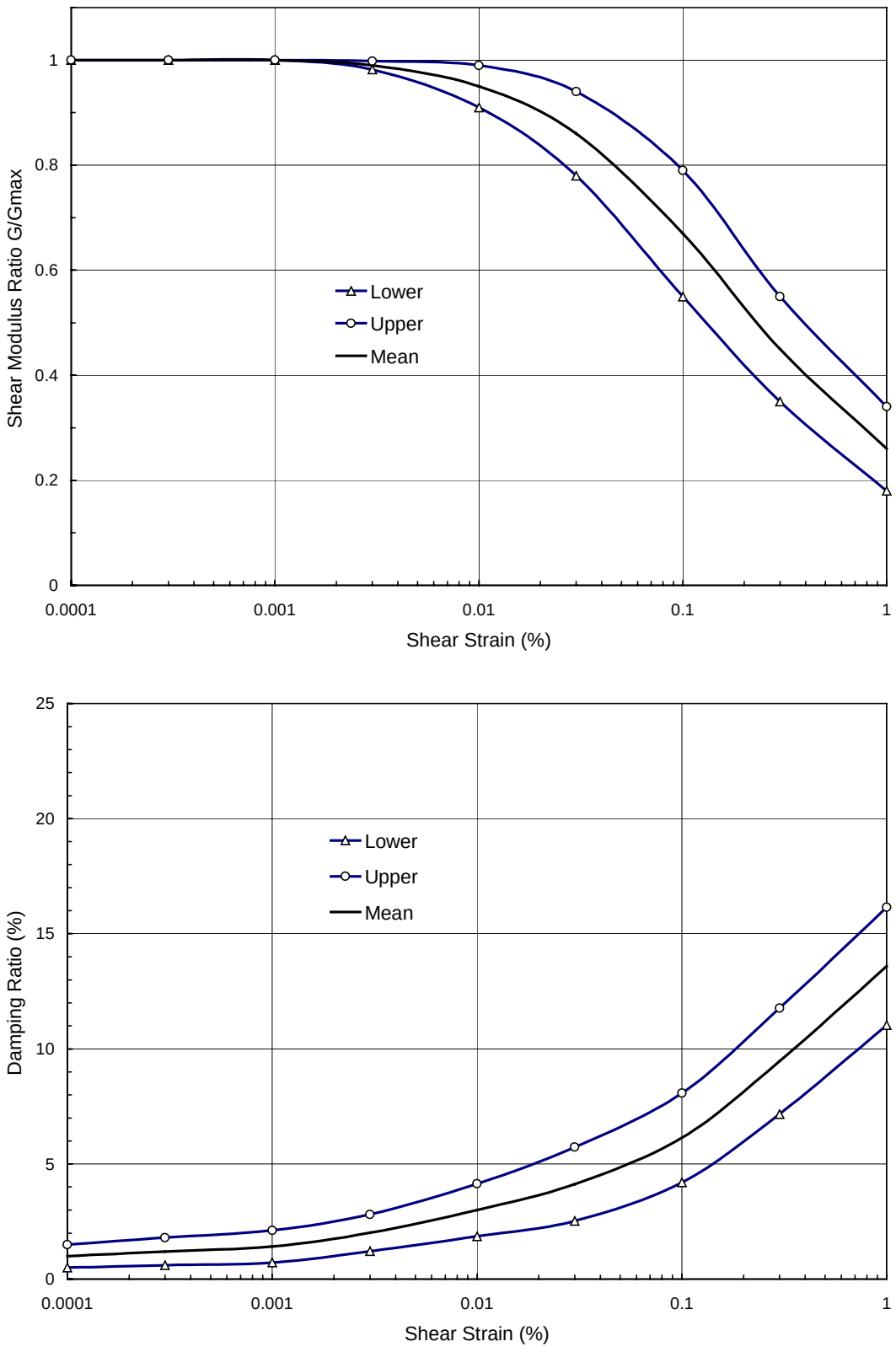

Figure 5-3 Shear Modulus Reduction and Damping Ratio Curves for Clays with PI = 50

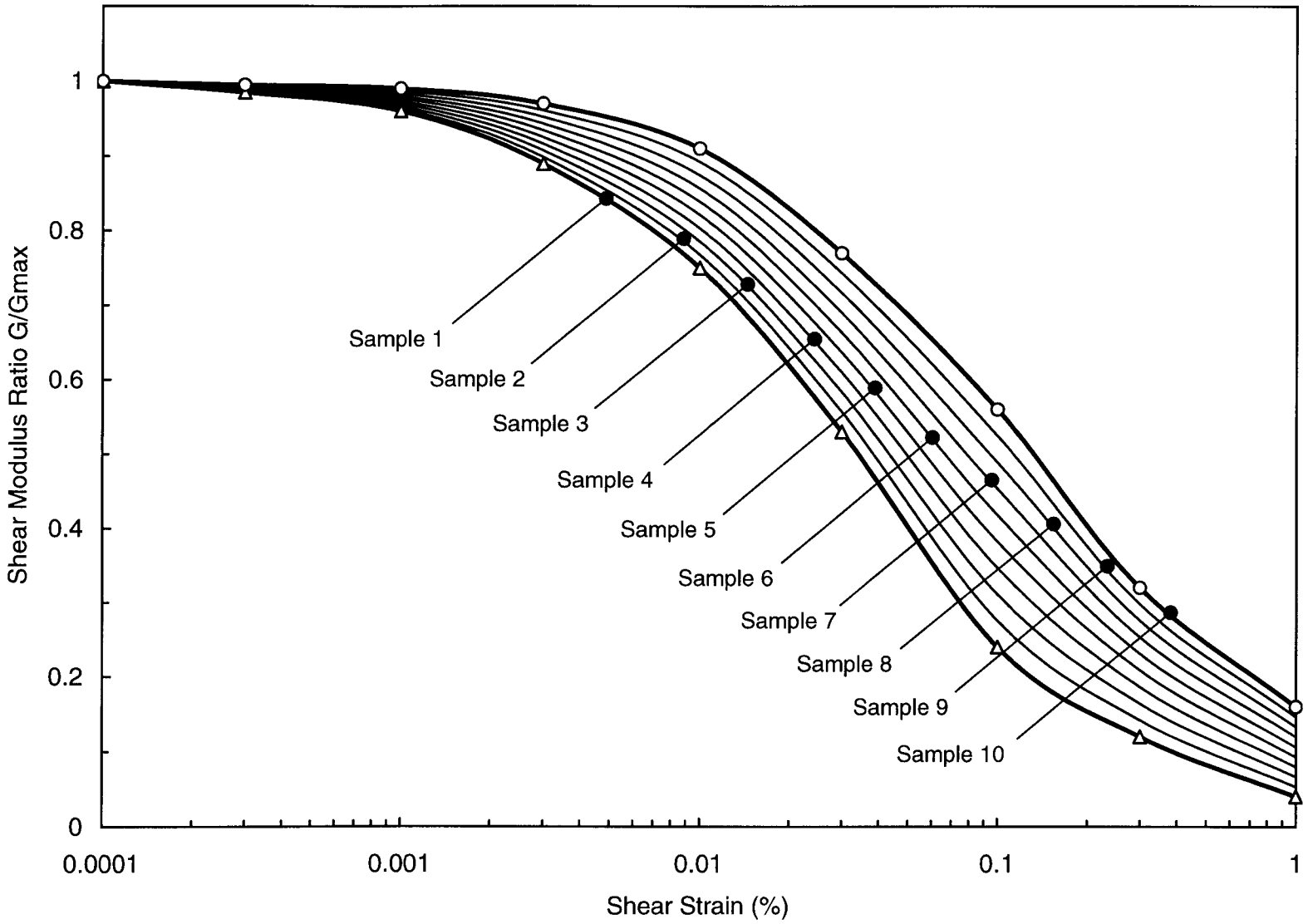

Figure 5-4 Ten Samples of Shear Modulus Reduction Ratio Curve for Clay with PI=15

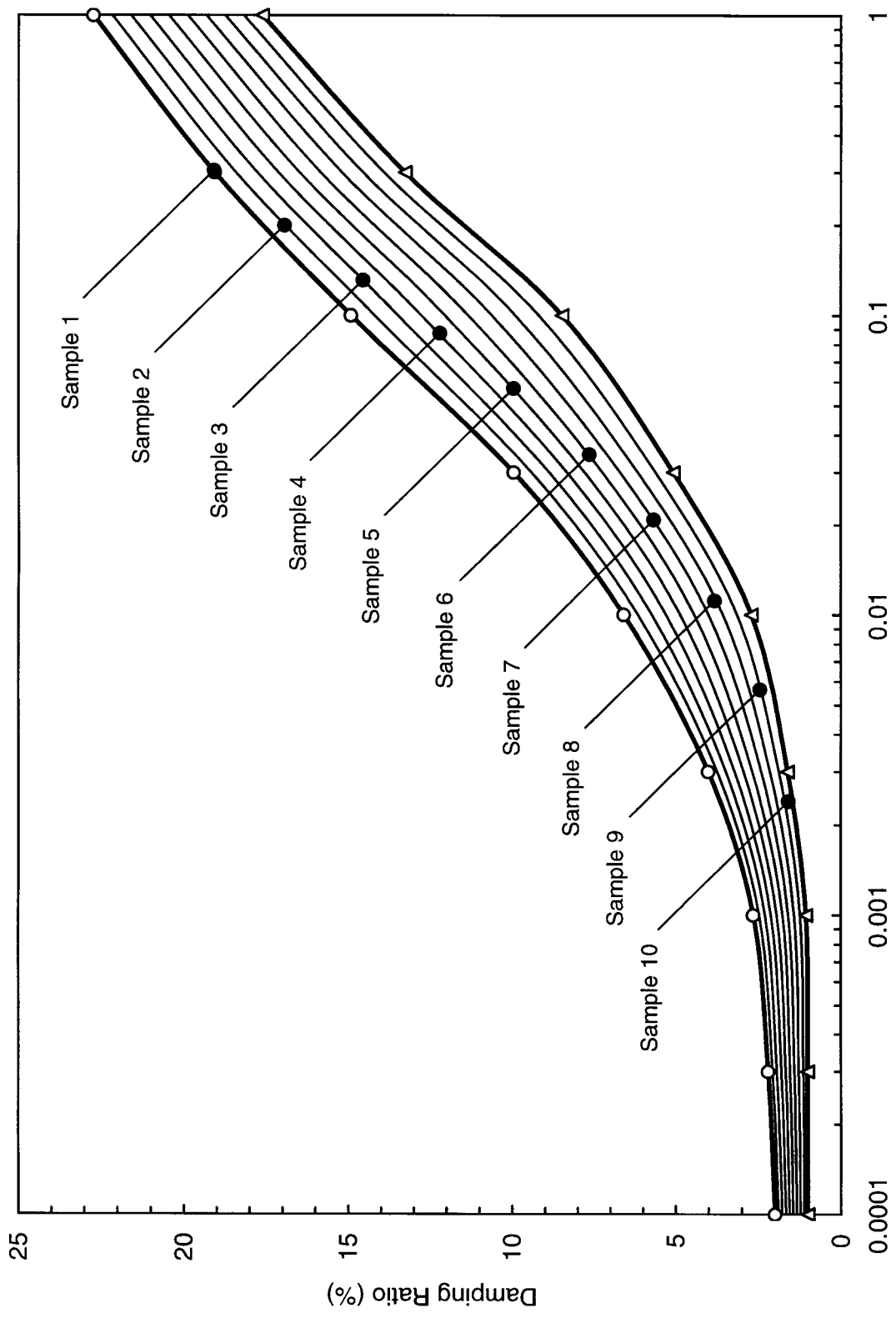

Figure 5-5 Ten Samples of Damping Ratio Curve for Clay with PI=15

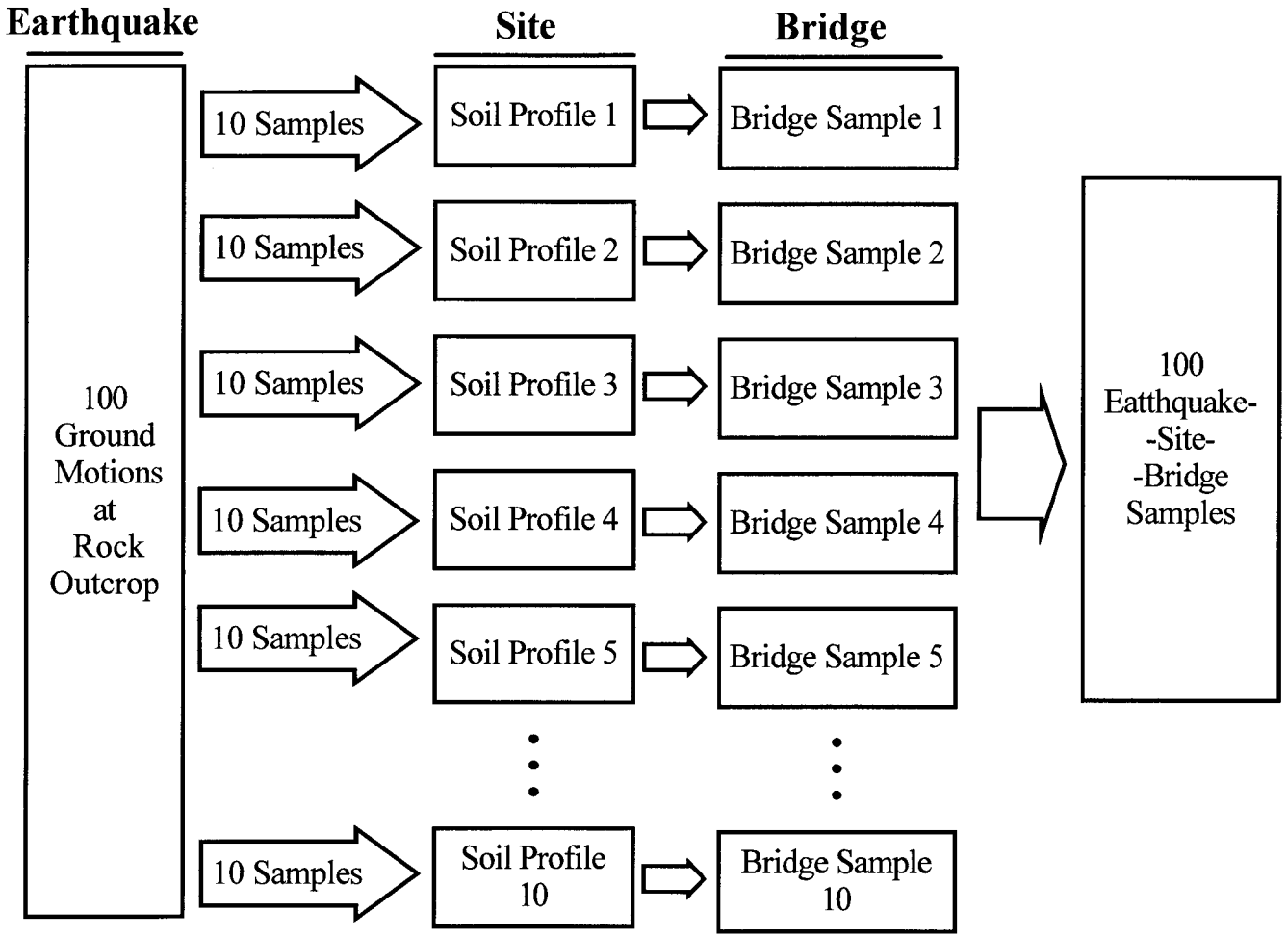

Figure 5-6 Generation of Earquake-Site- Bridge Samples

SECTION 6
PROBABILISTIC SEISMIC DEMAND

For each earthquake-site-bridge sample list in Table 5-8, a nonlinear time history analysis is carried out using the program SAP2000. The displacement ductility ratios of column 5 are computed as shown in Table 6-1. It is noted that SA and PGA of each input ground motion are also listed in the table.

The probabilistic characteristics of structural demand are described by a lognormal distribution.

$$\mu_d = \text{Ln}(\tilde{\mu}_d, \beta_d) \tag{6-1}$$

where $\tilde{\mu}_d$ is the median value of the structural demand and β_d is the logarithmic standard deviation, which are determined from the regression analysis of the simulated response data.

The expression used in the regression analysis is

$$\text{Ln}(y) = a + b\ \text{Ln}(x) + \varepsilon \tag{6-2}$$

where y is the displacement ductility ratio, x is SA or PGA, a and b are the unknown regression coefficients, and ε is a normal random variable with a zero mean and the standard deviation σ to represent the variation of the response data.

From the regression analysis of the response data with respect to SA, the median value of the structural demand is determined as

$$\text{Ln}(\tilde{\mu}_d) = 0.99 + 1.110\ \text{Ln}(\text{SA}) \tag{6-3}$$

The standard deviation σ is determined as 0.103. This indicates the regression line fits very well with the response data as shown in Figure 6-1.

From the regression analysis of the response data versus PGA, the median value of the structural demand is determined as

$$\text{Ln}(\tilde{\mu}_d) = 2.115 + 1.326\ \text{Ln}(\text{PGA}) \qquad (6\text{-}4)$$

The standard deviation σ is 0.309. This indicates that the displacement ductility ratios are scattered when they are plotted versus PGA as shown in Figure 6-2.

Table 6-1 Summary of Structural Response to Earthquakes

Sample ID	PGA (g)	SA (g)	T_s (sec)	Displacements (ft)		Relative disp. (ft)	Displacement ductility ratio μ_d
				Top	Bottom	Top-Bottom	
BSE001	0.15	0.35	0.55	0.0884	0.0564	0.0320	0.85
BSE002	0.16	0.41	0.55	0.1031	0.0657	0.0374	1.00
BSE003	0.20	0.45	0.55	0.1146	0.0727	0.0419	1.12
BSE004	0.13	0.27	0.55	0.0680	0.0436	0.0244	0.65
BSE005	0.18	0.51	0.55	0.1303	0.0788	0.0515	1.37
BSE006	0.12	0.17	0.55	0.0441	0.0281	0.0160	0.43
BSE007	0.11	0.27	0.55	0.0680	0.0434	0.0246	0.65
BSE008	0.08	0.17	0.55	0.0428	0.0274	0.0154	0.41
BSE009	0.10	0.14	0.55	0.0351	0.0224	0.0127	0.34
BSE010	0.07	0.13	0.55	0.0330	0.0210	0.0120	0.32
BSE011	0.16	0.18	0.53	0.0432	0.0266	0.0166	0.44
BSE012	0.20	0.38	0.53	0.0886	0.0548	0.0338	0.90
BSE013	0.10	0.21	0.53	0.0487	0.0300	0.0187	0.50
BSE014	0.09	0.18	0.53	0.0429	0.0264	0.0165	0.44
BSE015	0.09	0.15	0.53	0.0363	0.0225	0.0138	0.37
BSE016	0.28	0.68	0.53	0.1710	0.0759	0.0951	2.53
BSE017	0.33	0.91	0.53	0.2046	0.0782	0.1264	3.36
BSE018	0.15	0.24	0.53	0.0579	0.0357	0.0222	0.59
BSE019	0.19	0.39	0.53	0.0915	0.0565	0.0350	0.93
BSE020	0.10	0.16	0.53	0.0378	0.0232	0.0146	0.39
BSE021	0.16	0.23	0.51	0.0517	0.0315	0.0202	0.54
BSE022	0.23	0.73	0.51	0.1463	0.0776	0.0687	1.83
BSE023	0.18	0.41	0.51	0.0893	0.0543	0.0350	0.93
BSE024	0.25	0.71	0.51	0.1599	0.0777	0.0822	2.19
BSE025	0.29	0.78	0.51	0.1554	0.0775	0.0779	2.07
BSE026	0.09	0.23	0.51	0.0509	0.0310	0.0199	0.53
BSE027	0.10	0.19	0.51	0.0409	0.0249	0.0160	0.43
BSE028	0.18	0.48	0.51	0.1053	0.0639	0.0414	1.10
BSE029	0.28	0.73	0.51	0.1631	0.0769	0.0862	2.29
BSE030	0.22	0.40	0.51	0.0875	0.0533	0.0342	0.91
BSE031	0.24	0.48	0.51	0.1034	0.0583	0.0451	1.20
BSE032	0.32	0.65	0.51	0.1311	0.0641	0.0670	1.78
BSE033	0.28	0.89	0.51	0.1605	0.0664	0.0941	2.50
BSE034	0.23	0.26	0.51	0.0558	0.0320	0.0238	0.63
BSE035	0.14	0.29	0.51	0.0617	0.0352	0.0265	0.71
BSE036	0.12	0.29	0.51	0.0621	0.0354	0.0267	0.71
BSE037	0.17	0.35	0.51	0.0747	0.0426	0.0321	0.85
BSE038	0.25	0.37	0.51	0.0782	0.0446	0.0336	0.89
BSE039	0.28	0.45	0.51	0.0946	0.0540	0.0406	1.08

Table 6-1 Summary of Structural Response to Earthquakes (Continued)

Sample ID	PGA (g)	SA (g)	T_s (sec)	Displacements (ft)		Relative disp. (ft)	Displacement ductility ratio μ_d
				Top	Bottom	Top-Bottom	
BSE040	0.17	0.35	0.51	0.0735	0.0421	0.0314	0.84
BSE041	0.25	0.36	0.49	0.0714	0.0411	0.0303	0.81
BSE042	0.21	0.45	0.49	0.0888	0.0511	0.0377	1.00
BSE043	0.28	0.83	0.49	0.1594	0.0707	0.0887	2.36
BSE044	0.45	1.05	0.49	0.1996	0.0726	0.1270	3.38
BSE045	0.33	0.88	0.49	0.1687	0.0714	0.0973	2.59
BSE046	0.21	0.39	0.49	0.0763	0.0439	0.0324	0.86
BSE047	0.09	0.23	0.49	0.0457	0.0262	0.0195	0.52
BSE048	0.33	0.73	0.49	0.1549	0.0694	0.0855	2.28
BSE049	0.10	0.13	0.49	0.0257	0.0147	0.0110	0.29
BSE050	0.34	0.78	0.49	0.1577	0.0706	0.0871	2.32
BSE051	0.12	0.18	0.48	0.0349	0.0192	0.0157	0.42
BSE052	0.30	0.52	0.48	0.0983	0.0540	0.0443	1.18
BSE053	0.22	0.35	0.48	0.0664	0.0366	0.0298	0.79
BSE054	0.17	0.44	0.48	0.0847	0.0468	0.0379	1.01
BSE055	0.45	1.16	0.48	0.2265	0.0652	0.1613	4.29
BSE056	0.41	0.99	0.48	0.1605	0.0623	0.0982	2.61
BSE057	0.17	0.46	0.48	0.0873	0.0482	0.0391	1.04
BSE058	0.08	0.14	0.48	0.0260	0.0144	0.0116	0.31
BSE059	0.28	0.65	0.48	0.1224	0.0601	0.0623	1.66
BSE060	0.28	0.94	0.48	0.1509	0.0623	0.0886	2.36
BSE061	0.18	0.19	0.46	0.0340	0.0185	0.0155	0.41
BSE062	0.20	0.44	0.46	0.0790	0.0428	0.0362	0.96
BSE063	0.34	0.62	0.46	0.1121	0.0600	0.0521	1.39
BSE064	0.23	0.51	0.46	0.0927	0.0503	0.0424	1.13
BSE065	0.13	0.17	0.46	0.0300	0.0162	0.0138	0.37
BSE066	0.28	0.54	0.46	0.0988	0.0536	0.0452	1.20
BSE067	0.20	0.33	0.46	0.0582	0.0315	0.0267	0.71
BSE068	0.11	0.19	0.46	0.0337	0.0182	0.0155	0.41
BSE069	0.19	0.40	0.46	0.0724	0.0394	0.0330	0.88
BSE070	0.29	0.65	0.46	0.1173	0.0619	0.0554	1.47
BSE071	0.28	0.57	0.46	0.0996	0.0513	0.0483	1.29
BSE072	0.51	1.75	0.46	0.2428	0.0609	0.1819	4.84
BSE073	0.21	0.26	0.46	0.0457	0.0239	0.0218	0.58
BSE074	0.25	0.62	0.46	0.1086	0.0540	0.0546	1.45
BSE075	0.13	0.37	0.46	0.0646	0.0337	0.0309	0.82
BSE076	0.38	0.94	0.46	0.1426	0.0577	0.0849	2.26
BSE077	0.35	0.73	0.46	0.1296	0.0560	0.0736	1.96
BSE078	0.24	0.54	0.46	0.0942	0.0490	0.0452	1.20

Table 6-1 Summary of Structural Response to Earthquakes (Continued)

Sample ID	PGA (g)	SA (g)	T_s (sec)	Displacements (ft)		Relative disp. (ft)	Displacement ductility ratio μ_d
				Top	Bottom	Top-Bottom	
BSE079	0.14	0.34	0.46	0.0604	0.0316	0.0288	0.77
BSE080	0.21	0.57	0.46	0.0992	0.0517	0.0475	1.26
BSE081	0.10	0.22	0.45	0.0371	0.0191	0.0180	0.48
BSE082	0.15	0.21	0.45	0.0355	0.0183	0.0172	0.46
BSE083	0.22	0.39	0.45	0.0646	0.0332	0.0314	0.84
BSE084	0.32	0.64	0.45	0.1075	0.0531	0.0544	1.45
BSE085	0.16	0.24	0.45	0.0412	0.0211	0.0201	0.54
BSE086	0.13	0.20	0.45	0.0330	0.0170	0.0160	0.43
BSE087	0.41	1.03	0.45	0.1801	0.0578	0.1223	3.26
BSE088	0.24	0.45	0.45	0.0750	0.0384	0.0366	0.97
BSE089	0.33	0.84	0.45	0.1483	0.0564	0.0919	2.45
BSE090	0.20	0.48	0.45	0.0811	0.0415	0.0396	1.05
BSE091	0.11	0.09	0.44	0.0143	0.0072	0.0071	0.19
BSE092	0.34	0.76	0.44	0.1295	0.0507	0.0788	2.10
BSE093	0.21	0.30	0.44	0.0496	0.0248	0.0248	0.66
BSE094	0.27	0.43	0.44	0.0703	0.0350	0.0353	0.94
BSE095	0.39	1.13	0.44	0.1496	0.0529	0.0967	2.57
BSE096	0.37	0.75	0.44	0.1259	0.0512	0.0747	1.99
BSE097	0.47	1.02	0.44	0.1507	0.0526	0.0981	2.61
BSE098	0.28	0.43	0.44	0.0707	0.0352	0.0355	0.94
BSE099	0.24	0.45	0.44	0.0733	0.0366	0.0367	0.98
BSE100	0.21	0.42	0.44	0.0690	0.0344	0.0346	0.92

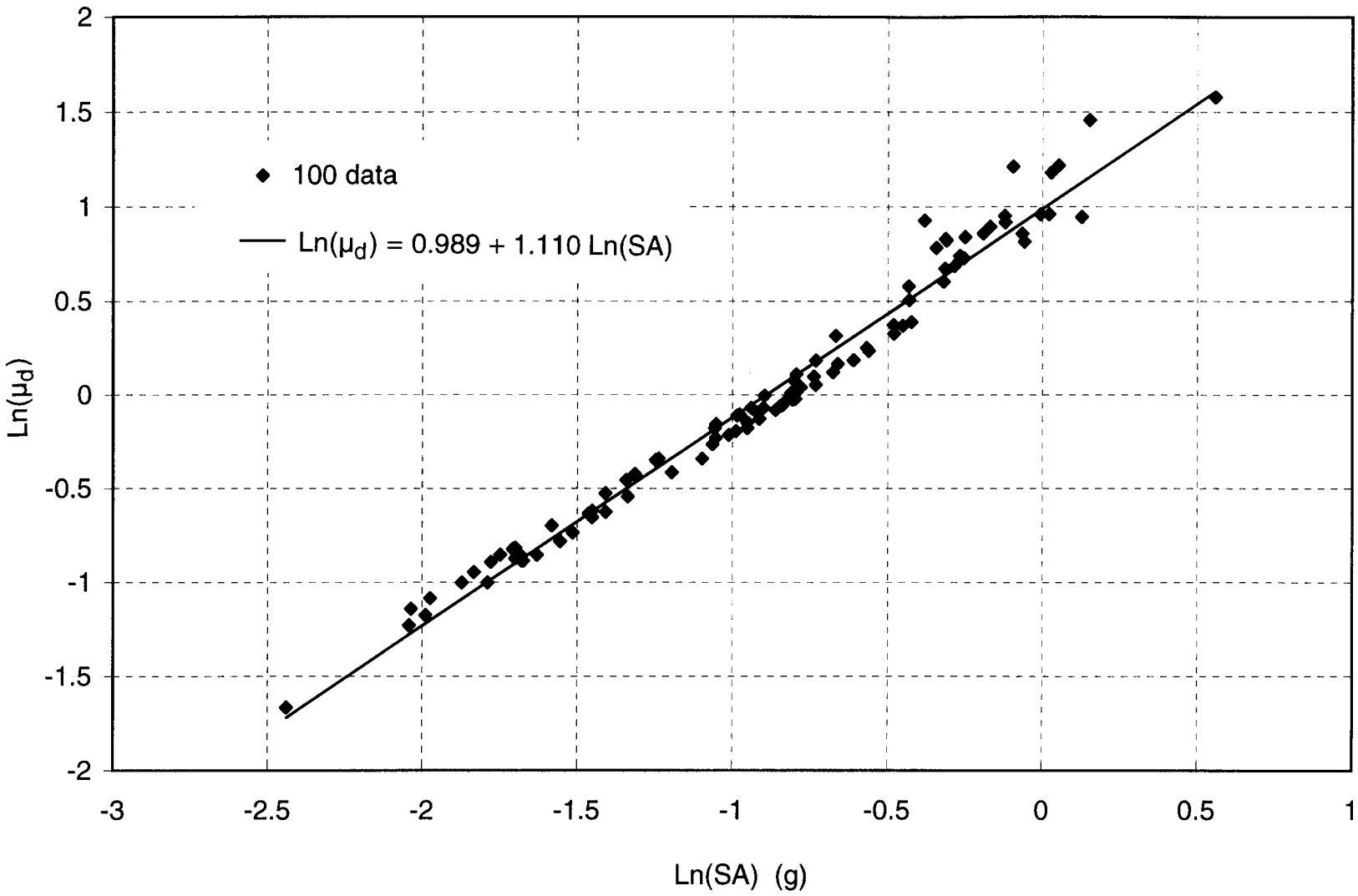

Figure 6-1 Regression Analysis of Displacement Ductility Ratio Versus Spectral Acceleration

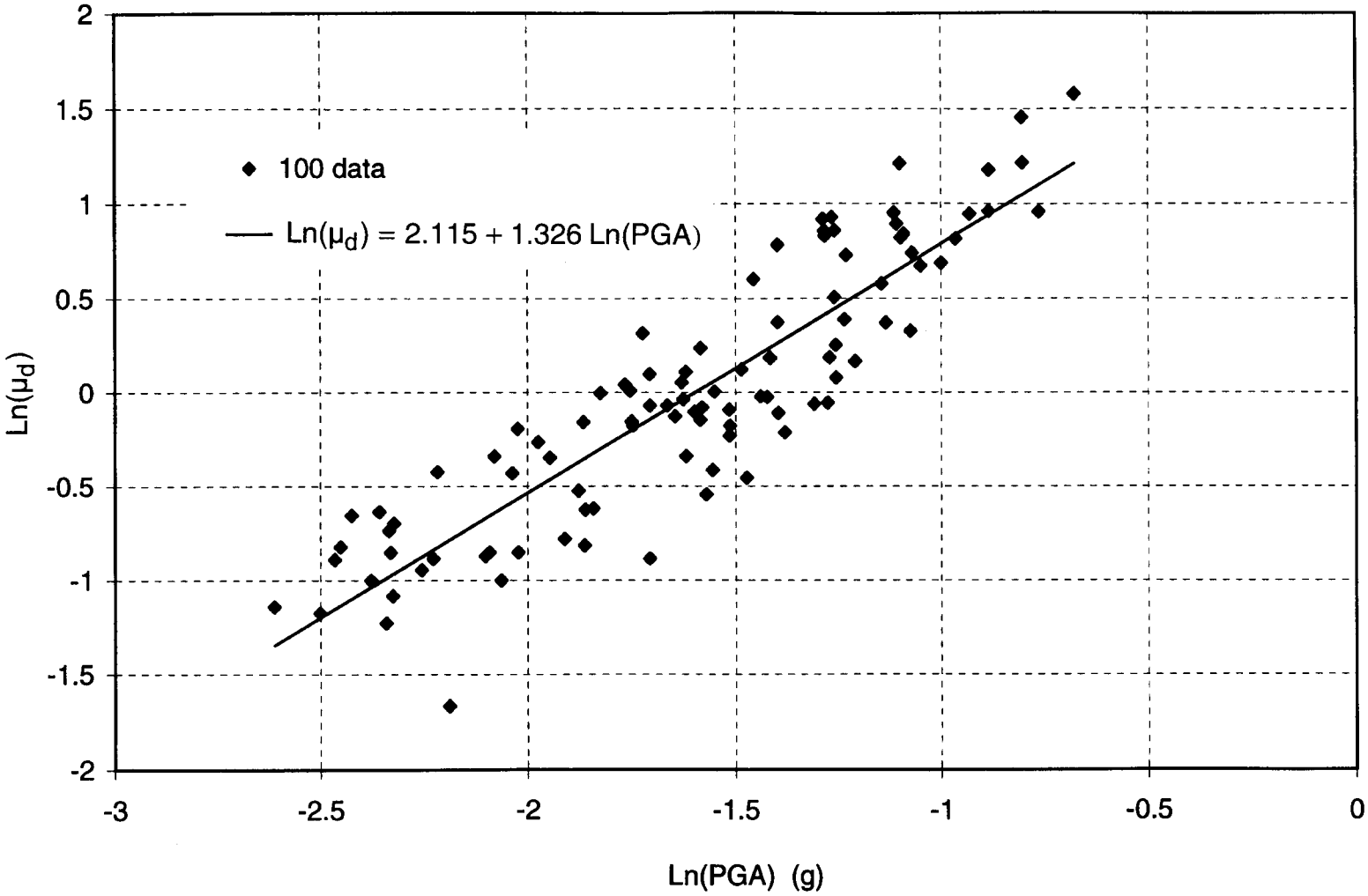

Figure 6-2 Regression Analysis of Displacement Ductility Ratio Versus Peak Ground Acceleration

SECTION 7
SEISMIC FRAGILITY ANALYSIS OF BRIDGE

The fragility curves of a bridge display the conditional probability that the structural demand (structural response) caused by various levels of ground shaking exceeds the structural capacity defined by a damage state. As shown in Table 4-19, the damage states used in this study are the five damage states for bridges defined in the HAZUS99. In this study, the five damage states are quantified in term of the relative displacement ductility ratios of bridge columns as shown in Table 4-20.

In this study, the probabilistic characteristics of structural capacity are described by a lognormal distribution.

$$\mu_c = \mathrm{Ln}(\tilde{\mu}_c, \beta_c) \tag{7-1}$$

where μ_c is the median value of structural capacity and β_c is the logarithmic standard deviation. The median values corresponding to various displacement ductility ratios are taken as those computed in Section 4 and are summarized in Table 7-1.

The probability that the structure demand μ_d exceeds the structural capacity μ_c can be computed using the following formula.

$$p'_f = P_r\left(\frac{\mu_c}{\mu_d} \le 1\right) \tag{7-2}$$

Since both μ_c and μ_d follow the lognormal distribution, the probability of exceeding a specified damage state p'_f can be determined as follows:

$$p'_f = \Phi\left[\frac{-\mathrm{Ln}(\tilde{\mu}_c / \tilde{\mu}_d)}{(\beta_c^2 + \beta_d^2)^{1/2}}\right] \tag{7-3}$$

Following the recommendations in HAZUS99, $(\beta_c^2+\beta_d^2)^{1/2}$ is taken as 0.4 when the fragility curve is expressed in terms of SA. It is taken as 0.5 when the fragility curve is expressed in terms of PGA. The fragility curves as a function of SA and PGA are shown in Figures 7-1 and 7-2, respectively.

Table 7-1 Median Structural Capacities Corresponding to Various Displacement Ductility Ratios

Displacement ductility ratio	Median value
μ_{cy1}	1.00
μ_{cy}	1.20
μ_{c2}	1.76
$\mu_{c\max}$	4.76

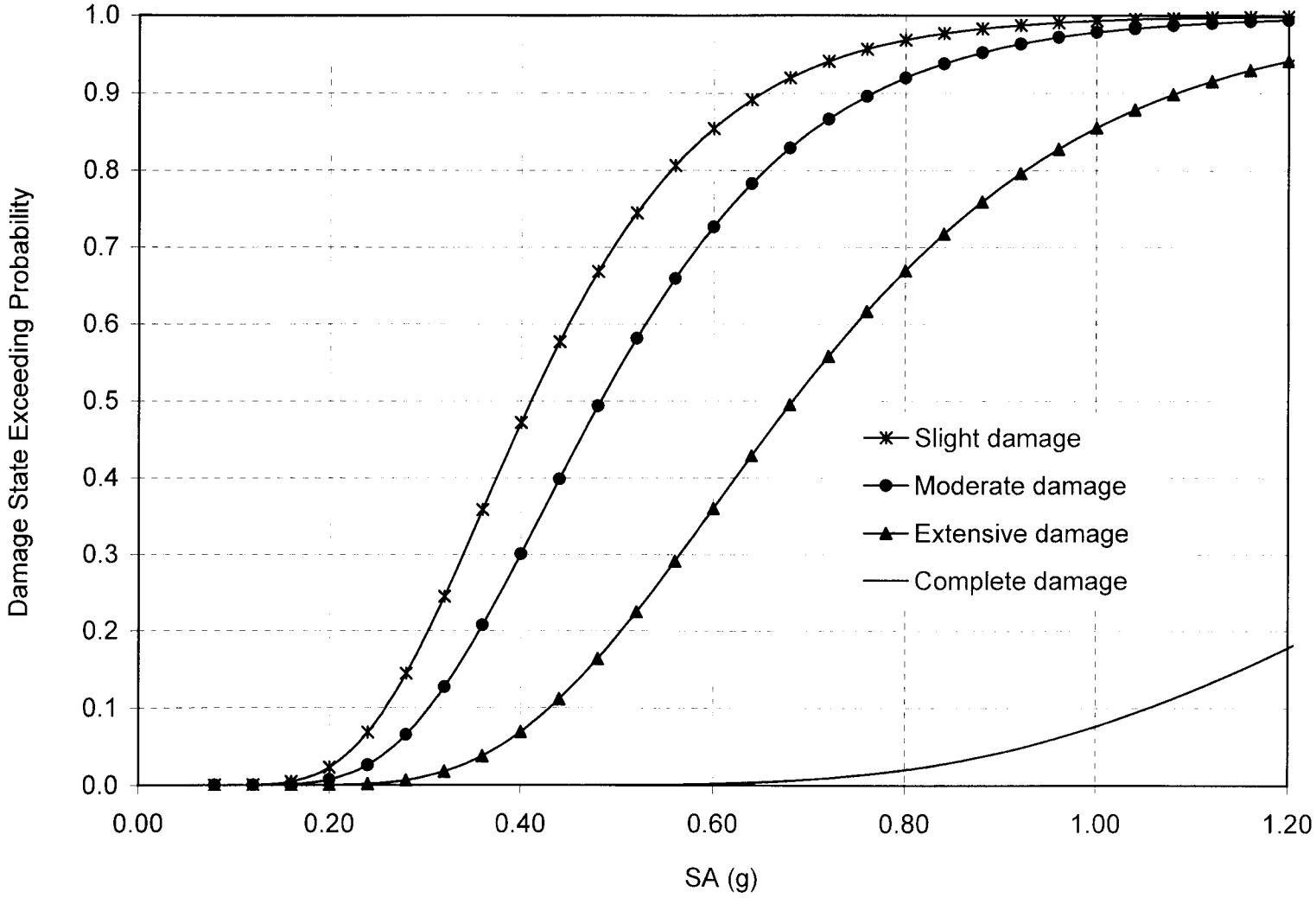

Figure 7-1 Fragility Curves of 602-11 Bridge as a Function of Spectral Acceleration

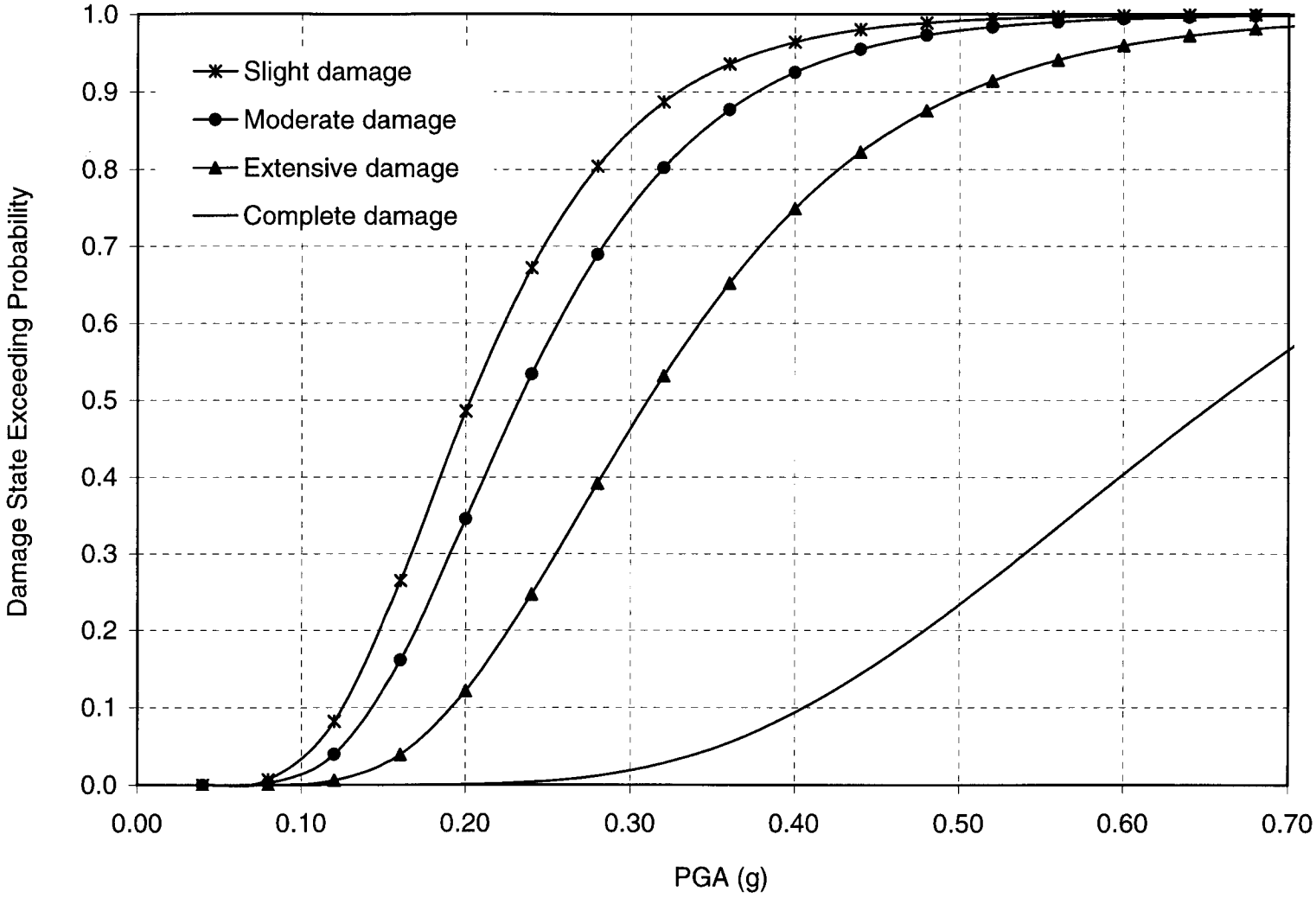

Figure 7-2 Fragility Curves of 602-11 Bridge as a Function of Peak Ground Acceleration

SECTION 8
DISCUSSIONS AND CONCLUSIONS

This report presents an analytical method for developing seismic fragility curves of highway bridges. In this method, appropriate models for seismic source, path attenuation, local site condition, and bridge are established and used to simulate the response of bridge to earthquakes. The uncertainties in the earthquake-site-bridge system are quantified by estimating uncertainties in the pertinent parameters that are used to define the analytical models. The advantage of this approach is that the assessment of uncertainties in these parameters can be easily verified and refined. Several issues pertinent to the use of analytical methods for the development of seismic fragility curves are discussed below.

Traditionally, the fragility curves of a structure are developed from random vibration analysis of structures. The advantage of random vibration analysis is that the probabilistic characteristics of structural response can be obtained analytically. However, random vibration analysis is most useful for linear structures because the principle of superposition is utilized in the analysis. To include nonlinear behavior of structures, the direct simulation is usually employed by performing nonlinear seismic response analysis of structures. It is noted that the direct simulation has become feasible in recent years because of the increase in computing power and storage capacities of personal computers and microcomputers.

In direct simulation, the number of simulations is a critical consideration. For those structures that can be represented by a model with a single degree of freedom or a few degrees of freedom, the number of simulations is not a problem. However, for those structures that cannot be represented by a simple structural model, for example, irregular buildings and curved bridges, a realistic structural model like a finite element model needs to be employed and the number of simulations is a critical consideration.

The choice of a parameter to represent the intensity of ground shaking is another consideration. Traditionally, peak ground acceleration (PGA) is used as the ground shaking parameter for the generation of fragility curves. The reason to use PGA as the ground shaking parameter is that it

is readily available from earthquake records. Thus, it is convenient to use PGA for the development of fragility curves when the curves are derived empirically from earthquake experience data. It is well known, however, that PGA is not a good measure of seismic demand on a structure. In the simulation, when PGA is used as the ground shaking parameter, the simulated structural response data are scattered and thus, the number of simulations needs to be increased. Conversely, the simulated response data are less scattered when spectral acceleration (SA) instead of PGA is used as the ground shaking parameter. However, it is difficult to apply the fragility curves expressed in terms of SA to a large inventory of structures because the determination of the fundamental periods of these structures is not trivial. Strictly speaking, spectral acceleration is a structural parameter and is not really a ground shaking parameter. Additional studies need to be conducted in order to find an appropriate pure ground shaking parameter for the expression of structural responses and fragility curves.

In most seismic fragility analyses, the probabilistic structural demand is described by a lognormal distribution. A lognormal distribution is defined by two parameters: the median value and the logarithmic standard deviation. It is noted that the median value can be determined from a few runs of simulation. On the other hand, a large number of simulation runs are required in order to determine the logarithmic standard deviation. For the practical fragility analysis of a complex structure, an overall logarithmic standard deviation may be used as recommended in HAZUS99 to reduce the number of simulation runs.

The fragility curves of bridges can be used to estimate the chance that a bridge will be damaged in a seismic event. In addition to fragility curves, the repair cost and the recovery time are also required for evaluating the seismic performance of a highway system. In the central and eastern United States, no data on the repair cost and recovery time are available because damaging earthquakes are very scarce. One way to develop such a database is through the survey of expert opinions. As an example, Hwang et al. (2000) have developed repair costs and recovery times for various degrees of damage to a 602-11 bridge based on the survey of experts in the state departments of transportation and consulting engineering companies.

SECTION 9
REFERENCES

Atkinson, G., and Mereu, R. (1992). "The Shape of Ground Motion Attenuation Curves in Southern Canada." *Bulletin of the Seismological Society of America*, 82, 2014-2031.

ATC 32: Improved Seismic Design Criteria for California Bridges: Provisional Recommendations (1996). Applied Technology Council (ATC), Redwood City, CA.

Basoz, N., and Kiremidjian, A. (1998). *Evaluation of Bridge Damage Data from the Loma Prieta and Northridge, California Earthquakes*. Technical Report MCEER-98-004, Multidisciplinary Center for Earthquake Engineering Research, Buffalo, NY.

Boore, D.M. (1983). "Stochastic Simulation of High-frequency Ground Motions Based on Seismological Models of the Radiation Spectra." *Bulletin of the Seismological Society of America*, 73, 1865-1894.

Boore, D.M., and Boatwright, J. (1984). "Average Body-Wave Radiation Coefficients." *Bulletin of the Seismological Society of America*, 74, 1615-1621.

Boore, D.M., and Joyner, W.B. (1991). "Estimation of Ground Motion at Deep-soil Sites in Eastern North America." *Bulletin of the Seismological Society of America*, 81, 2167-2185.

Boore, D.M. (1996). *SMSIM – Fortran Programs for Simulating Ground Motions from Earthquakes: Version 1.0.* Open-File Report 96-80-A, U.S. Geological Survey, Menlo Park, CA.

Brune, J.N. (1970). "Tectonic Stress and Spectra of Seismic Shear Waves from Earthquakes." *Journal of Geophysical Research*, 75, 4997-5009.

Brune, J.N. (1971). "Correction." *Journal of Geophysical Research*, 76, 5002.

Chiu, J.M., Johnston, A., and Yang, Y.T. (1992). "Imaging the Active Faults of the Central New Madrid Seismic Zone Using PANDA Array Data." *Seismological Research Letters*, 63, 375-394.

French, S.P., and Bachman, W.H. (1999). "Transportation facilities in Mid-America." *Proceeding of the 5th U.S. Conference on Lifeline Earthquake Engineering*, Seattle, WA, August 12-14, 1999, 582-591.

Guidelines for Determining Design Basis Ground Motions (1993). EPRI TR-102293, Electric Power Research Institute, Palo Alto, CA.

Hanks, T.C., and Kanamori, H. (1979). "A Moment Magnitude Scale." *Journal of Geophysics Research*, 84, 2348-2350.

Hanks, T.C., and McGuire, R.K. (1981). "The Character of High-Frequency Strong Ground Motion." *Bulletin of the Seismological Society of America*, 71, 2071-2095.

HAZUS99 User's Manual (1999). Federal Emergency Management Agency, Washington, D.C.

Hwang, H., and Lee, C.S. (1991). "Parametric Study of Site Response Analysis." *Soil Dynamics and Earthquake Engineering*, 10(6), 382-290.

Hwang, H., and Huo, J.R.(1994). "Generation of Hazard-consistent Ground Motions." *Soil Dynamics and Earthquake Engineering*, 13(6), 377-386.

Hwang, H., and Huo, J.R. (1998). "Probabilistic Seismic Damage Assessment of Highway Bridges." *Proceedings of the Sixth U.S. National Conference on Earthquake Engineering*, Seattle, WA, May 31-June 4, 1998, Earthquake Engineering Research Institute, Oakland, CA (on CD-ROM).

Hwang, H., Jernigan, J.B., and Lin, Y.W. (1999). "Expected Seismic Damage to Memphis Highway Systems." *Proceeding of the 5th U.S. Conference on Lifeline Earthquake Engineering*, Seattle, WA, August 12-14, 1999, 1-10.

Hwang, H., Jernigan, J.B., Billings, S., and Werner, S.D. (2000). "Expert Opinion Survey on Bridge Repair Strategy and Traffic Impact." *Proceedings of the Post Earthquake Highway Response and Recovery Seminar*, St. Louis, MO, September 5-8, 2000. Federal Highway Administration, Washington, D.C.

Idriss I.M. (1990). "Response of Soft Soil Sites During Earthquakes." *Proceedings of the H. B. Seed Memorial Symposium,* Berkeley, CA, 2, 273-289.

Idriss, I.M., and Sun, J.I. (1992). *SHAKE91, a Computer Program for Conducting Equivalent Linear Seismic Response Analyses of Horizontally Layered Soil Deposits, User's Manual.* Center for Geotechnical Modeling, Department of Civil and Environmental Engineering, University of California, Davis, CA.

Mander, J.B., Kim, D-K., Chen, S.S., and Premus, G.J. (1996). *Response of Steel Bridge Bearings to Reversed Cyclic Loading.* Technical Report NCEER-96-0014, National Center for Earthquake Engineering Research, State University of New York at Buffalo, NY.

Mander, J.B., and Basoz, N. (1999). "Seismic Fragility Curve Theory for Highway Bridges." *Proceeding of the 5th U.S. Conference on Lifeline Earthquake Engineering*, Seattle, WA, August 12-14, 1999, 31-40.

Priestley, M.J.N., Seible, F., and Calvi, G.M. (1996). *Seismic Design and Retrofit of Bridges*. John Wiley & Sons, Inc., New York, NY.

SAP2000, Integrated Finite Element Analysis and Design of Structures: Analysis Reference (1996). Computers and Structures, Inc., Berkeley, CA.

Seismic Retrofitting Manual for Highway Bridges (1995). Publication No. FHWA-RD-94-052, Office of Engineering and Highway Operations R&D, Federal Highway Administration, McLean, VA.

Shinozuka, M. (2000). "Development of Bridge Fragility Curves Based on Damage Data." *Proceedings of International Workshop on Annual Commemoration of Chi-Chi Earthquake*, September 18-20, 2000, Taipei, Taiwan, II, 14-25.

Vucetic, M., and Dobry, R. (1991). "Effect of Soil Plasticity on Cyclic Response." *Journal of Geotechnical Engineering*, 117 (GE1), 89-107.

Wallace, J.W. (1992). *BIAX, A Computer Program for the Analysis of Reinforced Concrete and Reinforced Masonry Sections.* Report No. CU/CEE-92/4, Department of Civil Engineering, Clarkson University, Potsdam, New York.